A STUDY, USING A SIMULATED SEA - WATER, OF THE DISPOSAL OF ACIDIC IRON EFFLUENT AT SEA

By

C. W. George, B.Sc., B.E. (Hons.) (Sydney)

SUBMITTED IN FULFILMENT OF THE REQUIREMENTS FOR THE DEGREE OF MASTER OF SCIENCE

University of Tasmania

Hobart

MARCH, 1977

TO MY WIFE

To the best of my knowledge this thesis contains no material which has been accepted for the award of any other degree or diploma in any University and contains no copy or paraphrase of material previously published or written by another person, except where due reference is made in the text.

Christ W George

ACKNOWLEDGEMENTS

I wish to express my appreciation to Professor H. Bloom for his supervision and guidance during the period this research was undertaken.

I wish to thank fellow research students and staff of this department for valuable research discussions and their continued encouragement.

Thanks are due to Mrs. H. Hen, Mrs. B. Dix and Mrs. S. Petrie for their assistance in the preparation of this thesis.

Finally, I gratefully acknowledge the receipt of the Tioxide Australia Pty. Ltd. Research Scholarship and thank the Company for its help and interest.

CONTENTS

CONTENTS (continued)

Abstract

The titanium dioxide pigment industry at present disposes of a large quantity of acid-iron waste by dumping it at sea. The ensuing interactions result in a red discolouration of the environment which is a source of increasing public concern. A study has been made of the reactions that occur when an effluent solution of ferrous sulphate in sulphuric acid is added to sea-water.

On addition of the effluent solution there is an initial rapid reaction between the effluent acid and the bicarbonate buffer of sea-water. The ferrous iron content is dispersed, is subsequently oxidised and precipitates as a form of ferric hydroxide. In sea-water ferrous iron solubility is controlled by the solubility of ferrous carbonate. Solubility calculations, based on available thermodynamic data at $25^{o}C$, show that for the composition of typical industrial effluents there is little possibility of ferrous carbonate precipitating on effluent dispersion in sea-water.

The kinetics of the ferrous oxidation reaction has been determined by following changes in dissolved oxygen concentration and pH in samples of a simulated artificial sea-water. The kinetics can be best described by the rate expression:

$$\frac{-d(Fe^{2+})}{dt} = k_B (Fe^{2+}) (O_2) (OH^-)^2$$

where k_B has a value of $5.7 \pm 0.6 \times 10^{16}$ litre^3 mole^{-3} min^{-1} at $25^{o}C$ for artificial effluents.

This is in agreement with the expression established for ferrous oxidation in low ionic strength natural bicarbonate waters by other workers.

The product of ferrous oxidation has been examined by infra-red spectroscopy and by X-ray diffraction and has been found to be poorly crystalline lepidocrocite, γ-FeOOH. Average crystallite sizes for the oxidation precipitates formed have been estimated and have been found to lie in the range 5.5 nm to 14 nm.

The relevance of the results to the real situation has been verified by experiments with real sea-water samples and samples of an industrial titanium pigment waste, though there appears to be some component in the actual waste used which retards the ferrous oxidation reaction.

ABBREVIATIONS

The following abbreviations and conventions are used in this thesis:

(A) = concentration of species A (as appears in the text).

[A] = concentration of species A (as appears on the diagrams).

$(Fe^{2+})_I$)
) = initial ferrous iron concentration -mg/litre
$[Fe^{2+}]_I$)

Alk = alkalinity of solution - equivalents/litre

C_T = total inorganic carbon content of solution - moles/litre

CHAPTER 1

INTRODUCTION - ACIDIC FERROUS SULPHATE EFFLUENT

1.1 TITANIUM DIOXIDE MANUFACTURE

The titanium pigment industry, barely established before 1930, has enjoyed a rapid rate of growth since the Second World War. Because of its brilliant whiteness, high refractive index, chemical stability and non-toxicity, titanium dioxide (TiO_2) is extensively used as a pigment in the paint and allied industries and is finding increasing application in many other industries, such as in plastics and paper manufacture. The chemical manufacturing process on which the titanium pigment industry was originally based is called "the sulphate process", and this process accounts for the bulk of the world's titanium dioxide production at the present time (1).

At most factories using the sulphate process the starting point in the manufacture of titanium pigments is ilmenite ($FeO \cdot TiO_2$), a combination of titanium oxide and iron oxides which is commonly obtained as a black beach sand. The raw sand is dried, ground to a fine powder and then reacted with concentrated sulphuric acid. On completion of acid digestion the iron present, which has been simultaneously dissolved, is fully reduced to the ferrous state. The resulting solution is then cooled to remove the iron by precipitation as hydrated ferrous sulphate ($FeSO_4 \cdot 7H_2O$). After filtration or passing through a centrifuge the remaining titanium solution is refined and the titanium is precipitated as titanium hydroxide.

Calcination of the hydroxide under controlled conditions forms the basic titanium dioxide. Subsequent treatment by both grinding and chemical surface coating produces the differing grades of pigment for specific industrial requirements (2). A flowchart of the process is given in Figure 1.

Because of the high proportion of iron in ilmenite, the most abundant titanium ore, the quantity of ferrous sulphate formed in the sulphate process is substantial, the rate being roughly 3.5 kilogrammes per kilogramme of titanium dioxide (3). Unfortunately hydrated ferrous sulphate, known commercially as "copperas" or "green salt", can only be utilized to a limited extent. A relatively small amount is used as a flocculant for biological sludges. Larger amounts are used in sulphuric acid manufacture but the high water of crystallisation content presents problems in the roasting process (4), and more economic raw material alternatives are readily available. Because of its solubility and acidic nature waste copperas cannot be dumped as solid fill. Consequently, most pigment manufacturers redissolve their waste copperas in the spent acid remaining at the end of the sulphate process (Figure 1). This yields a final acidic effluent relatively high in iron and produced in large quantity. For example, the final effluent from the 32,000 tonne Tioxide Australia Pty. Ltd. plant at Burnie, Tasmania, has an average composition of 30 gm /l Fe and 73 gm/l H_2SO_4 (7.3% $FeSO_4$ and 6.6% H_2SO_4 on a weight basis) and is produced at an average rate of around 70 m^3/hr (5).

FIGURE 1 - THE SULPHATE PROCESS FOR THE MANUFACTURE OF TiO_2 PIGMENT

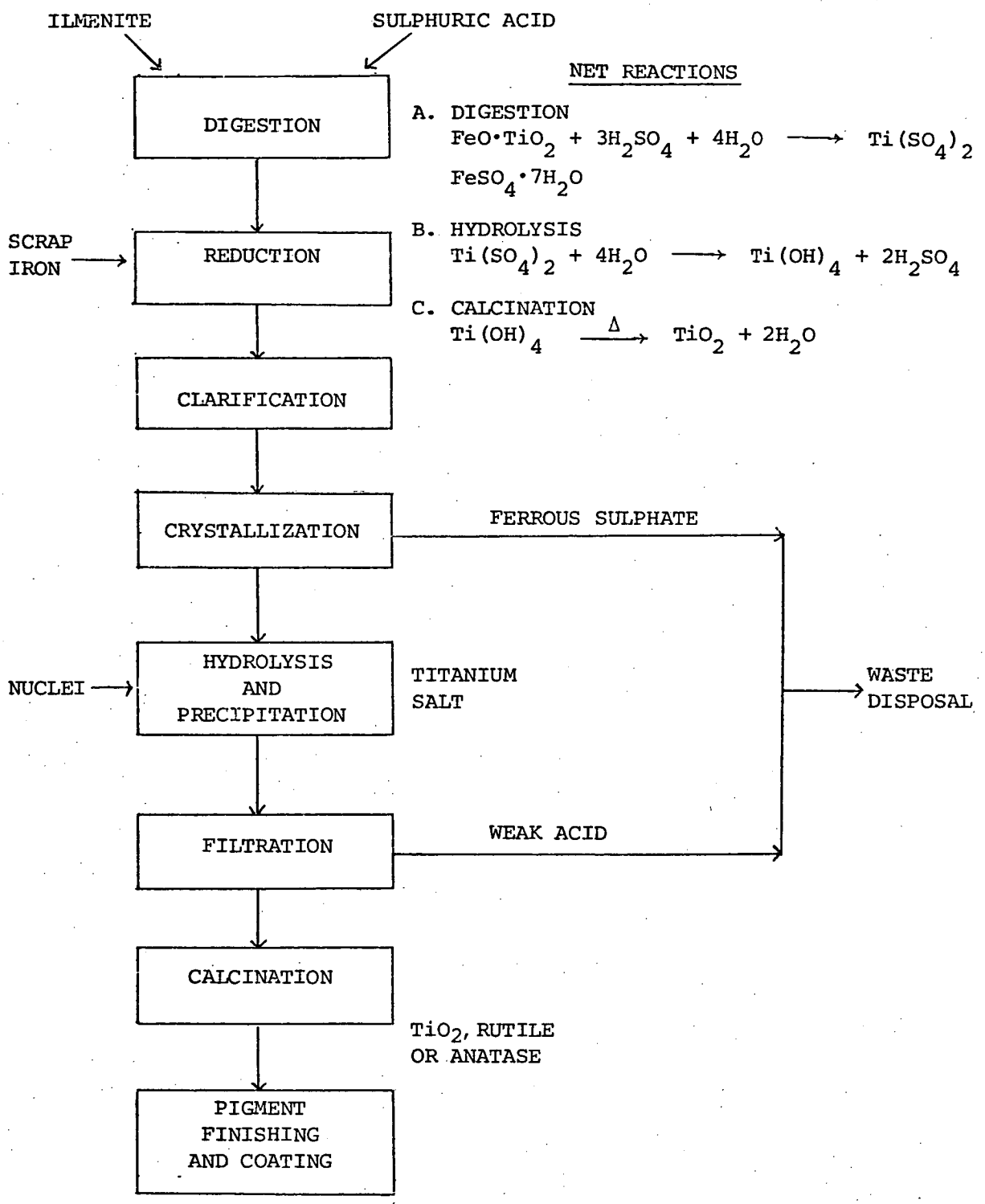

1.2 TREATMENT OF LIQUID EFFLUENT

Both the titanium pigment industry and the steel industry have for many years been faced with the problem of disposing of huge quantities of waste solution containing ferrous sulphate and free sulphuric acid. In the steel industry the product is the result of treating sheet steel with hot sulphuric acid to remove scale and rust, a process known as pickling. The waste liquor has generally the same composition as that discharged from titanium plants (6). Because of the high concentration of free acid and contained iron in the effluent simple treatment schemes such as neutralization and removal of precipitated iron are necessarily expensive, and such treatment still leaves the problem of the disposal of the large quantities of iron sludge produced. In addition, it is naturally preferable to manufacturers to try to recover their waste sulphuric acid from the effluent for reuse. However, in spite of an enormous amount of research over the last fifty years complete and economic regenerative processes for acidic ferrous solutions have yet to be developed.

A vast amount of literature and patents concerning the treatment of spent sulphuric acid pickle liquor exists and is continually being added to. Existing treatment methods have recently been reviewed by Lacey (7). The most common include neutralization and precipitation with lime or other alkaline materials and crystallization of the ferrous salt by cooling, evaporation, or chemical treatment. Steel manufacturers have an advantage over pigment manufacturers in that certain neutralizing materials, such as limestone, are used in large quantities in the steel-making process and are thus available at little extra cost (7). Lacey and Lawson have

proposed a new treatment process based on the bacteriological oxidation of ferrous iron and the precipitation of jarosite, a basic ferric sulphate (8).

The waste disposal problems of titanium dioxide producers have also been recently reviewed (9). As expected, most proposed treatment methods are identical to those investigated by the steel industry. Grishaeva (10) has presented a technical and economical evaluation of commercial scale and laboratory methods for processing spent sulphuric acid from pigment manufacture, but makes no mention of ferrous sulphate disposal. He concludes that methods based on neutralization with lime or boiling down the spent acid to higher H_2SO_4 concentrations are not economical. A stepwise treatment of pigment effluent to produce fertilizers, such as $(NH_4)_2SO_4$, and Fe ochre pigment is one of several treatment methods under recent investigation (11). In the present absence of any economic treatment or regenerative process, and faced with a large disposal problem, the majority of "sulphate process" pigment manufacturers employ the relatively cheap expedient of dumping their acidic ferrous sulphate effluent at sea. With increasing community awareness of pollution, however, the environmental effects of wastes discharged to the sea are coming under closer and closer investigation, and this method of disposal is a growing source of controversy.

In 1973 the United States Environmental Protection Agency conducted a survey of the major inorganic chemical industries in order to help formulate effluent limitation guidelines. It was found that the sulphate process for producing titanium dioxide had the greatest waste load of all the inorganic processes studied (12). Of the five sulphate process plants studied in the U.S.A. none was considered exemplary with regard to the treatment of its wastes.

Those producers with plants on the coast were generally barging their acidic ferrous liquid waste to sea, but USEPA did not consider this method of disposal satisfactory and believes the future of this alternative to be very uncertain.

In an economic analysis of proposed effluent guidelines, USEPA considered two separate treatment approaches for sulphate process plants - acid neutralization and acid recovery (13). The exemplary method of acid neutralization was regarded to be with limestone, followed by lime treatment to raise the pH to approximately 8 so as to precipitate iron and other metallic oxides and hydroxides. This treatment reduces the waste load discharge to the solubility limits of calcium sulphate. When costed, it was found that the investment in treatment facilities necessary for acid neutralization and acid recovery represented 55% and 26% respectively of the cost of the net plant (13), indicating the sizable investment relative to existing plant required to attain zero discharge of waterborne wastes. Of the major inorganic chemicals, TiO_2 stood out as the product where the estimated effluent treatment costs represented the highest proportion of both selling price and profit margin. The economic analysis concluded that if strict effluent controls were enforced then several sulphate process producers would be faced with shutdown decisions.

Because of the magnitude of the effluent disposal problem facing the titanium pigment industry, and to a somewhat lesser extent the steel industry, both have developed alternative processes to lessen their waste load. In the steel industry hydrochloric acid is increasingly replacing sulphuric acid in the pickling baths (14). Whilst the advantages of hydrochloric acid in the pickling process itself are well known, acceptance of the more expensive acid has been due

also to relatively simple regeneration processes for treatment of iron-containing hydrochloric acid effluent liquors (7).

The alternative process for the manufacture of titanium dioxide is "the chloride process" developed in the early 1950's by American technology. The majority of new pigment plants built since 1956 are based on the chloride process and this method of production now accounts for approximately 20% of the world's pigment output (2). The basic raw material - rutile, containing 95 + % TiO_2, is mixed with petroleum cake or other carbon-containing material and exposed to chlorine at a temperature of 1000^{o}C. The titanium chloride formed is separated from other chlorides by distillation and reacted with oxygen at 1000^{o}C. Titanium dioxide and chlorine are obtained. The drawback to this process is that, in comparison with ilmenite the raw material rutile is in short supply.

Much work has been undertaken into the upgrading of ilmenite into a "synthetic rutile" suitable for use in the chloride process and a "titanium slag" suitable for use in the sulphate process. In the latter case, ilmenite is treated metallurgically with coal and lime for the purpose of removing its iron content (15). However, until this enriched raw titanium dioxide is available in large quantities, and given the large investment in sulphate process plants around the world, the titanium pigment industry will continue to be faced with the problem of disposing of large volumes of acidic ferrous sulphate effluent in the foreseeable future.

1.3 THE DISPOSAL OF EFFLUENT AT SEA

The disposal of acidic ferrous sulphate effluent at sea represents a large cost advantage over chemical treatment options and is achieved either by barging or by pumping through direct submarine pipelines. Some titanium dioxide manufacturers have transferred their plants to the coast in order to reduce the distance tc the sea (15). The use of the ocean as a dumping ground utilizes the alkaline nature of sea-water and relies on rapid dilution to neutralize the spent acid in the effluent and disperse its iron content. A rapid initial dilution is necessary to avoid any toxic effects on the marine environment in the area immediately around the outfall. Ocean currents are then relied upon for further dilution and dispersion.

Published environmental studies of marine pollution resulting from the discharge of acid-iron waste from titanium dioxide manufacture centre on two major dumping areas. Since 1950 a titanium plant of the National Lead Company has been disposing of its acid waters in an approved region 10-13 miles off the New Jersey (New York) coast. Discharge of tanker loads of similar liquid waste into an area of the German Bight began in May 1969.

Not long after barge dumping commenced off the New York coast, Redfield and Walford (16) investigated the effect of disposal on the fisheries and on the composition of the sea water.

The waste, discharged into the propeller water of the tanker to achieve adequate initial dilution, contained 10% $FeSO_4$ and 8.5% H_2SO_4 and was being dumped at a rate of about 4,050 tonnes per day. Observations were made in the wake of the barge to determine the pH value and concentration of iron,as ferrous sulphate,at various depths and at various distances from the barge. Redfield and Walford found

that "within thirty seconds of discharge the waste is diluted with more than 250 volumes of sea water and causes only a temporary deviation from the normal chemical balance. On discharge the waste acid is rapidly neutralized, ferrous ions are oxidized and, as the sea water is saturated with respect to ferric ions, the iron is precipitated as colloidal ferric hydroxide. Sulphate, being one of the main constituents of sea water, is easily absorbed. Ferric hydroxide causes turbidity and does not settle very rapidly; this is advantageous as the precipitate is distributed widely by currents before settling to the bottom. The oxidation process is fairly slow and no more than 3-4 per cent of the oxygen present is used" (16). Biological investigations showed that the disposal of the waste temporarily immobilized the zooplankton in the relatively small area of discharge but had no detectable effect on the bottom fauna or fish population.

Subsequent studies of the dumping area (17, 18) have shown no evidence of serious pollution and the region has become a good fishing ground. Vaccaro and co-workers made an in-depth study of the ecological consequences arising from 22 years of barge disposal. They found that only 10-20% of the iron measured in the New York Bight was in true solution or occurred as particles less than 1μm in diameter, while the remaining iron fraction was in the form of particulate matter. The maximum concentration of iron in the water column (832 μg/l) suggested a maximum in-situ concentration of one part waste in 39,000 parts of sea water. There was a positive correlation between Fe:C in zooplankton and the amount of particulate iron present in the sea water, but there was no corresponding indication of adverse effects on the benthic population. The report concluded, "present indications are that the disposal of acid-iron waste in the New York Bight appears to influence standing crops in minor ways considering the magnitude and

nature of the waste material involved" (18).

In an investigation into the ocean disposal of titanium waste (14% $FeSO_4$ and 10% H_2SO_4) in the German Bight, Rachor (19) states that on discharge the waste acid is neutralized, ferrous iron is oxidized and the precipitated hydrated ferric oxide forms flakes which float above the bottom sediment with little or no permanent deposition. However, with time, the numbers of both individuals and species of macrofauna were found to have increased and the flakes of hydrated ferric oxide had not hindered the settlement of new species nor of some species previously found in the area. Weichart (20) studied physical and chemical changes in the water and on the sea bed resulting from the effluent discharge. Dilution of the acid waste was found to be rapid and about two hours after the release the pH value (initially about 6) had returned to nearly normal (pH 8), the oxygen concentration was nearly normal, and the iron concentration (initially 40 mg/l) was 2 mg/l, with no immediate effects on the sea bed. Six months after the first discharge the polluted zone was found to cover about 500 km^2 and the maximum concentration of iron in the water was 500 µg/l. Reviewing the results of waste dumping in the German Bight, Steinert (21) notes that although according to prediction and experiment it was reasoned that the discharge of "dilute iron rich acid" and red mud (from bauxite beneficiation) must have a devastating effect on the fauna, the opposite has happened. He states that the hydrographic and sedimentologic processes of deposition following waste dumping have been given little consideration and calls for work to solve such questions as what size particle arises on iron hydroxide precipitation.

Several workers have undertaken laboratory toxicity studies with acidic ferrous sulphate effluent. After experiments with copepod species, Grice and Wiebe concluded that acid-iron wastes are a minor factor affecting the distribution of zooplankton (22, 23). Similarly,

ferric hydroxide flakes have been found to have mechanical effects on mussels with no evidence of acute toxicity (24). Smith et al (25, 26) studied the effect of lime neutralized iron hydroxide suspensions on the survival, growth and reproduction of both the juvenile brook trout and flathead minnow and determined safe levels of suspended iron. It was assumed that impaired visibility due to high turbidity prevented the fish from feeding which in turn resulted in slow growth in high Fe concentrations.

Although environmental studies have, as yet, shown no adverse effects of acidic ferrous sulphate waste dumping on marine life, the so-called "visual pollution" due to the discolouration of the sea by precipitated ferric hydroxide is a continual source of public protest. Italian fishermen recently protested violently at the dramatic red hue taken on by the sea as a result of waste disposal by barging from a titanium dioxide plant at Scarlino (27). The problem of ocean discolouration particularly applies to those pigment manufacturers who discharge their waste to the sea by direct pipeline. In this case, as well as the discolouration of offshore waters, local coastlines and beaches can be subject to staining with a concomitant rise in public outcry. Some producers have found that discolouration can be reduced by extending their pipelines further out from shore to take advantage of natural ocean currents (28).

Madeley, in a discussion of the waste disposal problems of the British chemical industry, believes that "the submarine pipeline as a form of effluent disposal should remain with us for many years, and in fact increase its application. It has been shown to offer an economic as well as an environmentally acceptable solution when properly designed and controlled, compared with other methods" (29). He notes the procedures for the correct siting of marine pipelines and outfalls and examines the dispersal and dilution of effluents from

these outfalls. Weber (15) also believes that the possibility of the sea as a dumping ground will become increasingly important for the inorganic chemicals industry in the future.

Titanium pigment manufacturers who dispose of their waste through submarine pipelines are also faced with problems arising from the fact that, as noted by Rachor (19), ferric hydroxide tends to float above the ocean floor with little or no permanent deposition. This means that in the absence of natural dispersion currents large floating "deposits" of ferric hydroxide can be formed in relatively shallow coastal waters, easily stirred up by storm activity. Apart from the resultant periodically increased visual pollution, such floating deposits are themselves of possible pollution concern on two accounts. Firstly, it is argued that the productivity of coastal waters can be affected by reduction of light penetration due to large amounts of suspended matter (29). Secondly, ferric hydroxide precipitates are known to be able to concentrate and accumulate heavy metals from dilute solutions.

In December 1973 the Tasmanian Department of the Environment undertook a study of the distribution of heavy metals from industrial sources along a section of the North-West coast of Tasmania and out 21 km to sea. Among the industries located in the study section is the titanium dioxide plant of Tioxide Australia Pty. Ltd., which discharges its acidic ferrous sulphate effluent to the sea by means of a direct submerged pipeline. The Department's report (30) noted that "a gigantic red 'cloud' of iron-rich suspended material, at least 20 km across, was found to be either generated in the study area or to be drifting at lower depths during the period of the survey. A similar red-brown discolouration of the sea was observed several times during the survey

period." The 'cloud' was found to contain high concentrations of heavy metals but the relative concentrations did not correspond closely with those in "pipe discharged iron-rich liquor." Although it was not possible to establish the precise nature of the cloud formation, the study concluded that "it possibly originates from the chemical precipitation of iron compounds in seawater..... and it is likely that heavy metals are taken up by the suspended particulates either by adsorption or biological accumulation."

Thus it can be seen that the future of ocean disposal of acidic ferrous sulphate wastes from titanium dioxide manufacture is by no means guaranteed. The practice, particularly when achieved by means of a direct submarine pipeline, will continue to come under close environmental and public scrutiny. In order that a rational consideration of the issues involved can take place it is necessary that, in addition to gathering data by environmental monitoring, the chemistry of the effluent - sea water interaction be fully understood.

1.4 OBJECT OF RESEARCH

The disposal of liquid effluent at sea is an economic and indeed vital practice for many titanium dioxide producers. Up to date the majority of scientific investigations have concentrated, naturally, upon the environmental impact of such disposal with only a short consideration of the chemical processes taking place. Present indications are that the acid - iron waste does not disrupt the marine ecology to any large extent, though the ability of iron hydroxide suspensions to accumulate heavy metals may become of increasing concern. Possibly because of the concern with pollution, a precise study of the chemical interaction of acidic ferrous sulphate effluent with sea-water does not appear to have been made. Such a study would appear to be warranted, particularly given the fact that it is the visual discolouration of the sea following the ferric hydroxide precipitation process which greatly concerns the lay public. Moreover, the nature of the ferric hydroxide precipitate formed following ferrous iron oxidation and the resultant particle size are important parameters in ecological considerations (21).

The present laboratory study aimed to investigate some aspects of the chemical interaction resulting on the introduction of an acidic ferrous iron solution to sea-water. In particular, it was decided to concentrate on the following: the kinetics of the ferrous iron oxidation process, the accompanying depletion of oxygen in solution, the crystalline nature and crystallite size of the oxidation product formed, and the influence of solution pH and temperature. To aid in the study it was decided to make use of an "artificial" sea-water of constant composition. Results obtained with artificial solutions could then be compared with those obtained using samples of real sea-water and a real industrial effluent.

Finally, if the oxidation process is relatively slow then there is the possibility at high iron concentrations of the precipitation of ferrous iron compounds, as compared to ferric hydroxide precipitation. This suggested that a theoretical study of iron solubility in sea-water should initially be undertaken to provide the necessary background information for the work to follow.

1.5 REFERENCES

(1) "The Titanium Dioxide Industry" - Tioxide Australia Pty. Ltd., January 1974.

(2) "Progress" - a booklet produced by Tioxide Australia Pty. Ltd.

(3) Weber H. H. - Pure and Applied Chemistry, 29, 67 (1972).

(4) Beeken D. W. - The Industrial Chemist, p604 (December, 1960).

(5) Personal Communication.

(6) Bartholomew F. J. - Chemical Engineering, p 118 (August, 1950).

(7) Lacey D. T. - Rev. Pure and Applied Chemistry, 20, 23 (1970)

(8) Lacey D. T. & Lawson F. - "A New Method for Treating and Regenerating Spent Sulphuric Acid Pickle Liquor" - Dept. Chem. Eng., Monash University (1970).

(9) Bartolewski W. - Chemik,27(2), 44 (1974) (Polish).

(10) Grishaeva V. A. & Buryak K. A. - Tr., Nauch. - Issled. Inst. Udobr. Insektofungits.1970, No. 216, 3-15 (Russian).

(11) Ganz S. N. et al - Vop. Khim. Khim. Tekhnol.,30, 193 (1973) (Russian).

(12) "Development Document for Proposed Effluent Limitations Guidelines and New Source Performance Standards for the Major Inorganic Products Segment of the Inorganic Chemicals Manufacturing Point Source Category" - United States Environmental Protection Agency - August 1973.

(13) "Economic Analysis of Proposed Effluent Guidelines, Inorganic Chemicals, Alkali & Chlorine Industries (Major Products)" - United States Environmental Protection Agency - August 1973.

(14) Chem. & Eng. News, March 3, 38 (1969).

(15) Weber H. H. - Pure and Applied Chemistry, 29, 67 (1972).

(16) Redfield A. C. & Walford L. A. - National Research Council of the National Academy of Sciences, Publication No. 201, Washington D.C., 1951.

(17) Peschiera L. & Freiherr F. H. - J. Wat. Pollut. Control. Fed., 40, 127 (1968).

(18) Vaccaro R. F. et al - Water Res.,6(3), 231 (1972).

(19) Rachor E. - Mar. Pollut. Sea Life, FAO, 390 (1972).

(20) Weichart G. - Mar. Pollut. Sea Life, FAO, 186 (1972).

(21) Steinert H. - Frankfurtar Allgemeine Zeitung, No. 108, May 10 (1972).

(22) Grice G.D., Wiebe P. H. & Hoagland E. - Estuar. Coast. Mar. Sci., 1, 45 (1973).

(23) Ibid., p.51

(24) Winter J. E. - Mar. Pollut. Sea Life, FAO, 392 (1972).

(25) Smith E. J., Sykora J. L., Synak M. - Water Res., 6(8), 935 (1972).

(26) Smith E. J., Sykora J. L., Shapiro M. A. - J. Fish Res. Board Can., 30 (8), 1147, (1973).

(27) The Chemical Engineer, 303, 634 (1975).

(28) "Environmental Control" - Tioxide Australia Pty. Ltd. - 21.4.76.

(29) Madeley J. R. - J. Inst. Fuel, 46(383), 63, (1973).

(30) "Heavy Metals in the Marine Environment of the North West Coast of Tasmania" - Tasmania Department of the Environment, 1974.

CHAPTER 2

SOLUBILITY OF IRON IN SEA-WATER

2.1 THE STATE OF IRON IN NATURAL WATERS

Iron compounds are generously distributed in nature and play an important role in water supplies, waste waters and in limnology. Soluble ferrous iron at natural water pH levels is perhaps the most common, and sometimes a difficult-to-remove, contaminant in domestic water (1). The United States Public Health Service drinking water standard for iron is a low 0.3 mg/l (5.4×10^{-6} moles/l) (2) and water with a total Fe content above 1 mg/l is visually coloured and totally unacceptable for domestic supply (3). Because an understanding of the behaviour of iron in natural water can be gained by a detailed consideration of the kind of conditions that favour its solution, the chemistry of aqueous iron has received a lot of attention. An excellent review of the subject has been given by Stumm and Lee (4).

Iron may exist in solution in either the divalent, ferrous, or the trivalent, ferric, state. In oxygenated water ferrous iron is thermodynamically unstable and is oxidised to ferric iron. The rate of oxidation has been shown to be primarily dependent upon the hydrogen ion concentration (pH) and the temperature of the solution (4). The solubility of ferric iron is controlled in natural waters by the solubility of ferric hydroxide. Other insoluble ferric salts, such as the phosphate and sulphide, are of less practical significance (4). Different structural forms of insoluble ferric hydroxide are known: amorphous ferric hydroxide, ferric oxide hydroxide (FeOOH) and ferric oxide (Fe_2O_3). Their properties and mode of preparation were first extensively investigated by Feitknecht (5).

In most natural groundwaters and in the hypolimnetic waters of lakes and reservoirs iron exists principally in the reduced ferrous form (6). In the absence of carbonate and sulphide species the solubility of ferrous iron is controlled by ferrous hydroxide ($Fe(OH)_2$). However most natural waters contain a degree of dissolved calcium carbonate. The presence of calcium carbonate in carbon dioxide-containing water results in the buffering of natural waters at pH 6-8 (7). The buffering can be assumed to be described by the equilibria (6):

$$H_2CO_3 \rightleftharpoons H^+ + HCO^-_3 \; ; \; K_{25^oC} = 4.45 \times 10^{-7} \quad .....(2A)$$

$$HCO^-_3 \rightleftharpoons H^+ + CO_3^{2-} \; ; \; K_{25^oC} = 4.69 \times 10^{-11} .....(2B)$$

Although at natural pH levels the majority of dissolved inorganic carbon is in the form of the bicarbonate ion (HCO^-_3), in most alkalinity containing waters the carbonate ion (CO_3^{2-}) concentration, even at low pH, is sufficient to limit ferrous solubility. Consequently, in most natural waters the solubility of ferrous iron is controlled by the solubility of ferrous carbonate ($FeCO_3$). This applies up to a pH of about 9.

The solubility of ferrous iron in a bicarbonate containing water of alkalinity 2×10^{-3} equivalents per litre, as drawn by Stumm and Lee (4), is shown in Figure 2. The diagram indicates the principal soluble species contributing to ferrous solubility at different pH values. The alkalinity of a solution is the equivalent sum of bases titratable with strong acids and may be defined for natural waters by the equation:

$$(Alk) = (HCO_3^-) + 2(CO_3^{2-}) + (OH^-) - (H^+) .....(2C)$$

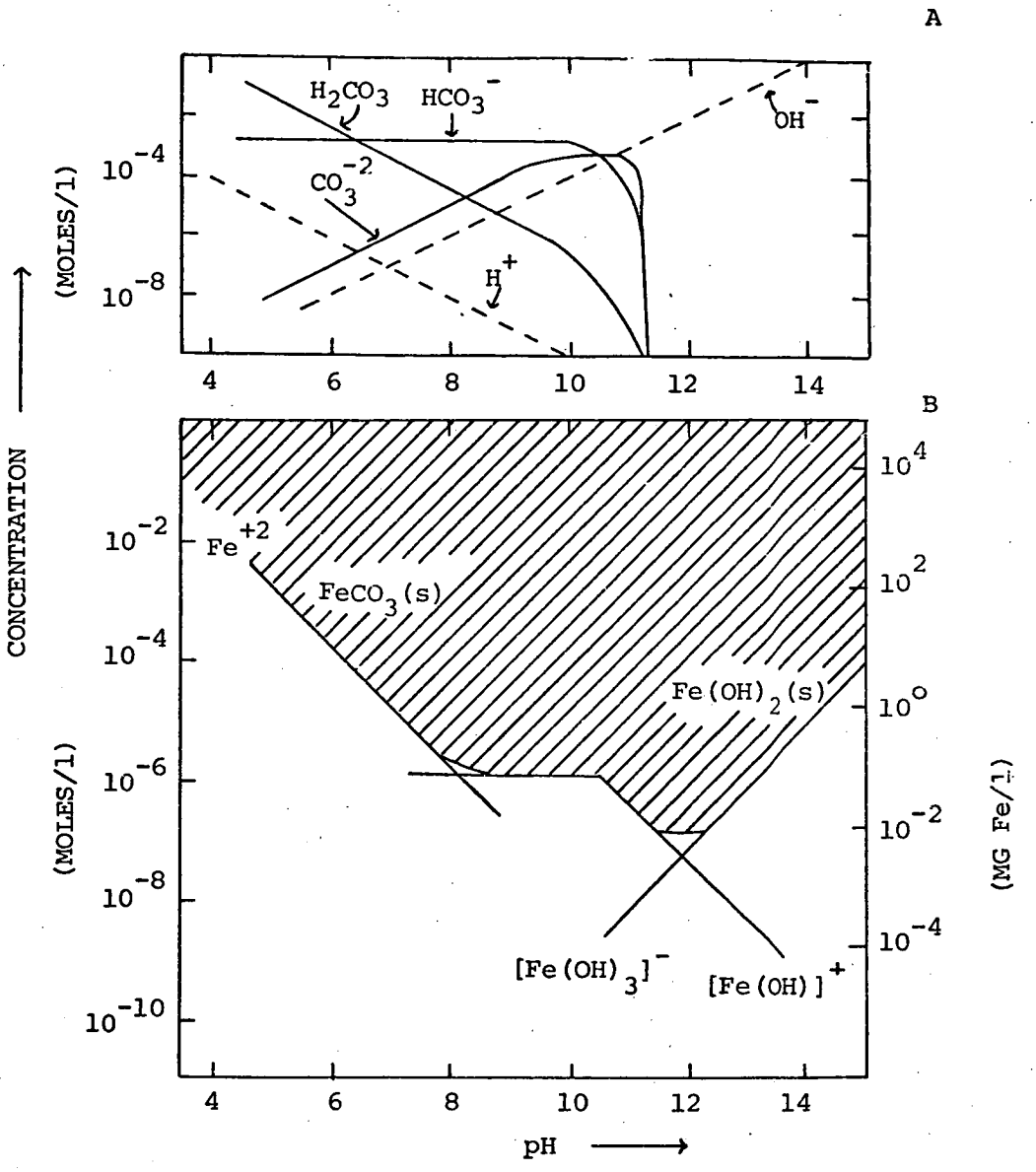

FIGURE 2 - SOLUBILITY OF FERROUS IRON IN A BICARBONATE CONTAINING WATER

ALKALINITY = 2×10^{-3} equivalents/litre (constant)

TEMPERATURE = 25°C

(As per Stumm & Lee (4))

A - pH-dependent distribution of carbonate species

B - Dependence of Fe(II) solubility on pH

Another parameter commonly used to describe a natural water is the total inorganic carbon content or sum of carbonate species, C_T. This is defined by:

$$C_T = (H_2CO_3) + (HCO^-_3) + (CO_3^{2-}) \quad \text{.....(2D)}$$

The distribution of the carbonate species as a function of pH and at a constant alkalinity is also illustrated in Figure 2. The distribution becomes zero at pH 11.3 since alkalinity includes the OH^- ion concentration.

Both ferrous and ferric iron are generally not very soluble in natural bicarbonate waters. In a water of alkalinity 2×10^{-3} equivalents/litre the maximum soluble concentration of ferrous iron at pH 8 and 25°C is calculated from equilibrium data to be about 10^{-6} moles/l (0.056 mg/l). For ferric iron the corresponding figure is 3×10^{-7} moles/l (0.017 mg/l) (8). Because ferrous constituents tend to display a greater solubility than do ferric constituents, oxidation of ferrous rich waters is usually accompanied by precipitation of ferric hydroxide. This forms the basis for the iron removal process in water treatment plants (9).

Most ground waters contain high concentrations of dissolved carbon dioxide and their pH is usually <7. As water is aerated in the treatment plant dissolved carbon dioxide is stripped out of solution, oxygen is entrained and the pH rises. If the pH is raised high enough then ferrous carbonate can precipitate, competing with the ferrous oxidation process. Thus under certain conditions, dependent on the respective rates of the oxidation and precipitation processes, iron can be removed from solution as a mixed precipitate of ferrous carbonate and ferric hydroxide. The situation can be regarded as analogous to that resulting when a ferrous iron solution is suddenly

introduced to a natural water.

It has been suggested that the formation of a mixed precipitate may prove advantageous in the water treatment process, particularly as regards the ease of filtration (3). Olson and Twardowski (9) state that whereas iron hydroxide precipitates as amorphous gelatinous masses, ferrous carbonate precipitates as large, easily filtered, crystalline particles. They also suggest that ferrous carbonate oxidises extremely slowly in an oxygenated water. In contrast, Stumm and Lee (4) point out that while the use of the better known equilibrium reactions and constants leads to solubility predictions in accordance with observed behaviour, under practical conditions pure crystalline solid phases with the given formulas $Fe(OH)_2$, $FeCO_3$ are not obtained, and that the occurrence of basic carbonates e.g. $(Fe(OH)_2 . FeCO_3$ (s)) is probable. Experimental findings as regards iron precipitates are discussed in Chapter 4.

Before moving to a discussion of iron solubility in sea-water, a note should be made on the iron-organic relationship in natural water. Many organic bases form very strong soluble iron complexes with ferrous and ferric ions and consequently may increase the solubility of aqueous iron. Complex formation with the organic acids, humic acid and tannic acid, has been found to retard the rate of ferrous iron oxidation (1) and in natural surface waters high concentrations of organic material such as humic acids and lignin derivatives are frequently associated with high concentrations of soluble iron (4). Plumb (10) found that up to 20% of the iron in the yellow stained waters of a natural lake was associated with organic matter. There is also evidence that organic compounds in natural waters act to stabilize colloidal ferric hydroxide (11).

2.2 CHEMICAL SPECIATION IN SEA-WATER

Chemically speaking, sea- water is roughly an aqueous 0.5M sodium chloride (NaCl) solution, 0.05M in magnesium sulphate ($MgSO_4$), and containing in addition a pinch or trace of just about everything imaginable. It is slightly alkaline with a normal pH of between 7.5 and 8.4 and is buffered primarily by the bicarbonate system (12). The major constituents of a typical sea-water of salinity (i.e. total salt content) 35 gms/kg are outlined in Table 1.

TABLE 1 - MAJOR SEA-WATER CONSTITUENTS(12)

Constituent	Concentration (gm/kg) in 35 ‰ seawater	Constituent	Concentration (gm/kg) in 35‰ seawater
Cl^-	19.353	K^+	0.387
Na^+	10.76	HCO_3^-	0.142
SO_4^{2-}	2.712	Br^-	0.067
Mg^{2+}	1.294	Sr^{2+}	0.008
Ca^{2+}	0.413		

The high ionic strength of sea-water, effectively 0.67 (13), sets it apart from the majority of natural waters and must be considered in any thermodynamic calculations. In a high ionic strength medium oppositely charged ions can be regarded as coming together to form an "ion-pair". The partners in an ion-pair are electrostatically attracted to one another and tend to "loiter" near one another, but the combination is not as strong as is the case with a complex ion. Like complex ions, ion-pairs can be characterised by a thermodynamic formation constant. They need not have a net charge. Horne (12) describes the difference between a true complex ion and a

mere ion-pair in terms of the degree of combination of the hydration sheaths of the separate charged species.

In order to determine the chemical form or forms of an elemental constituent in sea-water it is necessary to consider both simple chemical equilibria and redox potentials. Solutes may be present as hydrated ions, complex ions or ion-pairs. In the case of metal cations the particular species preferred is usually a sensitive function of the metal concentration and pH (14). Garrels and Thompson (15) developed a chemical model for sea-water from available thermodynamic data and from it calculated the degree of complexation between the major cations (Table 1) and the anions SO_4^{2-},HCO_3^- and CO_3^{2-}. Explicit in their calculations were the assumptions that the interactions between the ions under consideration resulted only in the formation of ion-pairs and that chloride complexes were negligible.

Zirino and Yamamoto (13) have expanded the approach developed by Garrels and Thompson to include higher order complex ions. Using available and estimated thermodynamic stability constants and individual ion activity coefficients, they developed a model for the speciation of divalent Cu,Zn,Cd and Pb ions in sea-water. The model was used to calculate the degree of interaction between each of the metal ions and the anions Cl^-, SO_4^{2-}, HCO_3^-, CO_3^{2-} and OH^- as a function of pH. Their calculations indicated that all four metals are complexed to a considerable extent in sea-water.

Whitfield (16) has examined the ion-association model and the buffer capacity of the carbon dioxide system in sea-water at 25^oC and 1 atmosphere total pressure. The equilibrium of the ocean with the atmosphere was simulated by allowing the model sea-water to equilibrate with carbon dioxide at a partial pressure of 3.3×10^{-4} atm

(33.4 N/m^2). At a typical pH of 8.2 the total inorganic carbon content, C_T (equation (2D)), of sea-water was calculated to be 0.0027 moles/litre, in good agreement with experimentally measured values.

Unlike the situation in fresh waters, the components of the carbonate system are complexed (both as complex ions and as ion-pairs) in sea-water with the cations present. For example, Garrels and Thompson calculate (15) that at pH 8 31% of the total bicarbonate ion present in sea-water ($HCO_{3_T}^-$) is complexed, leaving 69% as free ion ($HCO_{3_F}^-$). Whitfield (16) expanded this work to calculate the distribution, expressed as a percentage of C_T, of the components of the carbon dioxide system (both complexed and free) as a function of pH. In the normal pH range of sea-water more than 90% of the total inorganic carbon is found to be present in the form of the bicarbonate ion. Alkalinity (equation (2C)) can be regarded as being relatively constant at about 2.4×10^{-3} equivalents per litre (13).

2.3 IRON IN SEA-WATER

Iron is one of the more important minor constituents of sea-water. Apart from one work (20), the speciation of soluble iron in sea-water, both in the ferric and in the reduced ferrous form, would appear to have received little attention. Detailed study is hampered by a lack of thermodynamic data. Many authors have measured the concentration and distribution of iron in different oceanic waters, but measurements are frequently characterized by their lack of reproducibility (17). The erraticness of analytical results has been attributed to the presence, in situ, of colloidal particles of iron and the problem has been alleviated by recent refinements in analytical techniques. Literature data from 1953 to 1968 on the dissolved and particulate Fe contained in several sea-waters has been tabulated by Head (18). In a recent study Betzer (19) investigated particulate iron in the North Atlantic. The average concentration found in shallow open-ocean water was 0.177 µg/l.

As was the case with natural fresh waters, it is safe to say that ferric iron is the dominant form of iron in sea-water. Under the mildly oxidative conditions present in sea-water ferrous iron is unstable and is oxidized to ferric iron. The overall reaction in sea-water can be represented by (12):

$$4Fe^{2+} + O_2 \text{ (dissolved)} + 4H^+ \longrightarrow 4Fe^{3+} + 2H_2O \; ; E^0 = + 0.458 \text{ V} \quad \ldots\ldots\ldots (2E)$$

The positive potential indicates the reaction should go as written. The solubility of ferric iron in sea-water is controlled, like in other natural waters, by the solubility of ferric hydroxide (12).

2.4 FERRIC IRON SOLUBILITY IN SEA-WATER

2.4.1 Method of Calculation

Kester and Byrne (20) have calculated the relative amounts of the various soluble ferric iron sea-water complexes which contribute to total ferric solubility, from selected equilibrium constant data which best approximate the conditions in sea-water at 25^{0}C and one atmosphere pressure. The chemical forms of ferric iron were then related to the solubility of ferric hydroxide in sea-water to obtain an estimation of total ferric solubility as a function of pH.

The method employed by Kester and Byrne has been reproduced here and applied to both "normal" seawater and to an artificial seawater. The method, basically similar to the metal speciation approach of Zirino and Yamamoto (13), can be summarized as follows:

(a) Consider all the types of metal (ferric iron) species which might exist in solution. This involves a consideration of all possible ion-pairs and higher order complex ions and is dependent to some extent on available thermodynamic data. Call a particular species $ML(i)_n$, representing the n^{th} order complex between the metal M and the i^{th} ligand L(i). Let the overall formation constant of this species be $\beta(i)_n$.

(b) Using available thermodynamic data, activity coefficients (where applicable) and free ligand concentrations, rewrite the expression for $\beta(i)_n$ so as to obtain an expression for the concentration of each soluble species in terms of the concentration of the free uncomplexed metal (ferric iron). In general (13),

$$(ML(i)_n) = \beta(i)_n\ (M)\ (L(i))^n\ \frac{\gamma M(\gamma L\ (i))^n}{\gamma ML(i)_n} \qquad \ldots\ (2F)$$

where (M) = uncomplexed metal ion concentration

(L(i)) = free concentration of ligand

$\gamma M, \gamma L(i), \gamma ML(i)_n$ = thermodynamic activity coefficient of the respective species

Note that in the case of hydroxide complex species the expression can be re-arranged to include a (H^+) term, and is thus pH dependent.

(c) Calculate the metal (ferric iron) speciation and solubility as follows:-

The total soluble metal concentration in solution is given by the total of the dissolved species i.e.

$$(M)_{total} = (M) + \sum_n \sum_i (ML(i)_n) \qquad \ldots\ldots \quad (2G)$$

Substituting equation (2F) we have

$$(M)_{total} = (M) \left(1 + \sum_n \sum_i \beta(i)_n\ (L(i))^n\ \frac{\gamma M(\gamma L(i))^n}{\gamma ML(i)_n}\right) \qquad \ldots\ldots \quad (2H)$$

or more simply, allowing for the presence of hydroxide complexes,

$$(M)_{total} = (M)\ (1 + fn\ ((H^+))) \qquad \ldots\ldots \quad (2I)$$

Clearly then, the percentage contribution of any species to the total solubility can be calculated as a function of pH via the expression:

$$\%(ML(i)_n) = \frac{100\ (ML(i)_n)}{(M)_{total}} = \frac{100\ \beta(i)_n\ (L(i))^n\ \gamma M(\gamma L(i))^n/\gamma ML(i)_n}{(\ 1 + fn\ ((H^+)))} \qquad \ldots\ldots \quad (2J)$$

Moreover, if the solubility of the metal M is controlled by the solid species ML_x with solubility product K_{sp}, then:

$$(M) = K_{sp}/\gamma M(\gamma L)^x(L)^x \qquad \ldots\ldots (2K)$$

and the total solubility, as a function of pH, can be calculated by substituting equation (2K) into equation (2H).

The preceding approach was applied by Kester and Byrne (20) to calculate ferric solubility and ferric speciation in sea-water as a function of pH. Consideration of ferric organic complexes indicated that most types of organic compounds cannot compete with hydroxide for iron at the pH of sea-water.

2.4.2 Extension of Previous Calculations

In the present study the work of Kester and Byrne has been repeated and extended along two lines. Firstly, after consideration of a whole range of ferric complex species, Kester and Byrne found that ferric solubility is described almost solely by ferric hydroxide complexes. None of the other ligands present in sea-water can compete effectively with OH^- for iron. The complexes concerned are shown in Table 2 (Nos. 1 to 4), together with relevant equilibria data. Kester and Byrne found that above pH 8 soluble ferric iron is almost totally in the form $Fe(OH)_4^-$, and below pH 7 in the form $Fe(OH)_2^+$. A transition between the two species occurred from pH 7 to 8. However, Kester and Byrne did not consider the uncharged or undissociated molecular complex of ferric hydroxide, $Fe(OH)_3(d)$, a significant form of iron at the pH of sea-water and consequently omitted it in their calculations. This species has been suggested as an interpretation of the discrepancy between calculated solubilities and measured values for iron in sea-water (4). It was decided to include this species in the solubility calculations (No. 5, Table 2) and compare resulting solubility distributions.

Secondly, in the present project an "artificial" sea-water is used in kinetic studies. (Basically a solution of sodium chloride (NaCl) and sodium bicarbonate ($NaHCO_3$)). The composition of this artificial sea-water is outlined in Table 3 and it is discussed in detail in Chapter 3. Ferric solubility calculations were repeated

RELEVANT DATA FOR THE CALCULATION OF FERRIC IRON SOLUBILITY IN SEA-WATER

TABLE 2 - SOLUBLE SPECIES CONTRIBUTING TO FERRIC SOLUBILITY

Species	Reaction	Equilibrium Constant	Temp. (^{o}C)	Medium	Ref.
1. Fe^{3+}	$Fe^{3+} + 3OH^{-} \rightleftharpoons Fe(OH)_3(s)$	$10^{+37.5}$	18	0(Corr)	12
2. $Fe(OH)^{2+}$	$Fe^{3+} + OH^{-} \rightleftharpoons Fe(OH)^{2+}$	$6.8 \times 10^{+11}$	25	0(Corr)	4
3. $Fe(OH)_2^{+}$	$Fe^{3+} + 2OH^{-} \rightleftharpoons Fe(OH)_2^{+}$	$1.7 \times 10^{+21}$	25	0(Corr)	4
4. $Fe(OH)_4^{-}$	$Fe^{3+} + 4OH^{-} \rightleftharpoons Fe(OH)_4^{-}$	$1.3 \times 10^{+34}$	25	3M $NaClO_4$	20
5. $Fe(OH)_3$ (d)	$Fe(OH)_3(s) \rightleftharpoons Fe(OH)_3$ (d)	2.9×10^{-7}	25	0(Corr)	4

TABLE 3 - COMPARISON BETWEEN REAL SEA-WATER AND 'ARTIFICIAL' SEA-WATER

Property	Real Sea-Water (12)	Artificial Sea-Water
(Na^{+})	0.48 moles/l	0.42 moles/l
(Cl^{-})	0.56 moles/l	0.418 moles/l
$(HCO_{3_T}^{-})$	2.4×10^{-3} moles/l	2.4×10^{-3} moles/l
Ionic strength	0.67	0.42

TABLE 4 - ACTIVITY COEFFICIENTS

Species	ACTIVITY COEFFICIENT			
	Real S.W.	Ref.	Artificial S.W.	Ref.
Fe^{3+}	0.1	20	0.06	Calc.
$Fe(OH)^{2+}$	0.34	13	0.285	"
$Fe(OH)_2^{+}$	0.74	13	0.73	"
$Fe(OH)_4^{-}$	0.74	13	0.73	"
$Fe(OH)_3$ (d)	1.0	13	1.0	"
OH^{-}	Obtained directly as measured pH			

for this artificial solution, using activity coefficients calculated from the Davies modification of the Debye-Huckel expression (21). Activity coefficients for species in real sea-water were, in general, taken from Zirino (13). Values are given in Table 4.

2.4.3 Results and Discussion

The results of the solubility calculations are summarised in the solubility diagram, Figure 3. The detailed equations from which the solubility distributions were calculated are given in Appendix 1. It can be seen that the inclusion of the proposed soluble undissociated molecular $Fe(OH)_3(d)$ species makes a considerable difference to the calculated ferric solubility distribution. When included, this species predominates over the ferric hydroxide species over a pH range from 5 to 9, and raises the theoretical ferric iron solubility in sea-water by roughly two orders of magnitude. As expected, the inclusion of $Fe(OH)_3(d)$, using the suggested equilibrium constant (22), results in a theoretical solubility much closer (but still not equal) to the range of experimentally measured sea-water values (Fig. 3). However, until definite proof for such a species is forthcoming its existance must remain theoretical.

If $Fe(OH)_3(d)$ does not truly exist then an explanation is required for the relatively large difference between experimental values for iron solubility and the theoretical solubility of Kester and Byrne (lower curve, Fig. 3). If organic and phosphate complexes can be ruled out (as indicated by Kester and Byrne), then one explanation could be that experimental values do not reflect iron in true solution as measured samples have included particles of fine, stabilized, colloidal ferric hydroxide. Betzer and Pilson (19) define particulate

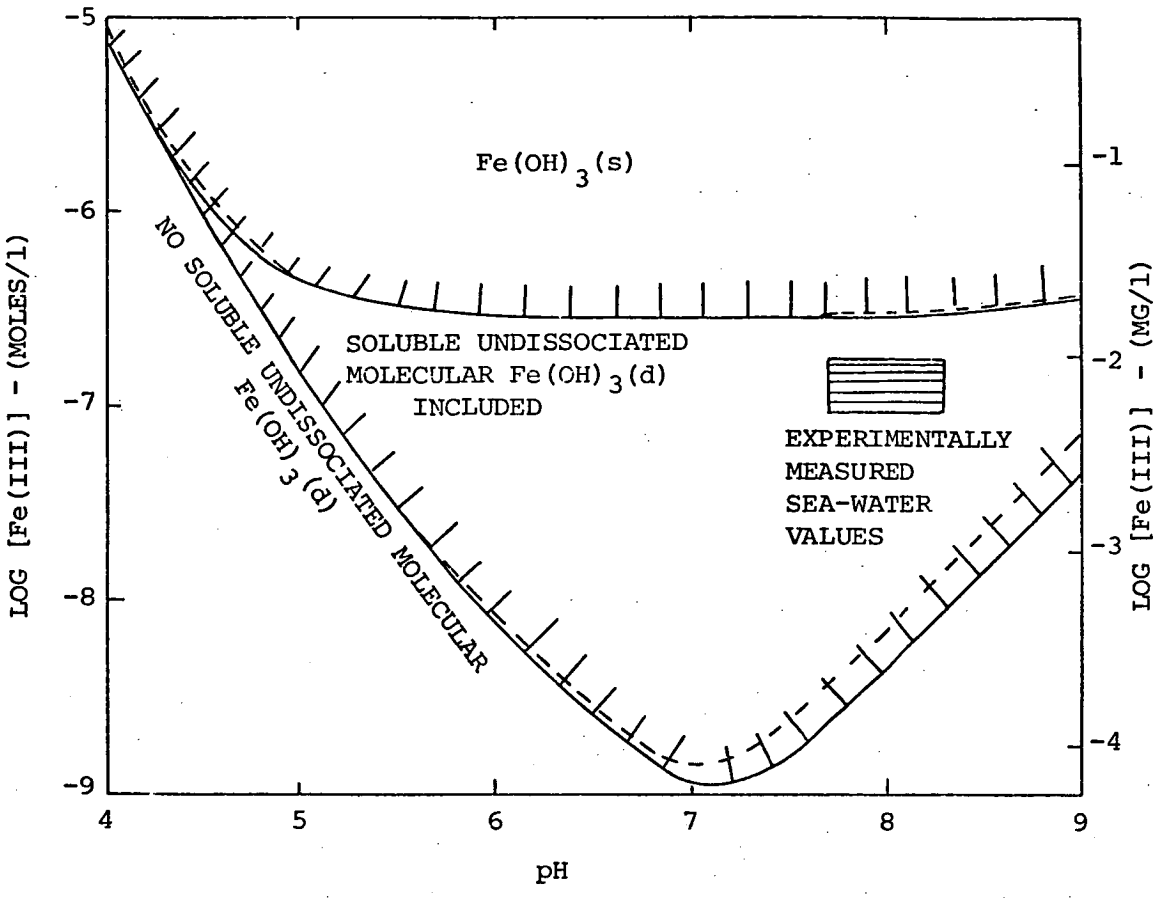

FIGURE 3 - CALCULATED SOLUBILITY OF FERRIC IRON IN SEA-WATER AS A FUNCTION OF pH

TEMPERATURE = 25°C

'REAL' SEA-WATER ———

'ARTIFICIAL' SEA- WATER - - - -

(Rectangular region represents analytically measured pH and iron concentration values (20))

iron as that retained by a 0.45μ filter, so any particular iron smaller in size is regarded as being in solution. A second explanation lies with the possible formation of soluble complexes between silica and iron. Kester and Byrne did not consider ferric silicate complexes as contributing to iron solubility, presumably because of a lack of thermodynamic data. However, Schenk and Weber (23) point out that dissolved silica is a major constituent of most natural waters (the concentration in sea-water is 3 mg/l (12)). They found that silicic acid greatly retards the hydrolysis of ferric iron and suggest that this may be due to soluble complex formation.

Figure 3 also illustrates that, particularly for pH values less than 7, the theoretical ferric iron solubility in the 'artificial' sea-water used in this project is nearly identical to that calculated for real sea-water. This suggests that the artificial solution can serve as a reasonable approximation to sea-water in solubility related experiments.

2.5 FERROUS IRON SOLUBILITY IN SEA-WATER

2.5.1 Introduction

Ferrous iron solubility in natural fresh waters has already been discussed and is illustrated in Figure 2. Although ferrous solubility has been studied in groundwaters, a theoretical study of ferrous iron solubility and speciation in sea-water does not appear to have been made. Such a study is applicable to the situation arising when a reducing environment exists in the sea (e.g. due to the presence of H_2S or anaerobic sediments (12)) or when a solution rich in ferrous iron is introduced into the sea. It is the latter case we are interested in here. A delineation of ferrous solubility is of interest as, given a slow rate of ferrous oxidation, ferrous iron compounds may deposit on the sea-bed. As has been previously mentioned, the situation is analogous to that arising in some groundwater treatment plants (section 2.1).

The question of ferrous solubility arises on a consideration of the formation of marine sedimentary iron ores. The particular mineral obtained when a ferrous-rich leach solution enters the sea depends on the redox potential (Eh) and the acidity (pH) of the environment. In oxygen-rich surface waters limonite ($Fe(OH)_3$) is formed, low pH CO_2-rich waters favour siderite ($FeCO_3$), while in H_2S containing water pyrite (FeS_2) is formed (24). This suggests that in the absence of sulphide species and prior to oxidation the solubility of ferrous iron in bicarbonate-containing sea-water is controlled, as was the case in low ionic strength natural waters, by the solubility of ferrous carbonate.

2.5.2 Method of Calculation

The solubility and speciation of ferrous iron in both real sea-water and 'artificial' sea-water have been calculated using the method of Kester and Byrne (section 2.4.1). The complex ferrous species which were considered as possible contributors to ferrous solubility in sea-water are given in Table 5. No thermodynamic data for possible ferrous complexes with bromine, borate, phosphate and silicate anions could be found, and therefore, if such complexes do exist, their relative contribution to total soluble ferrous iron could not be assessed. It is worth noting that ferric ions generally have a stronger tendency to form complexes than ferrous ions (4), and as Kester and Byrne (20) found that bromide, borate and phosphate complexes contribute negligibly to ferric solubility in sea-water, it is likely these ligands can be safely discarded in a consideration of ferrous solubility. The same argument applies to organic ferrous complexes.

In their calculation of the pH-dependent speciation of divalent Cu, Zn, Cd and Pb ions in sea-water, Zirino and Yamamoto (13) found it necessary only to consider interactions with the anions Cl^-, SO_4^{2-}, HCO_3^-, CO_3^{2-} and OH^-. They also did not include polynuclear and mixed-ligand complexes. The species outlined in Table 5 would therefore seem to represent a reasonable starting point for a consideration of ferrous iron solubility in sea-water.

Relevant equilibria data which best approximate the conditions in sea-water at 25°C and one atmosphere pressure are also given in Table 5. To apply to the sea-water calculations those equilibrium constants with values corrected to zero ionic strength, sea-water activity coefficients were required (for the corresponding species involved). These were determined as before and a list is given in

RELEVANT DATA FOR THE CALCULATION OF FERROUS IRON SOLUBILITY IN SEA-WATER

TABLE 5 - SOLUBLE SPECIES CONTRIBUTING TO CALCULATED FERROUS SOLUBILITY

Species	Reaction	Equilibrium Constant	Temp (^{o}C)	Medium	Ref
Fe^{2+}	A. $Fe^{2+} + 2OH^{-} \rightleftharpoons Fe(OH)_2$ (s)	$6.3 \times 10^{+14}$	25	0 (corr)	12
	B. $Fe^{2+} + CO_3^{2-} \rightleftharpoons FeCO_3$(s)	$4.8 \times 10^{+10}$	25	0	12
$Fe(OH)^{+}$	$Fe^{2+} + OH^{-} \rightleftharpoons Fe(OH)^{+}$	$2.5 \times 10^{+5}$	25	0 (corr)	4
$Fe(OH)_2^{0}$	$Fe^{2+} + 2OH^{-} \rightleftharpoons Fe(OH)_2^{0}$	10^{+9}	Estimated		
$Fe(OH)_3^{-}$	$Fe^{2+} + 3OH^{-} \rightleftharpoons Fe(OH)_3^{-}$	$5.2 \times 10^{+9}$	25	0 (corr)	4
$FeCl^{+}$	$Fe^{2+} + Cl^{-} \rightleftharpoons FeCl^{+}$	2.3	20	2M $HClO_4$	12
$FeCl_2^{0}$	$Fe^{2+} + 2Cl^{-} \rightleftharpoons FeCl_2^{0}$	2.5	20	2M $HClO_4$	12
FeF^{+}	$Fe^{2+} + F^{-} \rightleftharpoons FeF^{+}$	≈ 10	-	-	25
$FeSO_4^{0}$	$Fe^{2+} + SO_4^{2-} \rightleftharpoons FeSO_4^{0}$	10	25	1M $NaClO_4$	25
$FeCO_3^{0}$	$Fe^{2+} + CO_3^{2-} \rightleftharpoons FeCO_3^{0}$	$7.9 \times 10^{+5}$	Estimated		
$Fe(HCO_3)^{+}$	$Fe^{2+} + HCO_3^{-} \rightleftharpoons Fe(HCO_3)^{+}$	$2 \times 10^{+2}$	Estimated		

TABLE 6 - ACTIVITY COEFFICIENTS

Species	Activity Coefficient			
	Real Sea-water	Ref.	Artificial Sea-water	Ref.
Fe^{2+}	0.34	13	0.285	Calc.
$Fe(OH)^{+}$, $Fe(HCO_3)^{+}$	0.74	13	0.73	Calc.
$Fe(OH)_3^{-}$	0.74	13	0.73	Calc.
$Fe\,CO_3^{0}$, $Fe(OH)_2^{0}$	1.0	13	1.0	Calc.
H_2CO_3	1.13	16	1.0	Calc.
HCO_3^{-}	0.68	15	0.73	Calc.
CO_3^{2-}	0.20	15	0.285	Calc.
OH^{-}	Obtained directly as measured pH			

TABLE 7 - LIGAND CONCENTRATIONS IN REAL 35°/oo SALINITY SEA-WATER

Ligand	Total Concentration (moles/l)	Free Concentration (moles/l)	Reference
OH^{-}	As given by measured pH		
Cl^{-}	0.56	0.56	20
SO_4^{2-}	0.029	0.0114	20
F^{-}	0.00007	0.000036	20
$HCO_3^{-}/CO_3^{2-}/H_2CO_3$	0.0027	pH dependent	16

Table 6. The stability (equilibrium) constants for the ferrous carbonate ($FeCO_3^o$) and ferrous bicarbonate ($FeHCO_3^+$) ion-pairs were estimated in the same manner as employed by Zirino (13). The constant for $FeCO_3^o$ was estimated from a correlated dissociation constant v's cation electronegativity graph, and that for $FeHCO_3^+$ via the relationship $\frac{\log \beta\ FeCO_3^o}{\log \beta\ FeHCO_3^+} = 2.5$. A value for the stability constant for the $Fe(OH)_2^o$ species was obtained by comparison with similar data for the Cu, Zn, Cd and Pb cations.

To calculate the degree of ferrous iron complexation in sea-water values for the free ligand concentrations (i.e. that proportion of each ligand not already complexed with the major sea-water cations) are required. These are summarised in Table 7. The free chloride concentration in artificial sea-water was 0.418 moles/l (Table 3). As carbonate species, both soluble and insoluble, are of paramount importance the free bicarbonate ion concentration ($(HCO_3^-{}_F)$) as a function of pH must be known. The free carbonate ion concentration ($(CO_3^{2-}{}_F)$) can then be calculated from the equilibrium relationship (reaction 2B) and so, by rearrangement, the expression for total ferrous solubility (equation 2H) can be written in terms of (H^+) and $(HCO_3^-{}_F)$ (see Appendix 2B).

The variation of $(HCO_3^-{}_F)$ with pH was calculated on the basis that the total inorganic carbon content of sea-water, C_T (equation 2D), remained constant over the pH range of interest. For real sea-water C_T has a typical value of 0.0027 moles/litre (section 2.2) and, as the artificial sea-water prepared had the same bicarbonate ion concentration at the normal pH of around 8 (see Table 3), it was assumed to have the same value for C_T as well. The assumption that

for the problem under consideration C_T remains constant, is based on the fact that the transfer of carbon dioxide across the sea-air interface is very slow (26), while in comparison the dissociation of dissolved carbon dioxide (reactions 2A and 2B) is very rapid (12). On the introduction of an acidic ferrous iron solution to sea-water there is a rapid change of pH with the formation of excess carbonic acid, H_2CO_3 (see section 2.6), but because the oversaturated solution only loses its excess carbon dioxide to the atmosphere at a very slow rate, the immediate effect is that the total inorganic carbon concentration remains the same. Calculations of ferrous solubility should therefore be made on the basis of a constant inorganic carbon content in solution.

In the case of real sea-water, the pH variation of $(HCO_3^-{}_F)$, expressed as a percentage of C_T, has been calculated by Whitfield ((16) and see section 2.2). His figures, applied to a constant C_T of 0.0027 moles/litre, were used to obtain the required bicarbonate distribution for use in calculations. For artificial sea-water the pH variation of $(HCO_3^-{}_F)$ was calculated by a consideration of the various carbonate equilibria involved and the degree of complex formation with sodium ions. The method and calculations are given in Appendix 2A.

After having obtained the pH variation of the free bicarbonate ligand concentration, $(HCO_3^-{}_F)$, in both real and 'artificial' sea-water, ferrous iron solubility was calculated using the method of Kester and Byrne (20) and employing the data given in Tables 5, 6 and 7. Ferrous solubility was assumed to be controlled in the presence of carbonate species by the solubility of ferrous carbonate and in the absence of carbonate species by the solubility of ferrous hydroxide.

2.5.3 Results and Discussion

The calculated pH variation of the carbonate species in artificial sea-water is illustrated in Figure 4. As can be seen, over the pH range 7.5 to 8.5 (normal pH range for sea-water) the bicarbonate ion, HCO_3^-, accounts for the majority of the inorganic carbon in solution and, of the HCO_3^- present, roughly 10% is complexed as an ion-pair with Na^+. The carbonate ion, CO_3^{2-}, has negligible concentration below pH 8. At pH values below 6 the carbonic acid species, H_2CO_3, is predominant.

The distribution can be compared with that of Stumm and Lee, Figure 2A, which was calculated on the basis of constant alkalinity. It can be seen from Figure 4 that for pH values between 4 and 8 alkalinity (equation 2C) is approximately equal to the HCO_3^- concentration, so that by assuming a constant alkalinity of 2×10^{-3} moles/litre Stumm and Lee have used a much higher bicarbonate ion concentration at pH<6.5 than used in the present calculations. This means that their calculated ferrous solubility (Figure 2B) will be much lower in this region. Although the bicarbonate ion is more highly complexed in real sea-water than in the simplified artificial sea-water, particularly due to the presence of the Mg^{2+} and Ca^{2+} cations (12), the general distribution of the carbonate species illustrated in Figure 4 can be taken as indicative of the carbonate distribution in a real sea-water of identical C_T.

The results of the ferrous iron solubility calculations are summarised in the solubility diagram, Figure 5. The detailed equations from which the solubility distributions were determined appear in Appendix 2B. Figures 6A and 6B show the calculated speciation of soluble ferrous iron as a function of pH.

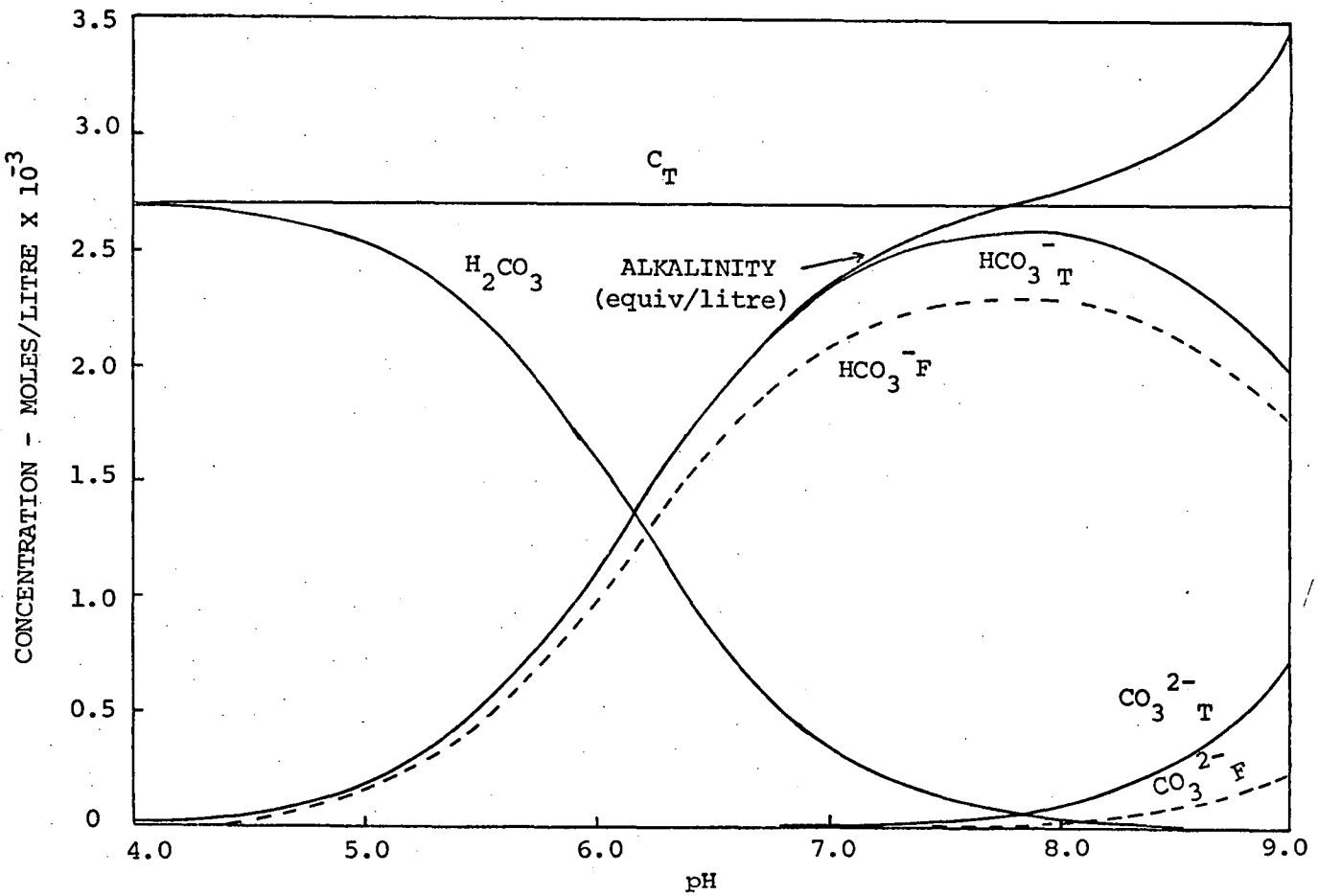

FIGURE 4 - THE pH-DEPENDENT DISTRIBUTION OF THE CARBONATE SYSTEM IN ARTIFICIAL SEA-WATER AT 25°C AND CONSTANT C_T

($C_T = 2.7 \times 10^{-3}$ moles/litre)

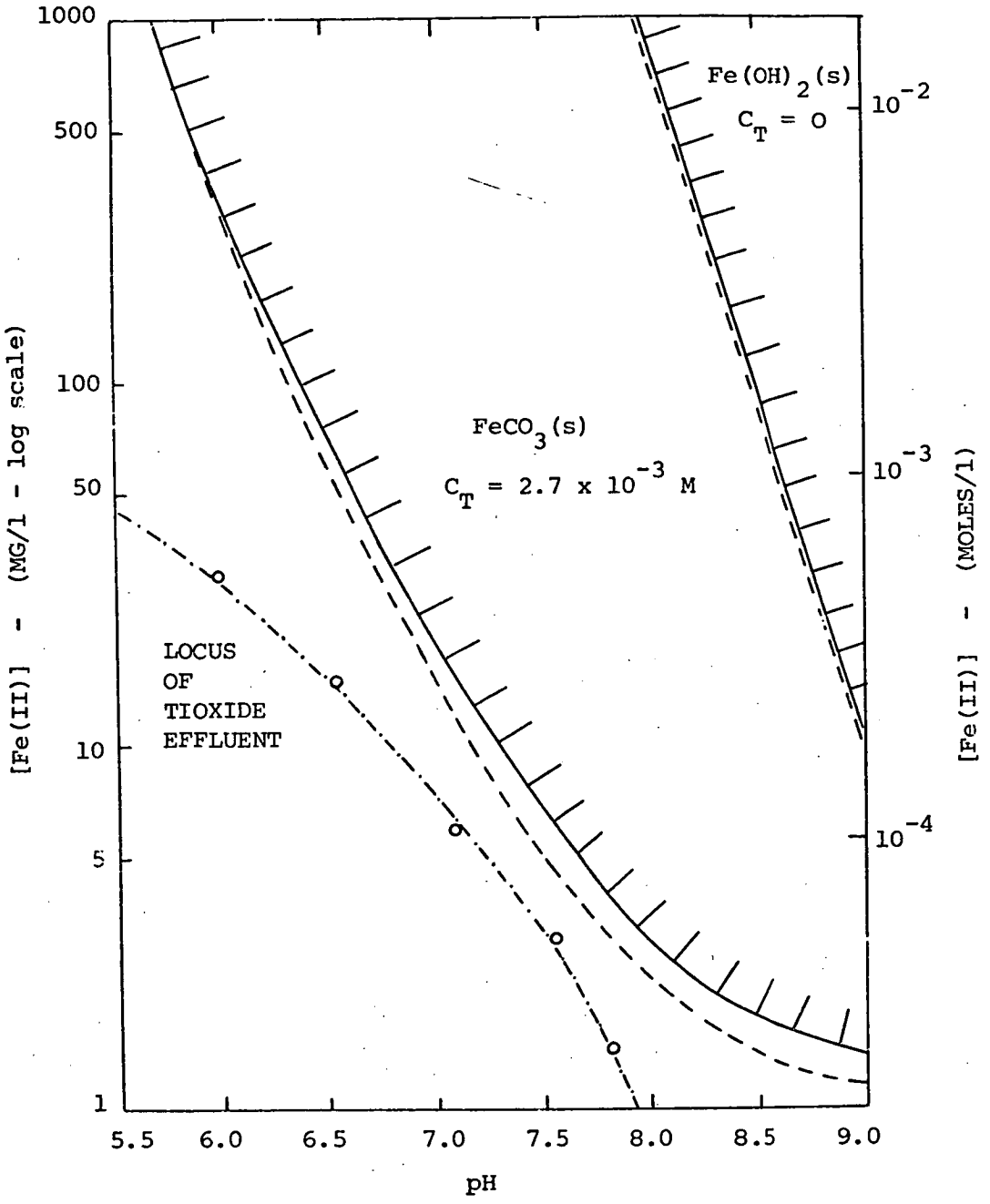

FIGURE 5 - CALCULATED SOLUBILITY OF FERROUS IRON IN SEA-WATER AS A FUNCTION OF pH

TEMPERATURE = 25°C

'REAL' SEA-WATER ———

'ARTIFICIAL' SEA-WATER - - - -

(For explanation of locus see Section 2.3)

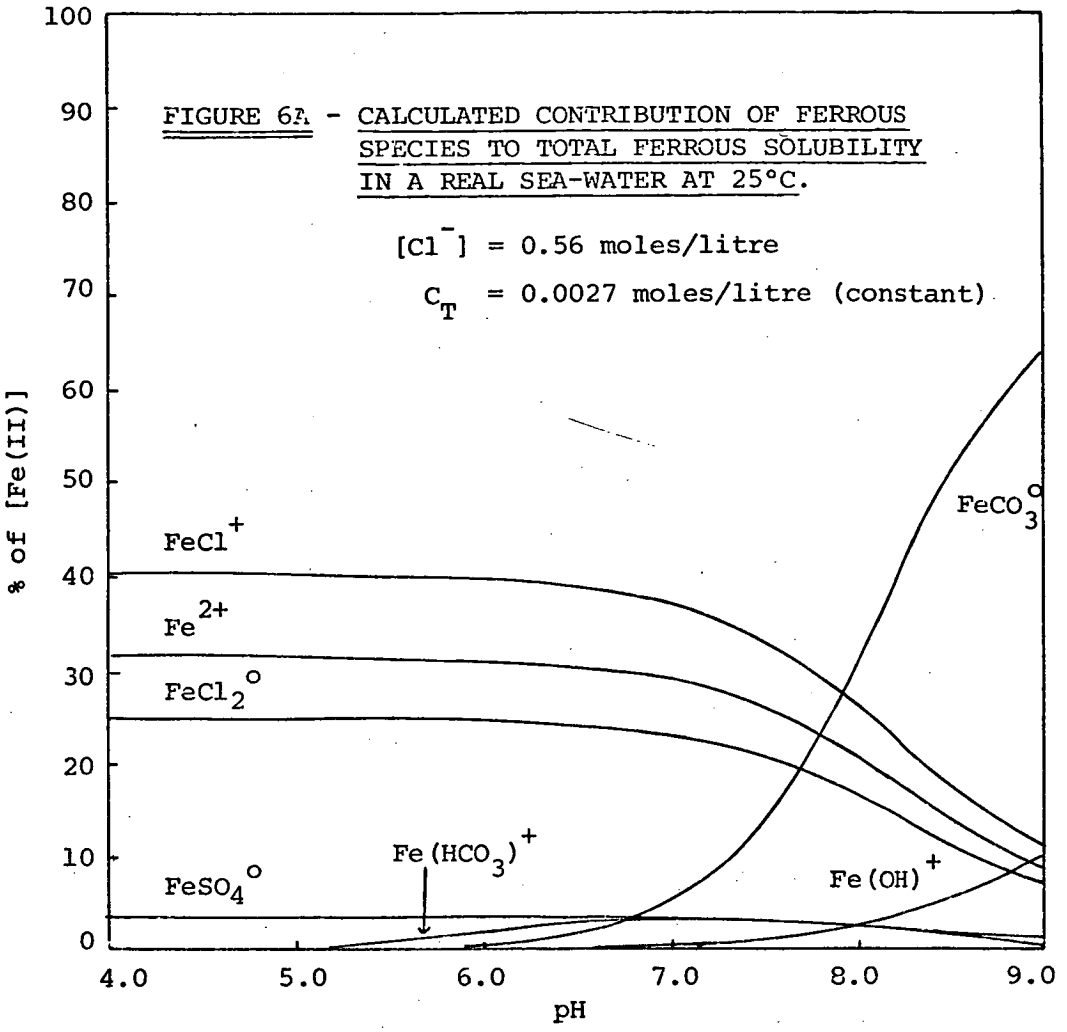

FIGURE 6A - CALCULATED CONTRIBUTION OF FERROUS SPECIES TO TOTAL FERROUS SOLUBILITY IN A REAL SEA-WATER AT 25°C.

$[Cl^-]$ = 0.56 moles/litre

C_T = 0.0027 moles/litre (constant)

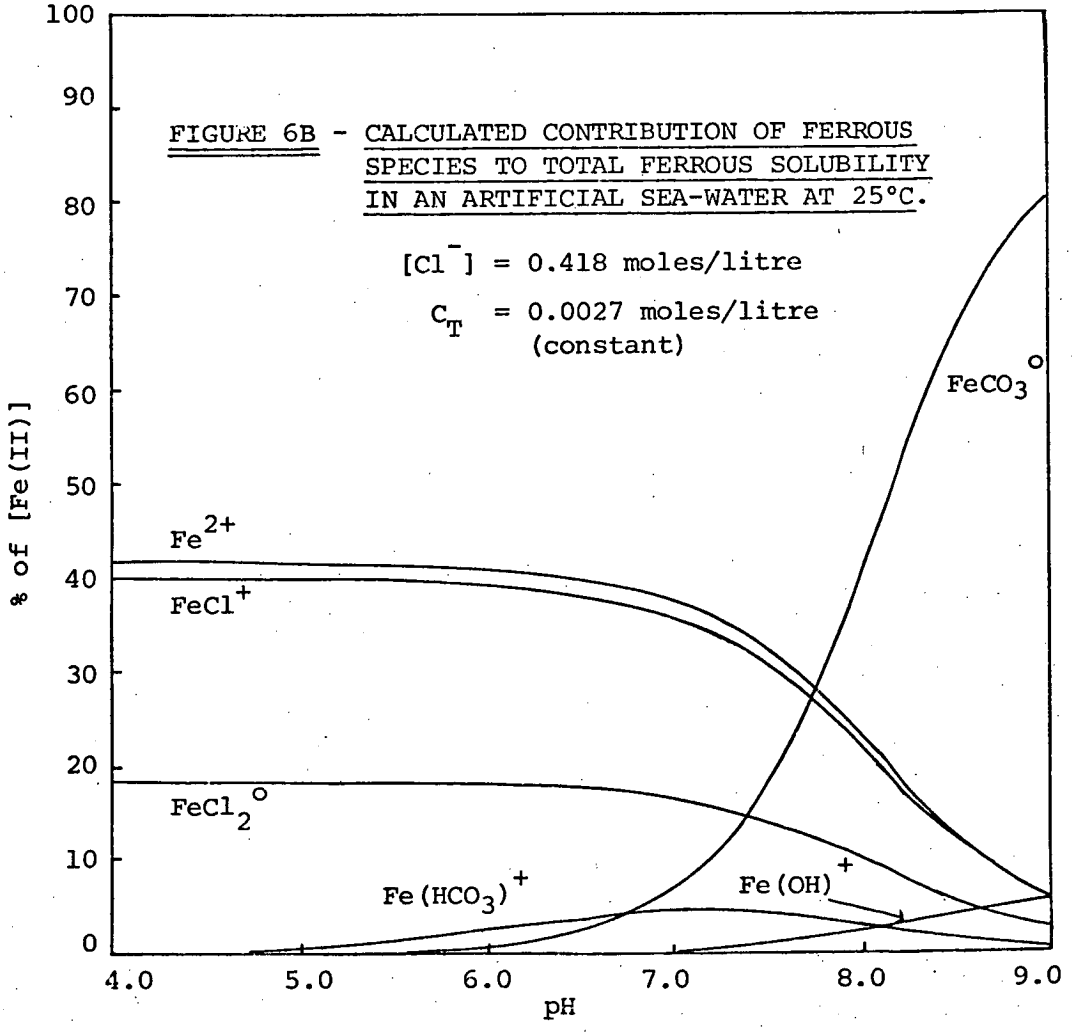

FIGURE 6B - CALCULATED CONTRIBUTION OF FERROUS SPECIES TO TOTAL FERROUS SOLUBILITY IN AN ARTIFICIAL SEA-WATER AT 25°C.

$[Cl^-]$ = 0.418 moles/litre

C_T = 0.0027 moles/litre (constant)

The speciation diagrams indicate that ferrous iron interacts primarily with the carbonate and chloride ions in sea-water. From pH 8 to 9 the majority of ferrous iron in solution is calculated to be in the form of the soluble ferrous carbonate ion-pair, $FeCO_3^o$. At pH values below 7, corresponding to the decrease in the bicarbonate ion concentration (Figure 4), soluble ferrous iron exists predominantly in the form of chloride species, $FeCl^+$ and $FeCl_2^o$, and as free ferrous ion, Fe^{2+}. Between pH 7 and 8 there is a transition between the carbonate ion-pair and the chloride species plus uncomplexed metal. The distribution of species contrasts with the speciation of soluble ferric iron, where it has been shown that soluble ferric hydroxide complexes predominate over the full pH range. It would appear that soluble ferrous hydroxide complexes contribute negligibly to ferrous iron solubility in sea-water over the pH range 4 to 9. Similarly, the sulphate and bicarbonate ion-pairs are of minor importance.

It is interesting to note that Zirino and Yamamoto (13) found that in sea-water lead interacts primarily with carbonate and chloride ions, cadmium with chloride ion, copper with hydroxide and carbonate ions, and zinc with hydroxide and chloride ions. They found that at the average sea-water pH of 8.1 the percentage of uncomplexed metal ion ranged from about 17% for zinc to about 1% for copper. Present calculations indicate that at pH 8.1 roughly 20% of ferrous ions are uncomplexed. Like the other divalent metals ferrous iron is thus complexed to a considerable extent. Although the actual calculated distribution of the soluble ferrous species can vary depending on the thermodynamic data used, the general information obtained as to the types of predominant species and the influence of pH is useful in an

understanding of total ferrous solubility in a sea-water medium.

The solubility diagram, Figure 5, shows that ferrous iron solubility increases dramatically as pH decreases. The increase is even more pronounced in a non-bicarbonate water where solubility is controlled by $Fe(OH)_2(s)$. At a constant pH the concentration difference between ferrous solubility described by $FeCO_3(s)$ and that described by $Fe(OH)_2(s)$ gives the theoretical quantity of Fe^{2+} which can be precipitated in sea-water as ferrous carbonate before the inorganic carbon content of solution is depleted. At pH 8.1 this quantity is calculated to be approximately 535 mg/l. The solubility of ferrous iron at pH 8.1 (average sea-water pH) is calculated to be 2.5 mg/l, though it must be remembered that in normal oxygenated water ferrous iron is unstable (being oxidized to ferric iron) so that this figure is only applicable to a temporary non-equilibrium situation.

The relative solubilities of ferrous iron and ferric iron can be compared by considering Figures 3 and 5. It is clear that the calculated ferrous iron solubility in sea-water is much greater than the calculated (and measured) ferric iron solubility. Consequently, one can expect the oxidation of ferrous iron in sea-water to be followed by the precipitation of a solid form of ferric hydroxide. The calculated ferrous solubility in sea-water is also greater than Stumm and Lee's (4) calculated ferrous solubility in a bicarbonate-containing natural fresh water (Figure 2B). As has been explained this is due, in part, to those authors' assumption of constant alkalinity, but it would appear that ferrous solubility in sea-water, particularly at pH<7, is also increased due to the high chloride concentration of the medium and the ability of ferrous iron to form soluble ferrous chloride complexes.

In the calculations undertaken possible ferrous-silicate complexes could not be assessed because of a lack of thermodynamic data. Similarly, the possibility of ferrous solubility in sea-water being controlled by that of ferrous silicate, $FeSiO_3(s)$, could not be adequately investigated. However Schenk and Weber (23), in an investigation of ferrous oxidation, found no precipitation occurred at a (Fe^{2+}) (H_4SiO_4) product greater than that encountered in a sea-water where Fe^{2+} is controlled by $FeCO_3(s)$ (assuming (H_4SiO_4) = 3mg/l (12)). We can thus infer that ferrous solubility is controlled by $FeCO_3(s)$ rather than by $FeSiO_3(s)$.

Finally, Figures 5 and 6 illustrate that, as was the case with ferric solubility, the artificial sea-water used in this project gives ferrous solubility predictions similar to those calculated for real sea-water. Both the ferrous speciation and the total ferrous solubility distributions of the two are alike. The simplified medium (Table 3) would thus seem to provide a good approximation to real sea-water for use in laboratory experiments related to iron solubility. The relatively small difference in $FeCO_3(s)$-determined solubilities is due to the higher Cl^- concentration in real sea-water, the higher degree of complexation of HCO_3^- (and thus smaller $(HCO_3^-{}_F)$) and the presence of SO_4^{2-} ions. This results in the calculated ferrous solubility in real sea-water being slightly higher than that calculated for the artificial sea-water.

2.6 INTERACTION OF INDUSTRIAL EFFLUENT WITH SEA-WATER

2.6.1 Introduction

The calculated ferrous solubility diagram, Figure 5, indicates that if ferrous carbonate is to precipitate on the introduction of an acidic ferrous sulphate effluent to sea-water then, keeping in mind the rate of ferrous oxidation, the effluent should have as low an acid to ferrous iron ratio as possible. The greater the depression of the normal sea-water pH, the greater the estimated ferrous solubility and so the less chance of ferrous precipitation. Any soluble ferrous iron will eventually be oxidized and the resulting ferric iron will precipitate as ferric hydroxide.

The possible advantage of $FeCO_3$ precipitation as opposed to $Fe(OH)_3$ precipitation is the suggestion by Twardowski ((9) and see section 2.1) that the former precipitates as large, separate, crystalline particles which are then, under water, relatively stable to subsequent oxidation. A precipitate of $FeCO_3$, if formed in sea-water, might thus be expected to settle to the sea-bed in contrast to the loose, poorly crystalline, floating flocks of $Fe(OH)_3$ which are observed to form on ferrous oxidation and which cause titanium dioxide producers the visual and other pollution problems outlined in Chapter 1. Clearly, whether or not $FeCO_3$ does precipitate in sea-water following the discharge of an industrial acid-iron waste depends on several factors, primarily the composition of the effluent, the rate of dilution by sea-water and the rate of ferrous oxidation.

The interaction of an acidic ferrous sulphate solution with sea-water can be considered to consist of two separate stages. Firstly, there is the rapid reaction between the sulphuric acid in the

solution with the bicarbonate buffer of sea-water. Secondly, there is the subsequent oxidation of the introduced ferrous iron (and consequent precipitation of $Fe(OH)_3$) at the pH resulting from the first reaction. If this pH is sufficiently high then ferrous precipitation may occur at the same time. Of course, in reality the picture is much complicated by the continued dilution and dispersion of the effluent with what can be regarded as "new fresh sea-water", so that the pH is continually rising back to normal and the ferrous concentration is continually decreasing. By necessity laboratory experiments are best carried out at a static, constant, dilution ratio. This simplifies the situation and allows a more detailed investigation of the processes taking place to be made. Such an approach is not unrealistic, as by undertaking work at various set dilution ratios it is possible to span at least part of the range of conditions encountered in the real situation. In this way the interaction of industrial effluent with sea-water can be thought of as "frozen" for study at different stages of dilution.

2.6.2 Dilution Experiments

As a preliminary investigation of the interaction reaction a series of dilution experiments were carried out using samples of realfiltered sea-water and a sample of an industrial titanium dioxide effluent. The sea-water, filtered through a 3μ millipore filter, was obtained via the marine research laboratory of the Tasmanian Fisheries Department. The industrial effluent was obtained from the Burnie plant of Tioxide Australia Pty. Ltd. and for the purposes of this report this effluent is classified as "Tioxide effluent".

Although it is known that the rate of ferrous oxidation is very

slow in highly acidic solutions (4), the Tioxide effluent was also stored in an air-tight plastic container prior to use to exclude oxygen. The degree of ferrous oxidation occurring between the time when the effluent was sampled and its use in the laboratory was thus kept to a minimum. The composition of the effluent is given in Table 8. The ferrous iron content was experimentally determined by titration with potassium permanganate solution, it being assumed that ferrous iron constituted the main oxidizable component of the effluent. Any minor component oxidizable by permanganate at low pH was assumed to be negligible in comparison.

The acidity of the effluent was estimated by means of pH-monitored titrations with a weak sodium hydroxide solution. Although at pH values above 5 the titration is disturbed by the precipitation of iron compounds, it was still possible to identify the inflection in the titration curve and thus estimate the equivalent volume of hydroxide required for neutralization. A consideration of the soluble ferrous species in the effluent indicated that $(Fe^{2+}) >> (Fe(OH)^{+})$ below pH 5 (4), so that none of the introduced hydroxide up to this point could be expected to be consumed by the soluble iron present. The estimated effluent acidity was checked by using the obtained value to calculate the expected pH values on the lower half of the titration curve and comparing with the measured experimental values. This involved a consideration of the sulphuric acid ionisation steps and a good agreement was obtained, indicating that the value given in Table 8 is reasonably correct.

TABLE 8 - COMPOSITION OF TIOXIDE EFFLUENT

(Sample A - Collected 2/10/75)

Component	Nominal Concentration (27)	Measured Concentration
Sulphuric Acid	74 gms/l	64 ± 2.5 gms/l
Acidity, H^+	1.5 moles/l	1.3 ± 0.05 moles/l
Ferrous Iron	30 gms/l	28.2 ± 0.3 gms/l (prior to use)

The dilution experiments were carried out by pipetting the required volume of Tioxide effluent into a stirred sample of freshly aerated sea-water. After one hour's stirring the pH was measured and the solution was then left to stand open to the air. Subsequent pH measurements were made every 24 hours. Room temperature was controlled at around 25°C and a negligible amount of sample evaporation was observed over the period of the experiment. On aeration the sea-water sample had a measured pH of 8.08 ± 0.02, well within the pH range observed, in-situ, in the ocean (12). Results are discussed in Section 2.6.4.

2.6.3 Prediction of Solution pH

The pH resulting on the introduction of a sulphuric acid solution to a bicarbonate-buffered natural water can be estimated by assuming that the buffering depends predominantly on the bicarbonate-carbonic acid equilibrium (equation 2A) i.e.

$$H_2CO_3 \rightleftharpoons H^+ + HCO_3^- \quad ; \quad K_{25^oC} = 4.45 \times 10^{-7} \text{ moles/litre}$$

This is a reasonable assumption as, as has already been shown (Figure 4),

these two carbonate species account for practically all the inorganic carbon content of solution below pH 8. The concentration of the carbonate ion, CO_3^{2-}, is negligible below pH8 and thus the influence of the second dissociation equilibrium (equation 2B) can be ignored as a first approximation. From the above reaction it can be seen that the addition of a quantity of acid to a buffered solution will cause an equivalent amount of bicarbonate ion to be converted to carbonic acid. Noting that at constant C_T, (HCO_{3T}^-) is basically equivalent to the solution alkalinity, (Alk) (see Figure 4), it can be derived that (28):

$$(H^+)_{End} = K \left(\frac{(H^+)_{Init} \times (Alk) \times K^{-1} + (H^+)_{Add}}{(Alk) - (H^+)_{Add}} \right) \quad \ldots . (2M)$$

Where $(H^+)_{Add}$ = quantity of acid added to solution

(Alk) ($\simeq (HCO_{3T}^-)$) = solution alkalinity

$(H^+)_{Init}$ = initial pH of solution

$(H^+)_{End}$ = final pH of solution

K = carbonic acid - bicarbonate dissociation constant

This equation is only valid when $(H^+)_{Add} < (Alk)$. If the amount of acid added exceeds the natural bicarbonate content of the solution then the resultant pH can be assumed to be determined by the amount of excess acid present. In the case of sulphuric acid the final pH is calculated by considering the dissociation steps:

$$H_2SO_4 \longrightarrow H^+ + HSO_4^- \; ; \text{ (complete)} \quad \ldots . \quad (2N)$$

$$HSO_4^- \rightleftharpoons H^+ + SO_4^{2-} \; ; \; K_a = 1.2 \times 10^{-2} \ldots . \quad (2O)$$

The preceding approach was applied to the real sea-water/Tioxide effluent dilution experiments carried out to estimate the pH values

resulting on interaction at different dilution factors (and prior to any decrease due to ferrous oxidation). The effluent acidity was assumed to be 1.3 moles/l as H_2SO_4 (Table 8). The alkalinity of the sea-water sample was found by titrating a freshly aerated sample with hydrochloric acid to the methyl-orange end-point (28). The obtained value of 2.33×10^{-3} moles/l was in excellent agreement with values recorded in the literature (12, 13). Equilibrium constants were modified for use in sea-water by the use of the activity coefficients of Zirino (13) and Whitfield (16). Examples of the calculations made are given in Appendix 3.

2.6.4 Results and Discussion

The results of the dilution experiments for dilution factors ranging from 1:50 to 1:50,000 are given in Table 9, together with the respective pH values calculated on the basis of the sulphuric acid-bicarbonate ion reaction. Because of the high acidity of the Tioxide effluent it can be seen that a dilution of at least 1:1000 is required to maintain solution pH above a value of 6.

TABLE 9 - pH CHANGES IN SOLUTION ON THE ADDITION OF TIOXIDE EFFLUENT TO REAL SEA-WATER AT DIFFERENT DILUTION FACTORS (Initial pH = 8.08 , Temperature = 25°C)

Dilution Factor	Approx. Initial Fe^{2+} Conc. (mg/l)	Calculated End pH	Measured pH (± 0.02)		
			After 1 hr	After 24 hrs	After 48 hrs
1:50	565	1.71	1.88	1.87	1.86
1:100	280	2.02	2.16	2.14	2.14
1:500	56	3.57	3.51	3.50	3.48
1:1000	28	6.02	5.97	6.02	5.77
1:2000	14	6.52	6.51	6.71	7.39
1:5000	5.6	6.99	7.07	7.69	7.87
1:10,000	2.8	7.28	7.55	7.82	7.93
1:20,000	1.4	7.53	7.82	7.92	8.02
1:50,000	0.6	7.78	8.06	8.06	8.07

As well as following the pH changes in solution, any solid products formed in the dilution experiments were naturally of interest. A very small amount of white precipitate was produced at dilutions of 1:100 and 1:500, although the corresponding pH values were too low to suggest iron precipitation. The precipitate was presumably calcium sulphate, formed because of the increased sulphate ion concentration in solution and the low Ksp of this salt. The quantity of precipitate was too small to analyse. At dilutions ranging from 1:1000 to 1:20,000 an orange precipitate was observed to form, the amount greatly decreasing in quantity as the dilution factor increased. This precipitate, clearly a form of ferric hydroxide, was extremely fine but gradually

settled on standing. Where the amount of precipitate formed was sufficient, it was collected by filtration, washed, dried and then analysed as outlined in Chapter 4. Over the dilution ratios investigated there was no precipitate formed which could be identified as ferrous carbonate.

Values from Table 9 corresponding to the measured pH after one hour and the accompanying initial ferrous iron concentration have been superimposed on the ferrous solubility diagram, Figure 5, and joined to give a "locus of Tioxide effluent". Oxidation of ferrous iron in solution is usually accompanied by a decrease in pH due to the hydrolysis of the ferric iron produced. This is represented by the reaction:

$$4\ Fe^{2+} + 10\ H_2O + O_2 \longrightarrow 4\ Fe(OH)_3\ (s) + 8\ H^+ \ldots\ (2L)$$

However, because the sea-water oxidation of the ferrous iron in Tioxide effluent is a slow process, as will be shown in Chapter 3, and because, in addition, the ferrous concentrations superimposed on Figure 5 are small (<50 mg/l), the respective pH values measured one hour after adding the effluent are not far removed from those resulting immediately after the two solutions have been mixed. This is also borne out by a comparison of the measured pH's with values calculated solely on the basis of the acid-buffer interaction (see Table 9 and below). It is this rapid reaction which predominantly determines the solution pH.

The locus on Figure 5 can thus be taken as representing the ferrous concentration/pH range spanned immediately after Tioxide effluent is introduced into a real sea-water. As can be seen, at no stage does the locus intercept the calculated region in which ferrous carbonate precipitation could be expected. These results thus indicate that with an effluent of composition as given in

Table 8, there is little if no possibility of ferrous carbonate precipitating in sea-water. The immediate results refer to a sea-water temperature of 25°C, but a consideration of Figure 5 shows that even at the point of closest approach the solubility of $FeCO_3$ would have to be decreased by at least a factor of two for precipitation of $FeCO_3$ to be likely. The drop in temperature required for such a factor to be achieved is likely to be at least 20°C, so that the conclusions drawn seem valid for the normal temperature range spanned in coastal waters.

As mentioned, Table 9 compares calculated pH values with experimentally measured values. It can be seen that the calculated pH's are in very good agreement with pH values measured one hour after effluent addition, particularly at dilution factors under 1:5000. This indicates two things: firstly, that the rapid initial interaction between Tioxide effluent and alkaline sea-water, due to the contained sulphuric acid reacting with the natural ocean carbonate buffer, has been successfully modelled; and secondly, that pH changes in solution due to ferrous oxidation are minimal within the first hour after interaction. The difference between the measured and calculated pH values (< 0.3 pH unit) at high experimental dilution factors can be partially attributed to the higher experimental error involved in obtaining these high dilutions and also to the fact that at the higher pH values there is more likelihood of the CO_3^{2-} ion taking part in the buffering mechanism. Also, where moderate additions of acid have been made the influence of other species in the buffering of sea-water cannot be discarded. Both the silicate system and general ion-pair formation are known to contribute to the buffering of sea-water (12,16).

Finally, looking at Table 9 it can be seen that at dilutions lower than 1:1000, where the sea-water buffer has been destroyed, the final pH remains constant with time. These low pH values have also been observed to quench the ferrous oxidation reaction. However, at dilutions of 1:2000 and above, where the bicarbonate buffer has not been destroyed, there is a gradual return of solution pH to normal. The solution slowly loses carbon dioxide to re-establish equilibrium with the atmosphere and the pH consequently rises as the bicarbonate buffer is restored. Clearly the transfer of CO_2 between solution and atmosphere occurs at a very slow rate compared to the rate of the effluent - sea-water interaction.

2.7 REFERENCES

(1) Jobin R. & Ghosh M.M. - Jour. A.W.W.A., 64(9), 590 (1972).

(2) Ghosh M.M. - Jour. A.W.W.A., 65(5), 348 (1973).

(3) Cleasby J.L. - Jour. A.W.W.A., 67(3), 147 (1975).

(4) Stumm W. & Lee G.F. - "The Chemistry of Aqueous Iron" - Schweiz. Zeitsch. Fur. Hydrol., 22, 295 (1960).

(5) Feitknecht W. - Z. Elektroch., 63, 34 (1959).

(6) Ghosh M.M. - Aqueous Environ. Chem. Met. 1974, p 193-217, Ann Arbor Science, Michigan (Rubin A.J. ed).

(7) Hem D.J. - U.S. Geol. Survey, Water Supply Papers, 1473, (1959).

(8) Stumm W. - Jour. A.W.W.A., 53(2), 228 (1961).

(9) Olson L.L. & Twardowski C.J. Jr. - Jour. A.W.W.A., 67(3), 150 (1975).

(10) Plumb R.H. Jr. & Lee G.F. - Water Res., 7(4), 581 (1973).

(11) Hutchinson G.E. - "A Treatise on Limnology", Vol. 1 (J. Wiley & Sons, N.Y. 1957).

(12) Horne R.A. - "Marine Chemistry" - (J. Wiley & Sons, 1969).

(13) Zirino A. & Yamamoto S. - Limnol. Oceanog., 17(5), 661 (1972).

(14) Coyne L. - J. Chem. Educ., 52(12), 796 (1975).

(15) Garrels R.M. & Thompson M.E. - "A chemical model for sea-water at 25^{o}C and 1 atmosphere total pressure" - Amer. J. Sci., 260, 57 (1962).

(16) Whitfield M. - Limnol. Oceanog., 19(2), 235 (1974).

(17) Cooper L.H.N. - Jour. Marine Biol. Assoc. U.K., 27, 279 (1948).

(18) Head P.C. - Jour. Marine Biol. Assoc. U.K., 51, 891 (1971).

(19) Betzer P.R. & Pilson M.E.Q. - J. Mar. Res., 28(2), 251 (1970).

(20) Kester D.R. & Byrne R.H. Jr - "Chemical Forms of Iron in Sea Water". Taken from collection of papers from a conference "Ferromanganese Deposits on the Ocean Floor" held at Arden House, Harriman, New York and Lamont-Doherty Geological Observatory, Columbia University, Palisades, New York, Jan 20-22, 1972, p107-116.

(21) Davies C.W. - "Ion Association" - (Butterworths, 1962).

(22) Gayer K.H. & Woontner L. - J. Phys. Chem., 60, 1569 (1956).

(23) Schenk J.E. & Weber W.J. Jr. - Jour. A.W.W.A., 60(2), 199 (1968).

(24) Borchert H. - "Formation of Marine Sedimentary Iron Ores", in J.P. Riley & G. Skirrow, eds., "Chemical Oceanography", Vol. 2, Chap. 18 (Academic Press, London, 1965).

(25) Sillen L.G. & Martell A.E. - "Stability Constants of Metal - Ion Complexes" , Chem. Soc. London, Spec. Publication No. 17 (1964).

(26) Harvey H.W. - "Biological Chemistry and Physics of Sea-Water" (Cambridge University Press, 1928).

(27) Personal Communication.

(28) Huhn W. - Fortschr. Wasserchem. Ihrer Grenzgeb., No.13, 147 (1971).

CHAPTER 3

KINETICS OF FERROUS IRON OXIDATION

The ferrous iron concentration/pH range spanned when a typical industrial acidic ferrous sulphate effluent is discharged to the sea has now been delineated. Soluble ferrous iron will eventually be oxidised and will precipitate as a form of ferric hydroxide. A detailed understanding of the precipitation process taking place in sea-water requires that the kinetics of the oxidation of the introduced ferrous iron be known. Prior to formulating an experimental programme aimed at investigating the oxidation kinetics it was necessary to review previous work undertaken on ferrous iron oxidation, particularly that involving aerated acidic liquors and bicarbonate-containing waters.

3.1 OXIDATION OF FERROUS IRON IN ACIDIC LIQUORS

The majority of proposed treatment methods for acidic ferrous liquors rely on the conversion of ferrous iron to ferric iron and the subsequent precipitation of ferric compounds. Because the oxidation of ferrous iron has been found to be the rate-controlling step in many processes the kinetics of the oxidation stage has been the subject of much investigation. A high rate of oxidation of ferrous iron is required in order to limit the size of treatment equipment and the consequent capital costs.

The amount of literature concerning the oxidation of ferrous iron by molecular oxygen in aqueous acidic solutions is vast and it is not possible, nor relevant, to cover it at depth here. Among the more recent reviews appearing on the subject have been those by Tamura (1) and by Klinghoffer (2). Much of the existing literature is in the form of registered patents. Generally speaking, it has been found that an increase in temperature causes an increase in the rate of Fe^{2+} oxidation in aerated acids, and the rate increases with decreasing pH in HCl but decreases with decreasing pH in H_2SO_4. The presence of copper ions in solution accelerates the oxidation. Among the different proposed mechanistic schemes describing ferrous oxidation Weiss' radical-chain scheme is the most widely accepted (3).

Concerning the oxidation of ferrous sulphate in sulphuric acid solution by air there is broad agreement on the important factors in the kinetic expression, namely ferrous concentration, pH, temperature and the effect of cupric ions. The rate expression:

$$\frac{d\,(Fe^{3+})}{dt} = k(Fe^{2+})^2\,(O_2) \qquad \ldots\ldots\ (3A)$$

where k decreases with decreasing pH, was first proposed by Pound in 1939 (4), has been verified by George over the temperature range 25-40^{o}C (5), by Cornelius and Woodcock (6), and is incorporated in many proposed equations (7). The depressing effect of H_2SO_4, increasing with concentration and temperature, has been remarked upon by several workers and is believed to be due to the suppression of ferric hydrolysis (8).

There is disagreement in the literature as to whether the rate equation is of second order with regard to ferrous iron concentration under all conditions. Huffman and Davidson (9) propose that at 30.5°C:

$$\frac{d(Fe^{3+})}{dt} = k(Fe^{2+})(O_2) \quad \ldots\ldots (3B)$$

and Hine and Yasuda (10), investigating ferrous oxidation by dissolved oxygen in electrolyte solutions, also found that the rate exhibited a first-order dependence on ferrous iron concentration with the rate constant,k,greatly dependent on pH. Saprygin and Gusar (11) have recently found that the kinetics of $FeSO_4$ oxidation by molecular oxygen in H_2SO_4 solutions exhibits a complex dependence on $FeSO_4$ concentration. At less than 50 mg/l Fe^{2+} the rate was found to be proportional to (Fe^{2+}) (equation 3B) but at greater than 100 mg/l Fe^{2+} the rate was proportional to $(Fe^{2+})^2$ (equation 3A).

Many substances are known to catalyse the oxidation of ferrous sulphate solutions. Apart from copper, phosphoric acid, amino acids, activated carbon and silicic acid have all been found to accelerate the formation of Fe^{3+}. Huffman and Davidson (9) state that the rate of oxidation is dependent upon the anion present and increases as the complexing affinity of the anion to ferric ion increases. The use of biological oxidation to improve the oxidation rate is a new field of much interest. Lacey (12) has reported a 500,000 fold increase in oxidation rate by the use of the bacterium Thiobacillus ferro-oxidans.

Although the studies of ferrous oxidation in acid solution yield valuable clues as to the mechanism of the reaction and the rate-determining species,it should be noted that the kinetic express-

ions found need not necessarily apply directly to bicarbonate-containing waters such as sea-water.

3.2 OXIDATION OF FERROUS IRON IN NATURAL WATERS

Because of its importance in the deferrization of natural drinking waters, the kinetics of ferrous iron oxidation in low ionic strength bicarbonate waters has received a deal of attention. A very early study of iron oxidation in the carbonic acid-bicarbonate buffer system of natural waters was made by Just in 1908 (13). The first comprehensive study of ferrous oxidation in natural waters was made by Stumm and Lee in 1961 (14). They found that in bicarbonate solutions the rate of oxygenation of ferrous iron follows the law:

$$-\frac{d\,(Fe^{2+})}{dt} = k(Fe^{2+})\,(O_2)\,(OH^-)^2 \quad \ldots\ldots \quad (3C)$$

where k values tend to be smaller in solutions of lower alkalinity. The corresponding stoichiometric relationship describing the oxidation of ferrous iron to ferric iron and the subsequent hydrolysis of the latter is (15):

$$4\,Fe^{2+} + 10\,H_2O + O_2 \rightleftharpoons 4\,Fe(OH)_3 + 8H^+ \quad \ldots\ldots \quad (3D)$$

Stumm and Lee determined the oxidation kinetics by carrying out a series of experiments at constant pH and with constant partial pressure of oxygen in solution. This was achieved by bubbling a predetermined mixture of CO_2 and air through the test solution for the duration of each run. The concentration of ferrous iron remaining at a given time was determined photometrically by analysing aliquots taken from the reaction vessel. Runs were carried out in the pH range 6.0 to 7.5 and alkalinity was varied from 9×10^{-3} to 3.9×10^{-2} equivalents

per litre. The bicarbonate -CO_2 buffers were prepared by bubbling CO_2-air mixtures through dilute (<4 x 10^{-2}M) Na_2CO_3 solutions. All experiments were conducted with dissolved ferrous iron concentrations of less than 5 x 10^{-5}M (<3 mg/l) so that "no precipitation of ferrous carbonate was encountered even though the conditions of the experimental runs that were made above pH 7 were such that the solubility product for $FeCO_3$ was occasionally exceeded."

As well as establishing the rate expression for ferrous oxidation, Stumm and Lee investigated the effect on the reaction of different chemical species. They found that "catalysts (especially Cu^{2+}) in trace quantities, as well as anions which form complexes with ferric iron (e.g. $H_2PO_4^-$), increase the reaction rate significantly, while small amounts of Fe(III), Cl^-, SO_4^{2-} have no effect on the reaction rate".

The kinetic equation of Stumm and Lee has been verified in subsequent work by Schenk and Weber (16) and by Jobin and Ghosh (17). Both sets of workers carried out oxidation experiments along the experimental guidelines set by Stumm and Lee, using prepared bicarbonate buffer systems of low ionic strength to simulate conditions in natural ground waters. Some of the results of Schenk and Weber are summarized in Figure 7. As expected from the kinetic expression (3C), it can be seen that the rate of ferrous oxidation is greatly dependent on the pH of solution. Below pH 6 the reaction is effectively quenched.

Jobin and Ghosh studied the effect of buffer intensity and organic matter on the oxygenation of ferrous iron in ground waters at pH 6.8. Recent work by Ghosh (15) has extended this study over a pH range from 5.5 to 7.2. It was found that the buffer capacity of a water at values higher than 4.0 x 10^{-3} equiv/l has a definite influence on the oxidation of Fe(II) in HCO_3^- solutions. However, below this

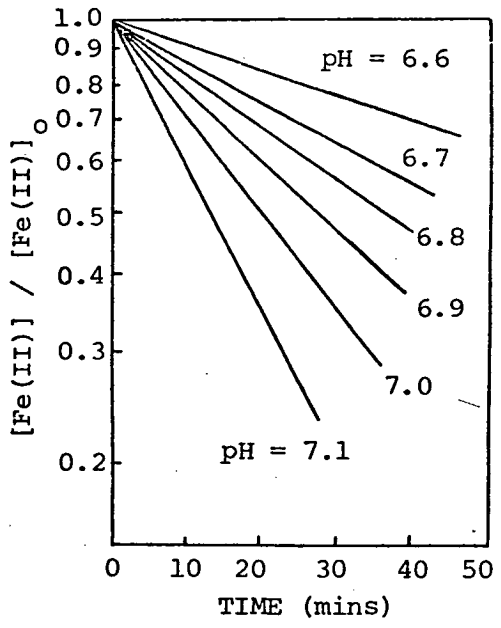

$$-\frac{d[Fe(II)]}{dt} = k[Fe(II)].P_{O_2}.[OH^-]^2$$

TEMPERATURE = 25°C

P_{O_2} = 0.2095 atmospheres

ALKALINITY = 30-50 x 10^{-3} equiv/l

$[Fe(II)]_o$ < 3 mg/l

FIGURE 7 - RATE OF OXIDATION OF FERROUS IRON IN A BICARBONATE WATER (Schenk & Weber (16))

value the kinetics conform to the rate equation of Stumm and Lee, with the overall rate constant, k, being basically invariant. The apparent lack of dependence of the oxygenation rate on the buffer capacity at values below 4.0 x 10^{-3} equiv/l has been attributed to "the slow response of the bicarbonate buffer system to localized acidity changes induced by the oxygenation reaction" (14). The parameter, buffer capacity, is related to the pH and alkalinity of a natural water. Whitfield (18) shows that in the pH range 4 to 10 sea-water has a buffer capacity of less than 6.0 x 10^{-4} equiv/l.

Other researchers have found kinetic expressions in accordance with that of Stumm and Lee. Van Suc (19) investigated the time required for Fe^{2+} removal from natural water by $Fe(OH)_3$ precipitation. For normal cases, with (Fe^{2+}) < 10 mg/l, excess (O_2), and pH 6.5 - 8.5 with bicarbonate buffering, his equations simplified to:

$$-\frac{d(Fe(II))}{dt} = K(Fe(II))$$

where K varied with pH and temperature. Stumm and Lee found that the temperature dependence of the ferrous oxidation reaction in bicarbonate waters was substantial. For a given pH the rate

increased about 10-fold for a 15°C temperature increase, and the apparent activation energy was calculated to be 23 kcal (9.6×10^4 joules/mole). The majority of experimental investigation has been carried out at a temperature of 25°C.

Although the Weiss radical-chain mechanism is in accordance with a first-order dependence of the oxidation rate on both ferrous ion and dissolved oxygen concentration, it does not explain the second-order dependence of the rate on hydroxyl ion concentration which is observed in neutral buffered solutions. Goto et al (20) have proposed a new mechanism consistent with the rate expression of Stumm and Lee, where the rate-determining step is assumed to be the reaction between the species $FeOH^+$ and O_2OH^-. It is suggested that the reaction between these species is most likely diffusion controlled.

3.3 PRESENT KINETIC STUDIES

3.3.1 Approach

The present work is concerned with the oxidation resulting when an acidic ferrous sulphate iron solution is introduced to sea-water. Although the kinetics of ferrous iron oxidation has been established for a low ionic strength bicarbonate water, as far as can be ascertained no study would appear to have been made of ferrous oxidation in a high ionic strength bicarbonate water such as sea-water. Horne (21) notes that the kinetics of marine chemical reactions represents a very important, yet largely unexplored, field.

On the introduction of a sulphuric acid/ferrous sulphate solution to sea-water there is an initial rapid interaction between the effluent acid and the bicarbonate buffer of the salt water- see Section 2.6. There will also be a degree of ferrous iron oxidation (or perhaps even ferrous carbonate precipitation and redissolution)

occurring in this initial period, but it is to be expected that the bulk of ferrous oxidation will take place at the pH values resulting from the acid-buffer reaction. The range of pH/ferrous iron concentration values spanned on the continuing dilution of a typical industrial effluent is illustrated in Figure 5. It can be seen that in the pH range 6 to 7.5 the initial ferrous concentration in sea-water varies from roughly 30 mg/l to 3 mg/l. These results are in good agreement with the findings of Weichart (22) who, on studying the discharge of tanker loads of titanium dioxide factory waste waters into the sea off Germany, found that immediately after effluent release the sea-water concerned had a pH of about 6 with a corresponding iron concentration of around 40 mg/l. Two hours after discharge the pH had returned to nearly normal (pH 8), the solution oxygen concentration was nearly normal and the iron concentration was 2 mg/l.

The nature of the ferrous oxidation reaction occurring in sea-water differs in several important aspects from the ferrous oxidation studies carried out by previous workers. Firstly, as mentioned, there is the high ionic strength of the medium, due principally to the high sodium chloride content of sea-water. Secondly, the ferrous iron concentrations involved are much greater than those employed by Stumm and Lee and others, who carried out all their work at concentrations less than 3 mg/l to avoid ferrous carbonate precipitation. The increased solubility of ferrous iron in sea-water has already been attributed to the ability of ferrous iron to form soluble chloride complexes - Section 2.5. It is worth repeating that Saprygin and Gusar (11) have found that the kinetics of ferrous sulphate oxidation change from a first-order ferrous ion dependence to a second-order dependence as ferrous concentration increases. Thirdly, the majority of previous

oxidation studies have been carried out under carefully controlled conditions of constant pH and constant oxygen concentration in solution. Neither of these conditions is likely to be encountered in the real case of the sea-water oxidation reaction.

It was decided to investigate the kinetics of the ferrous oxidation reaction occurring in sea-water on the addition of an acidic ferrous sulphate solution by monitoring the resultant pH and oxygen concentration changes in solution. From the stoichiometric equation, 3D, it can be calculated that oxygen will be consumed in solution at a rate of around 1 mg/l per 7 mg/l ferrous iron oxidised. As aerated sea-water has an oxygen concentration at 25^{o}C of roughly 7 mg/l (21), an initial ferrous iron concentration of at least 10 mg/l is required in order to obtain a meaningful degree of oxygen consumption for kinetic analysis. There is also a practical limit on the pH range that can be studied, governed by the speed of the oxidation reaction. With the results of previous workers in mind (Figure 7), and the known range of conditions relevant to industrial effluent dispersal (Figure 5),it was decided to carry out oxidation experiments in the pH range 6 to 7 with initial ferrous iron concentrations ranging from 60 to 10 mg/l. This also ensured that the quantity of ferric hydroxide produced in each run would be sufficient for subsequent precipitate analysis (see Chapter 4).

For the purposes of the kinetic studies it was decided to make use of 'artificial' sea-water and 'artificial' effluents. The former is discussed in Section 3.3.2 and the latter were designed so as to achieve the conditions outlined above. Several different 'artificial' sulphuric acid/ferrous sulphate solutions were used so that the influence of the acid/iron ratio of the effluent could be quantitatively assessed. Experiments were undertaken to determine the influence of oxygen transfer across the air-water interface and of temperature on the oxidation reaction. For

comparison purposes several kinetic runs were also carried out using samples of real filtered sea-water and samples of Tioxide industrial effluent. A detailed description of the experimental procedure is given in Section 3.3.3.

3.3.2 Artificial Sea-Water

It is often difficult to obtain meaningful physio-chemical measurements on selected samples of real sea-water because of its complexity and instability, both inorganic and biological (21). A synthetic or 'artificial' sea-water is thus often employed in the laboratory in 'sea-water' experiments to minimize biological effects and to provide a reproducible solution of known composition. The advantage of using a known reproducible medium to simulate the behaviour of real sea-water is particularly evident in kinetic studies where rates of reaction can be dramatically affected by the presence of variable trace elements. The oxidation of ferrous iron is known to be very susceptible to the presence of trace impurities (14).

For these reasons it was decided to carry out the bulk of ferrous oxidation kinetic studies using an "artificial sea-water" of set composition. The results were later compared with those obtained using samples of real sea-water to test the validity of this approach. It is worth noting that Stumm and Lee used a synthetic low ionic strength ground water in their experiments.

The synthetic solution used in the present work was kept as simple as possible so that, if it proved necessary, other constituents of sea-water could be progressively added later. In this way it was hoped to isolate the species most influencing ferrous iron oxidation. The basic medium, referred to in this report as "artificial sea-water", was limited to a solution of sodium chloride (NaCl) and sodium bicarbonate ($NaHCO_3$), the latter establishing the required bicarbonate buffer system in solution. The salts were added to de-ionized distilled water accord-

ing to the artificial sea-water recipe of Kester et al (23). Analytical reagent grade chemicals were used and after dissolution air was bubbled through the solution until a steady pH value was attained. This tended to equilibrate the artificial sea-water with atmospheric gases, removed the excess CO_2 resulting from the conversion of HCO_3^- to CO_3^{2-} (23) and ensured that the solution was saturated with oxygen. After aeration and equilibration at the required temperature (25^oC or 12^oC) artificial solutions were found to have pH values in the range 8.25 to 8.45, well within the range established for aerated surface ocean waters (21).

The formula of artificial sea-water and a comparison with the known composition of real sea-water has already been given in Table 3 and is repeated in more detail in Table 10. As already mentioned, sodium and chloride ions are by far the most abundant chemical species in sea-water (21). Table 10 shows that the sodium and chloride ion concentrations in the artificial sea-water of this work are lower than the corresponding values in real sea-water, while the bicarbonate ion concentration is the same. The discrepancy arises because of the method of following the sea-water recipe of Kester et al. This was intentional. If required, sulphate ions can now be added to the artificial solution in the correct proportion as found in real sea-water by adding the formula weight of Na_2SO_4. Similarly, the correct proportion of magnesium can be attained by adding a volumetric amount of soluble $MgCl_2$. The omission of the major sea-water divalent ions is the prime cause why the artificial sea-water has a lower ionic strength than real sea-water.

However, although the synthetic solution does represent a very simplified model for real sea-water, it does contain a major amount of the principal sea-water ions and the bicarbonate buffer system is correctly modelled. Moreover, as shown and discussed in Chapter 2, in

TABLE 10 - COMPOSITION OF ARTIFICIAL SEA-WATER (21, 23)

Salt	CONCENTRATION		Element	CONCENTRATION	
	Gm/kg Soln	Gm/l @ 25°C		Artificial Sea-water (moles/l)	Real Sea-water (moles/l)
NaCl	23.93	24.45	Na^+	0.420	0.48
$NaHCO_3$	0.196	0.200	Cl^-	0.418	0.56
			HCO_3^- (pH 8.2)	2.4×10^{-3}	2.4×10^{-3}
			(Ionic strength)	(0.42)	(0.67)

spite of the differences in composition, the pH dependent solubility of both ferrous iron and ferric iron has been calculated to be basically the same for artificial sea-water as for real sea-water. The artificial solution thus provides a good, simple, reproducible medium that can be used to simulate real sea-water in an introductory investigation of the kinetics of ferrous iron oxidation.

3.3.3 Experimental Method

A schematic diagram of the experimental apparatus used in the kinetic studies is shown in Figure 8A. The reaction vessel consisted of a 3-litre capacity sealable perspex cylinder which could be suspended in a thermostatically controlled water bath. The major dimensions of the vessel are given in Figure 8B. Holes, sized so as to provide a tight fit, were drilled through the reactor lid to enable pH electrodes and an oxygen sensor to be inserted into the solution in the vessel. Other suitably sized holes enabled the insertion of

FIGURE 8 - APPARATUS

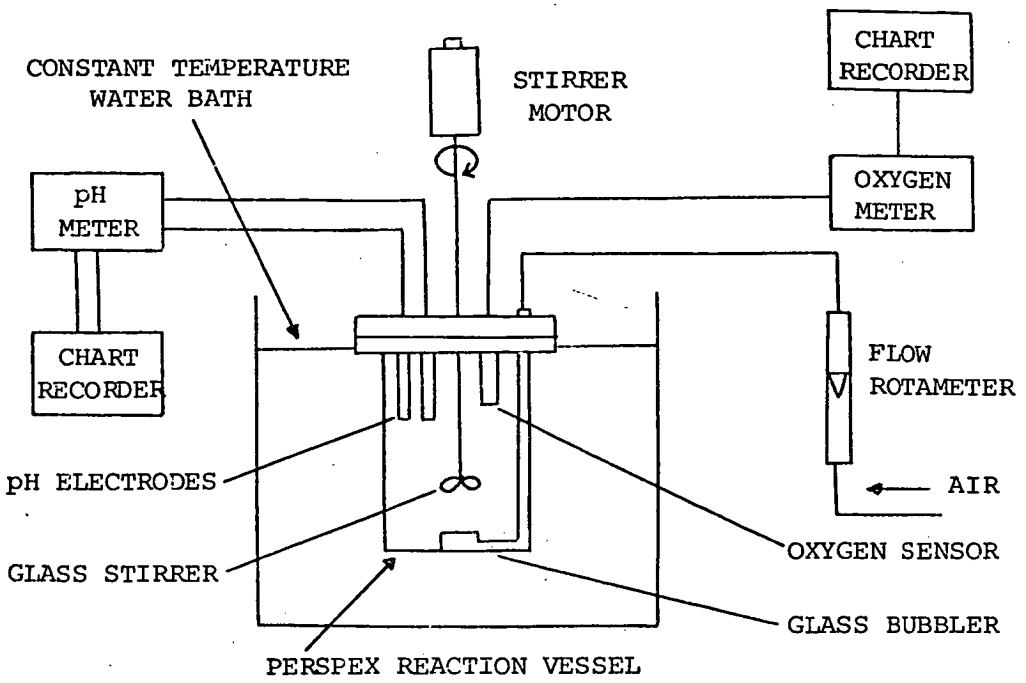

A - SCHEMATIC DIAGRAM OF EXPERIMENTAL APPARATUS

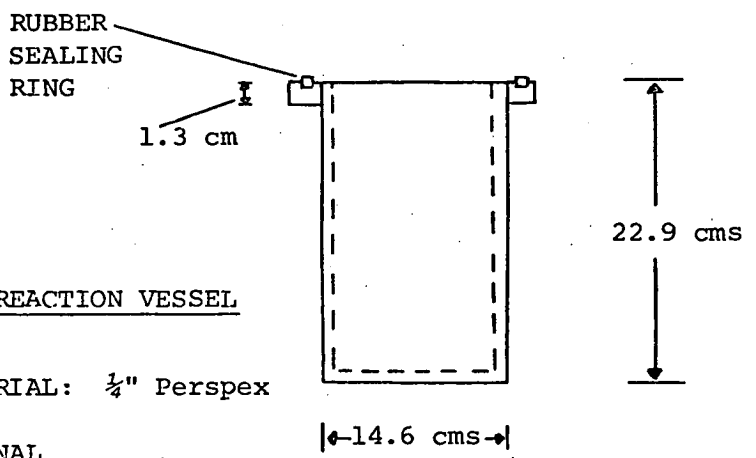

B - REACTION VESSEL

MATERIAL: ¼" Perspex

NOMINAL VOLUME: 3 Litres

LID THICKNESS: 1.3 cms

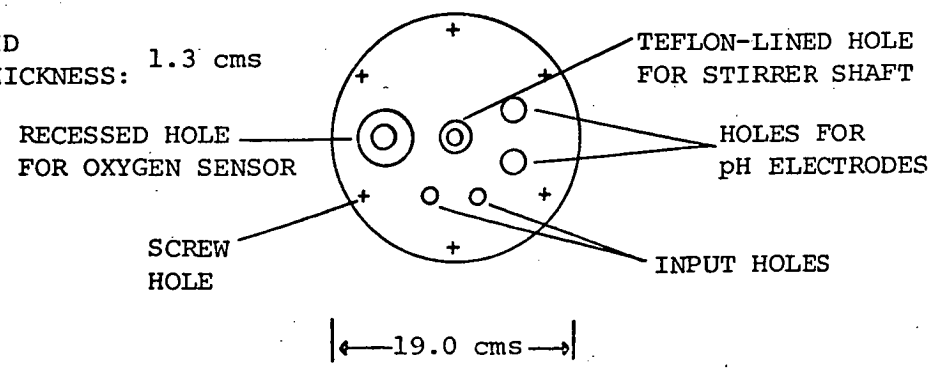

the glass impeller of a variable speed stirrer, a glass bubbler and allowed solution addition or withdrawal.

All pH measurements were made with a Philips PR-9400 pH meter equipped with glass and calomel electrodes. The meter was calibrated before each run in the pH range 6 to 8 with two standard phosphate buffers (24). The oxygen sensor used to follow the depletion of oxygen in solution was a Beckman model No. 39553, attached to a Beckman Fieldlab oxygen analyser. The sensor was prepared and calibrated in the manner recommended by the manufacturer and measures the partial pressure of dissolved oxygen in solution by the polarographic principle, oxygen diffusing into a small electrolytic cell through a gas-permeable teflon membrane. Readings are obtained in concentration units of parts per million (ppm). Both instruments were attached to chart recorders to enable a continuous monitoring of readings.

Two types of kinetic run were undertaken. In the majority of runs, classified as "closed" runs, the vessel was completely full of solution so that negligible oxygen transfer could take place from the atmosphere into the solution under study. The general procedure for each "closed" run was as follows below. The vessel, minus lid, was filled with artificial sea-water (prepared as outlined in Section 3.3.2) and suspended in the water bath. The lid plus glass stirrer and bubbler was then fixed into place. While temperature equilibrium was being established, air was bubbled at a controlled rate through the stirred solution to ensure that it was saturated with oxygen and had attained a steady pH. The air flow was then ceased and the bubbler allowed to fill with solution (the volume concerned was negligible compared to the total volume of the vessel).

With the solution at the required temperature, the pH electrodes and oxygen sensor were then inserted and the volume of artificial sea-water adjusted so that the vessel was completely full, with negligible trapped air. When steady values of pH and oxygen concentration were being recorded for the well stirred solution, a pre-determined volume ($\leq$15 ml) was removed from the vessel and replaced with an equivalent amount of artificial effluent. The volume and concentration of the effluent added were determined by the pH and the initial concentration of ferrous iron required. The addition of effluent marked time zero for the run. After effluent addition the vessel was then "re-topped", if necessary, with artificial sea-water and the "input" holes were sealed to the atmosphere. The rate of the ensuing oxidation reaction was followed by monitoring the oxygen consumption in solution and the changes in pH over a set period of time (two hours in most cases).

After monitoring the oxidation kinetics the vessel was left in-situ, often over night, to enable the reaction to proceed to completion. The precipitate formed via the oxidation reaction was then collected by decantation and filtration, was washed with distilled water, dried in an oven at 60^{o}C for three hours, and analysed as discussed in Chapter 4.

The different artificial effluents used in the kinetic studies are outlined in Table 11. As with artificial sea-water, all solutions were prepared using de-ionized distilled water and reagent grade chemicals. Artificial effluent was made by dissolving 6.223 gms $FeSO_4.7H_2O$ (1250 mg Fe^{2+}) in 100 mls of the required sulphuric acid solution and was freshly prepared for each run. As well as the artificial sea-water/artificial effluent runs carried out,a series of closed kinetic runs were undertaken using samples of real sea-water

TABLE 11 — COMPOSITION OF ARTIFICIAL EFFLUENTS

EFFLUENT	FERROUS IRON CONTENT (gms/l=mg/ml)	SULPHURIC ACID CONTENT		ACID/IRON RATIO (w/w)
		(gms/l)	(ml/l @ 20°C)	
A	12.5	7.4	4	0.6
B	12.5	3.7	2	0.3
C	12.5	11.0	6	0.9
D	12.5	4.8	2.6	0.4

and real Tioxide effluent. The method of collection, storage and analysis of these samples has already been discussed in Section 2.6. The real sea-water samples showed no evidence of deterioration in the period between collection and use, and on aeration had measured pH values around 8.25, in excellent agreement with literature values (21) and only marginally less than the corresponding values obtained with the prepared artificial sea-water matrix. The measured saturated oxygen concentration in both real and artificial sea-water varied around 6.9 ppm at 25°C, again in very good agreement with established values. Oxygen solubility is determined by the temperature and the salinity of a solution (21).

Most of the closed kinetic runs were undertaken at a constant temperature of 25.0± 0.05°C to enable results to be compared with those of other workers. Several runs were also made, with the aid of a refrigeration unit attached to the water bath, at a temperature of 12.0± 0.1°C to investigate the effect of temperature on the ferrous iron oxidation reaction.

The second type of kinetic run undertaken in the present work was an "open" run in which the solution was left in contact with the air. This enabled atmospheric oxygen to transfer into solution, replenishing dissolved oxygen being consumed in the oxidation reaction. Open runs were carried out with 2.5 litres of solution in the reaction vessel (three quarters full) and with the "input" holes in the lid unsealed. With this volume in the reaction vessel both the pH electrodes and the oxygen sensor were still well immersed in solution. The influence of stirrer speed on the rate of oxygen transfer across the air-water interface was assessed by carrying out experiments investigating the rate of re-aeration of oxygen depleted artificial sea-water solutions. Solutions were de-oxygenated by bubbling nitrogen gas through them for a short period. Re-aeration runs were undertaken at several different stirrer speeds, and the results are analysed in Section 3.3.4. Apart from the smaller volume in the reaction vessel and the absence of precautions to exclude air during the ferrous oxidation reaction, the open kinetic runs were carried out in the same manner as described for the closed runs. All open runs were undertaken at 25^{o}C using artificial sea-water and artificial effluents.

3.3.4 Rate Analysis of Experimental Data

The results of each kinetic run, whether closed or open, can be expressed in terms of an oxygen consumption versus time curve and a corresponding pH versus time curve- see Section 3.4. It was required to analyse this rate data to try to obtain a consistent rate expression describing the ferrous oxidation taking place. As is the general procedure with rate analysis, it was decided to test the data with several proposed kinetic expressions, suggested by the work of previous researchers.

The net rate of oxygen consumption in sea-water following the introduction of a sulphuric acid/ferrous sulphate solution is equal to the rate of oxygen consumption due to the oxidation of ferrous iron minus the rate at which oxygen transfers into the solution from the atmosphere to replace the depleted oxygen content. In the case of the closed kinetic runs undertaken the latter can be taken to be zero. As regards the present work, preliminary closed experi-ments involving only

a stirred sample of artificial sea-water showed that over a two-hour period and more the Beckman oxygen sensor consumed negligible dissolved oxygen in determining oxygen concentration in solution. Any decrease in oxygen concentration recorded in subsequent work could thus be attributed wholly to the ferrous iron oxidation reaction.

CLOSED KINETIC RUNS

For these runs we can equate the measured rate of oxygen consumption directly with the rate of ferrous iron oxidation. From the stoichiometric relationship describing the oxidation reaction (3D) it can be seen that corresponding to each mole of oxygen consumed in solution four moles of ferrous iron will have been oxidised. The ferrous iron concentration remaining in solution can be related to the measured oxygen concentration at any particular time during a run by the expression:

$$(Fe^{2+}) = A - 4k\,(C_s - C)$$

where (Fe^{2+}) = ferrous concentration at time t - moles/litre

A = initial ferrous concentration - moles/litre

C = oxygen concentration in solution at time t - ppm

C_s = initial oxygen concentration - ppm

k = conversion factor between ppm and moles/litre

Further, from the stoichiometric relationship we have that:

$$-\frac{d(Fe^{2+})}{dt} = \frac{d(Fe^{3+})}{dt} = -4\frac{d(O_2)}{dt} = -4k\,\frac{dC}{dt}$$

We can now test the experimental results with the required kinetic expressions.

A. Assume that the oxidation reaction can be empirically described by the expression:

$$-\frac{d(Fe^{2+})}{dt} = k_A (Fe^{2+}) (O_2) \quad \ldots\ldots\ldots (3E)$$

Substituting the relevant relationships given above we find:

$$-\frac{dC}{dt} = \frac{k_A}{4} \left(A - 4k (C_s - C) \right) C \quad \ldots\ldots (3F)$$

Integration is achieved by completing the square and then using partial fractions.

Assuming that k_A is invariant with time, the solution is:

$$\ln \left(\frac{C}{C_s} \left(\frac{A^1 + kC_s}{A^1 + k (C-C_s)} \right) \right) = -k_A (A^1 - kC_s) t + \ln \left(\frac{A^1 + kCs}{A^1} \right) \quad \ldots (3G)$$

where $A^1 = A/4$

Thus, if the assumed rate expression is correct, a plot of the above left-hand side natural logarithm against time should yield a straight line of slope $-k_A (A^1 - kC_s)$, and the basic rate constant k_A can be found via the equation:

$$k_A = \text{slope}/(kC_s - A^1) \quad \ldots\ldots (3H)$$

Experimental data was analysed along these lines by means of a computer programme. The programme evaluated the slope of the required line by regression analysis and the degree of linearity was assessed by computing a correlation coefficient (25). A value for k_A, together with its appropriate error, was calculated for each run.

B. Assume that the oxidation kinetics is given by the expression:

$$-\frac{d(Fe^{2+})}{dt} = k_B (Fe^{2+}) (O_2) (OH^-)^n \quad \ldots\ldots (3I)$$

where n = 1 or n = 2 (N.B. for low ionic strength bicarbonate waters it is

established that n = 2 (15)). Whereas the first kinetic expression tested ignores the influence of pH on the oxidation reaction (or assumes that pH is included in the rate constant k_A), this expression attempts to take pH into account.

As will be shown in Section 3.4, pH during a run was not in fact constant after the initial rapid acid-buffer interaction, but decreased gradually due to the hydrolysis of ferric iron. This can be predicted from the stoichiometric relationship describing ferrous oxidation (3D), two moles of H^+ being produced per mole of Fe^{2+} oxidised. The actual pH value of the artificial sea-water/effluent solution is dependent not only on the hydrogen ions liberated by means of the oxidation reaction, but also on the buffer action of the bicarbonate system and on the amount of introduced effluent sulphuric acid. There is thus no simple expression relating the pH of solution to the amount of ferrous iron oxidised (and from there to the oxygen concentration), and consequently (OH^-) terms in proposed kinetic expressions need to be evaluated by numerical integration.

The extent of the decrease in pH resulting from ferric hydrolysis was found to vary according to the acidity of the artificial effluent used and the initial concentration of introduced ferrous iron, but generally speaking over the bulk of each run was less than 0.4 pH unit. It is thus possible, after allowing five minutes for the acid-buffer reaction to be complete, to sub-divide each run into small equal time periods over which, within experimental error, the pH of solution can be taken to be constant. For the majority of kinetic runs, monitored for two hours, pH could be regarded as constant over individual five minute periods and the runs were broken up accordingly.

From expression (3I), after substituting in terms of oxygen concentration, we have:

$$\int_{C_1}^{C_2} \frac{dC}{\left(A-4k(C_s-C)\right) C} = \frac{-k_B}{4} (OH^-)^n_{\Delta T} \int_{t_1}^{t_2} dt \quad \ldots\ldots\ldots (3J)$$

where $\Delta T = t_2 - t_1$, the time period over which pH is taken to be constant and C_2, C_1 are the corresponding measured oxygen concentrations in solution.

Integrating, and re-writing in terms of the overall rate constant k_B, we find:

$$k_B = 4 \ln \left(\frac{C_1 (A + 4k (C_2 - C_s))}{C_2 (A + 4k (C_1 - C_s))} \right) / (A - 4kC_s)(OH^-)^n_{\Delta T} \Delta T \quad \ldots(3K)$$

A series of k_B values can thus be calculated for each run and, if the rate expression and accompanying assumptions are correct, the k_B values both within and between runs will be similar. A computer programme was written to analyse the kinetic data of each closed run along these lines, calculating a series of "five minute" k_B values, and from these an overall k_B value, for each run. The scatter of calculated k_B values within a run, and thus the error associated with the overall k_B, is expressed by the standard deviation. Calculations were carried out assuming both a first-order and a second-order rate dependence on hydroxyl ion concentration i.e. with n = 1 and with n = 2.

OPEN KINETIC RUNS

In the case of the open kinetic runs carried out the amount of dissolved oxygen consumed by ferrous oxidation is offset by oxygen transfer into solution from the air,

$$\frac{-d\,(O_2)}{dt}_N = \frac{-d\,(O_2)}{dt}_R - \frac{d\,(O_2)}{dt}_A \quad \ldots\ (3L)$$

where $\frac{-d\,(O_2)}{dt}_N$ = net recorded rate of oxygen consumption

$\frac{-d\,(O_2)}{dt}_R$ = rate of oxygen consumption in ferrous oxidation reaction.

$\frac{+d\,(O_2)}{dt}_A$ = rate of transfer of oxygen from air into solution

The quantitative effect of leaving the reaction solution open to the atmosphere can be assessed by comparing the oxygen consumption curves of closed and open runs with the same initial ferrous iron concentration. However, analysing the experimental data with the purpose of obtaining a consistent rate expression is difficult and can only be achieved by making several assumptions:

1. Firstly, it is assumed that the rate of oxygen consumption in the oxidation reaction is given by expression A for the closed kinetic run. This assumption is reasonable when the amount of oxygen consumed exceeds by several factors the amount transferred into solution, as is the case over the period of the reaction monitored in the present work.

2. Secondly, it is assumed that the rate of oxygen transfer into solution is given by the expression (26):

$$\frac{d(O_2)}{dt_A} = k_R \left((O_2)_{Sat} - (O_2)\right) \quad \ldots.(3M)$$

where k_R is a re-aeration constant dependent on the stirrer speed in the vessel and $(O_2)_{Sat}$ is the saturated oxygen concentration. As mentioned in the experimental method section, this assumption was tested by following the rate of increase of oxygen concentration in a de-oxygenated artificial sea-water solution stirred at a constant set speed. Integration of (3M) yields the equation:

$$\ln \left(\frac{(C_s - C)}{(C_s - C_o)} \right) = -k_R t \quad \ldots \quad (3N)$$

where C_o = measured depleted oxygen concentration in solution at time zero (ppm)

C_s = saturated oxygen concentration (ppm)

C = oxygen concentration at time t (ppm)

Thus it can be seen that if the assumed re-aeration rate expression is correct, a plot of the above natural logarithm against time should yield a straight line of slope $-k_R$.

Results for re-aeration runs undertaken at three different stirrer speeds are given in Figure 9 and show that such a linear relationship is in fact obtained. Tabulated values for each re-aeration run are given for reference in Appendix 7. Obtained k_R values show a large variation with stirrer speed and were used in the subsequent rate analysis of the open kinetic runs.

Given that expression (3M) appears to be valid, we can now substitute into (3L) to obtain an overall expression for the net rate of oxygen consumption recorded in open kinetic runs. Integration of this expression will then yield a relationship giving expected oxygen concentration as a function of time and dependent

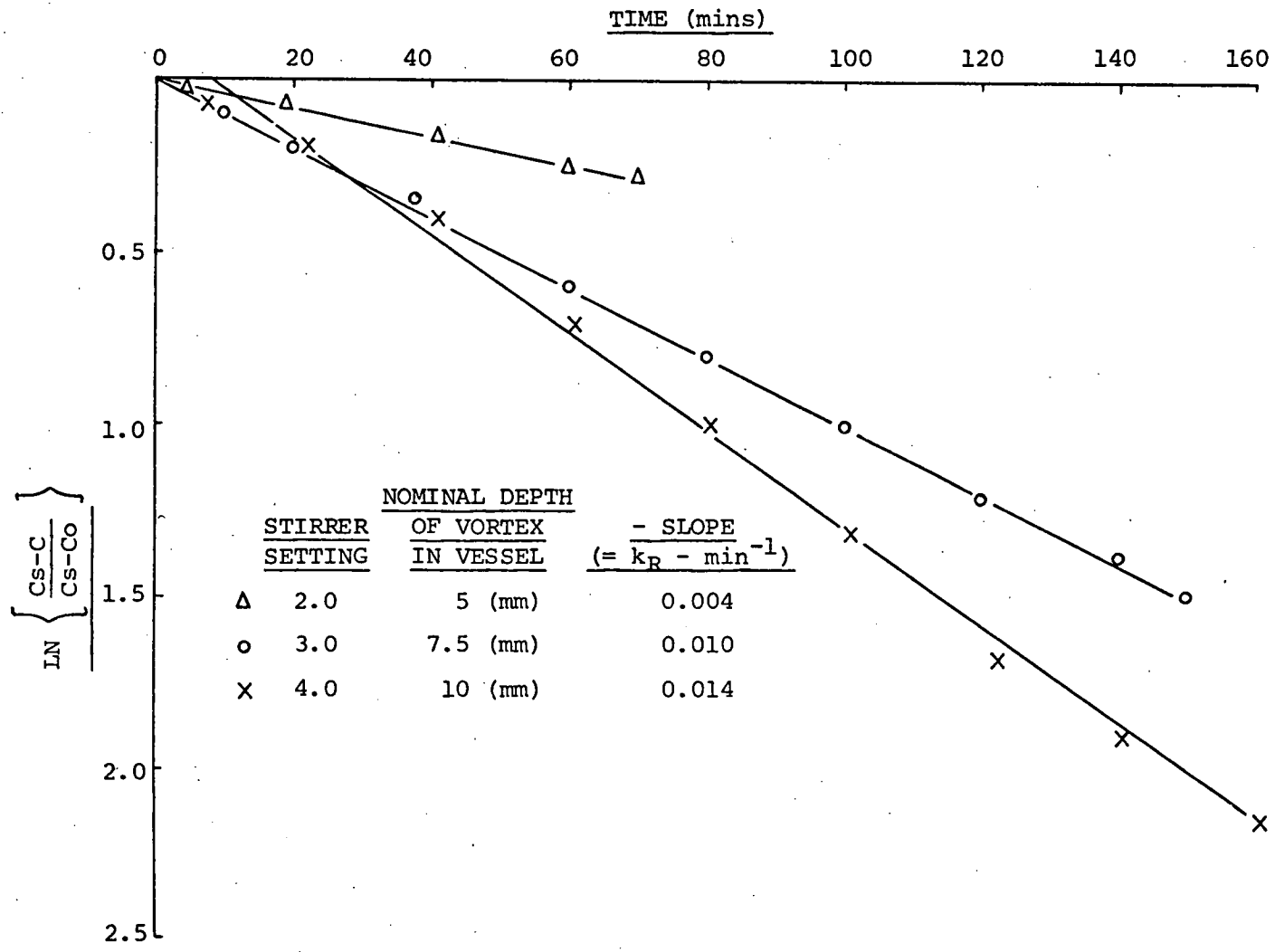

FIGURE 9 - LOGARITHM PLOTS FOR ARTIFICIAL SEA-WATER RE-AERATION RUNS

on the ferrous oxidation reaction rate constant, k_A. The mathematics and integration are complicated and are given in Appendix 4.

Because no simple linear plot exists from which a k_A value can be evaluated, k_A has to be found by trial and error, comparing calculated with obtained oxygen consumption curves. A computer programme was written to estimate a k_A value for each open kinetic run. Values can be compared with those obtained in the closed kinetic runs.

3.4 RESULTS AND DISCUSSION

3.4.1 Closed Kinetic Runs at 25°C

Typical oxygen consumption curves recorded for closed kinetic runs at 25°C are shown in Figures 10, 11, 14 and 15. All the runs shown were carried out using artificial sea-water and the artificial effluents outlined in Table 11. The progress of a run was marked by the increasing turbidity of the solution in the reaction vessel, the colour of the solution changing from a clear very pale green to an opaque brown/orange as oxidation proceeded. The degree of turbidity developed in a run was reflected by the amount of oxygen consumed. At relatively high values of oxygen consumption (>2ppm) it was possible to distinguish small flocks of precipitate in the reaction vessel. The brown/orange suspension remaining at the completion of the oxidation reaction took many hours to settle, but the final fine precipitate (a form of ferric hydroxide) could be collected after decantation by filtration, using fine-grade filter paper.

Figures 10 and 11 show the variation of oxygen consumption curves for a particular effluent as initial ferrous iron concentration increases (i.e. increasing volume of effluent added to reaction vessel). Initial ferrous iron concentration is designated as $(Fe^{2+})_I$. It is obvious that if oxidation proceeds to completion then overall oxygen consumption must increase with $(Fe^{2+})_I$. However, whether or not this relationship is achieved within the first two hours following effluent introduction depends on the kinetics of the ferrous iron oxidation reaction. If the reaction is effectively quenched then no oxygen will be consumed no matter how high the initial ferrous concentration. It can be seen from the diagrams that for effluents A and B the oxygen consumed in the first two hours does in fact increase with $(Fe^{2+})_I$, over the range of values investigated. However, a

FIGURE 10 - OXYGEN CONSUMPTION CURVES FOR EFFLUENT A @ 25°C.

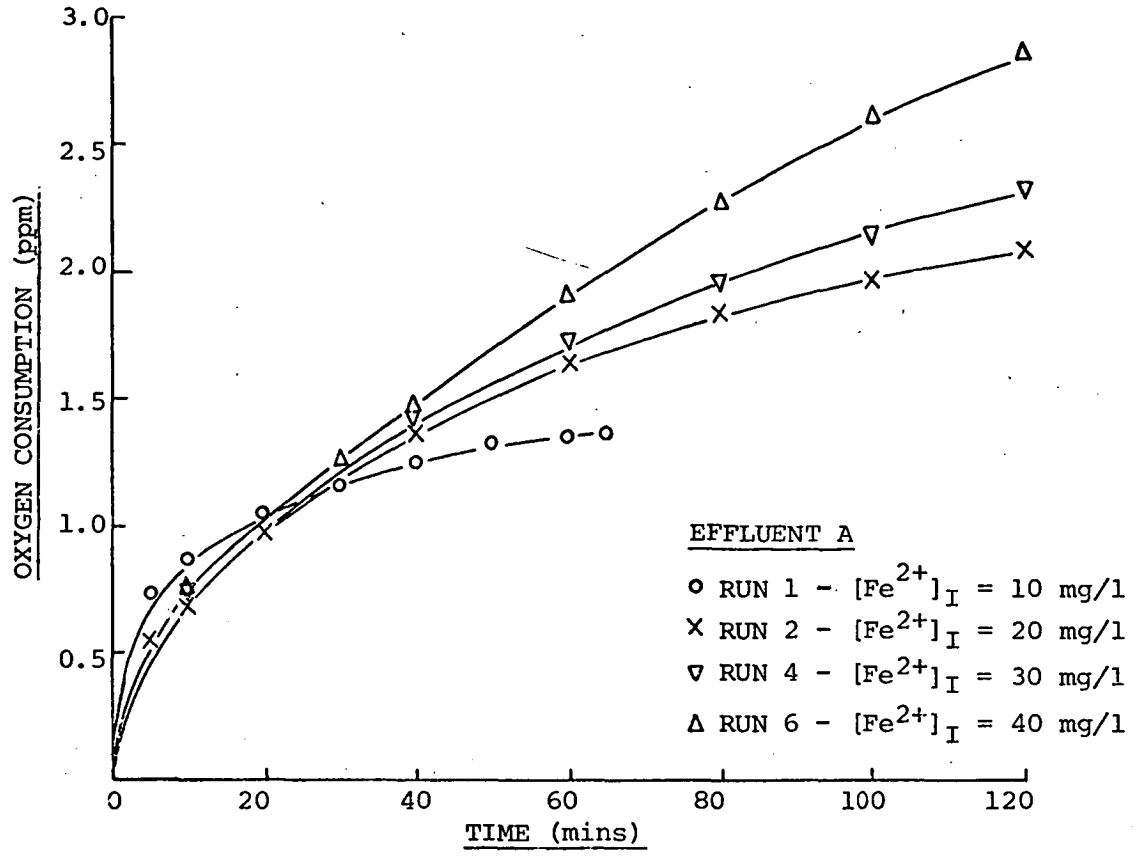

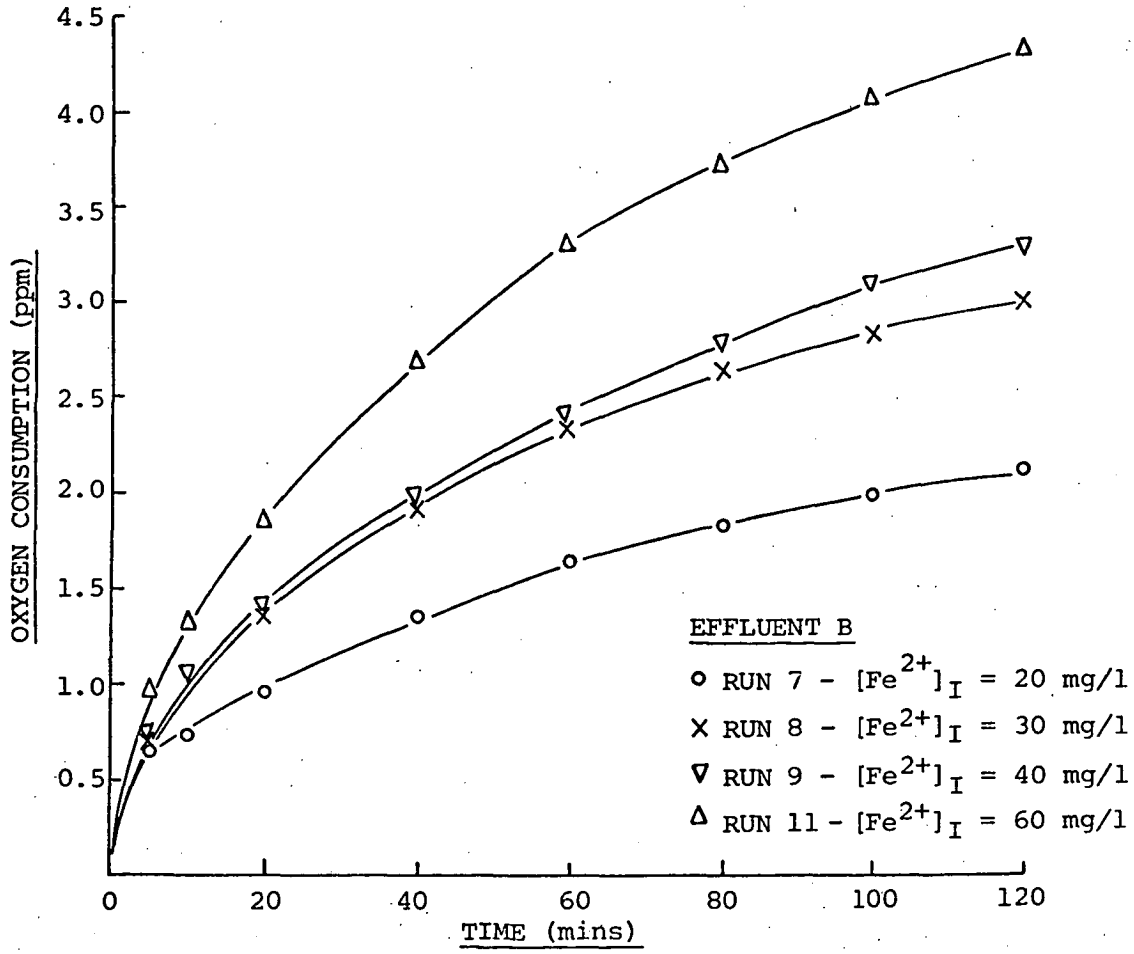

FIGURE 11 - OXYGEN CONSUMPTION CURVES FOR EFFLUENT B @ 25°C.

comparison of runs 13 and 15 involving the more acidic effluent, effluent C, (illustrated in Figure 14) shows the reverse situation with $(Fe^{2+})_I$ values of 40 mg/l and 60 mg/l. Clearly $(Fe^{2+})_I$ is not the only factor determining the kinetics of the ferrous oxidation reaction.

Typical recorded pH changes during a run are illustrated in Figures 12 and 13. It can be seen that by far the greatest change in pH occurs within the first few minutes of effluent introduction into the reaction vessel, a sudden rapid decrease occurring as the effluent sulphuric acid is neutralized by the bicarbonate buffer of the artificial sea-water. Thereafter the pH decreases very gradually due to the hydrolysis of the ferric iron produced by ferrous oxidation. It is worth noting that above pH 5 the bicarbonate buffer is still present in solution (Section 2.6.3), so that the pH changes following iron hydrolysis are gradual thanks to residual buffering action.

Figure 12 shows the variation of pH with time for selected runs involving artificial effluent A, corresponding to the oxygen consumption curves of Figure 10. As expected, as the effluent dilution factor decreases, not only does $(Fe^{2+})_I$ increase but the pH of solution decreases. In the case of effluents A and B, for the runs carried out, this decrease in pH is not sufficient to depress the relative greater oxygen demand caused by the greater amount of ferrous iron introduced into solution. However, such is the situation with the two runs involving effluent C which were previously mentioned.

The influence of pH on the kinetics of the oxidation reaction at $25^{o}C$ is most clearly illustrated in Figure 14. As can be seen, the rate of oxygen consumption for a constant initial ferrous concentration decreases directly as the acidity of the effluent used

FIGURE 12 - OVERALL VARIATION OF pH FOR CLOSED KINETIC RUNS @ 25°C.

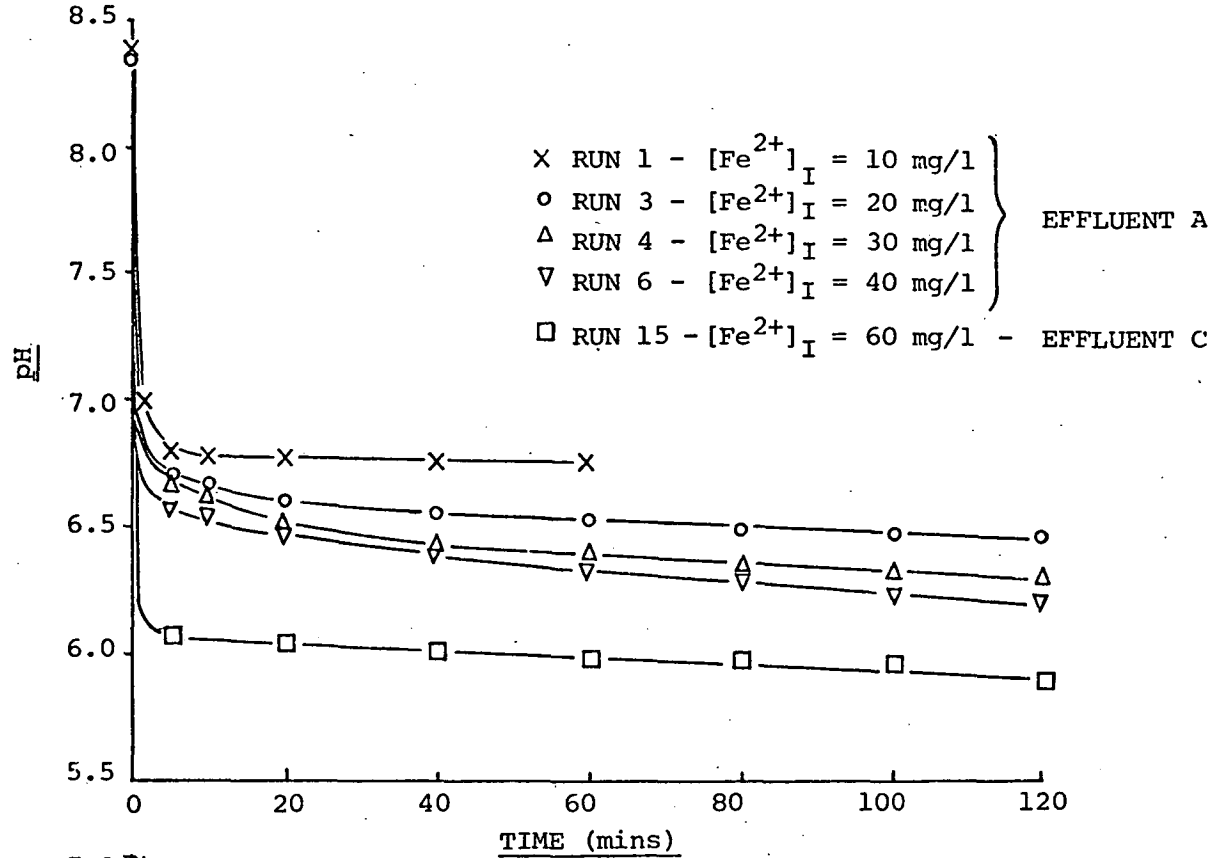

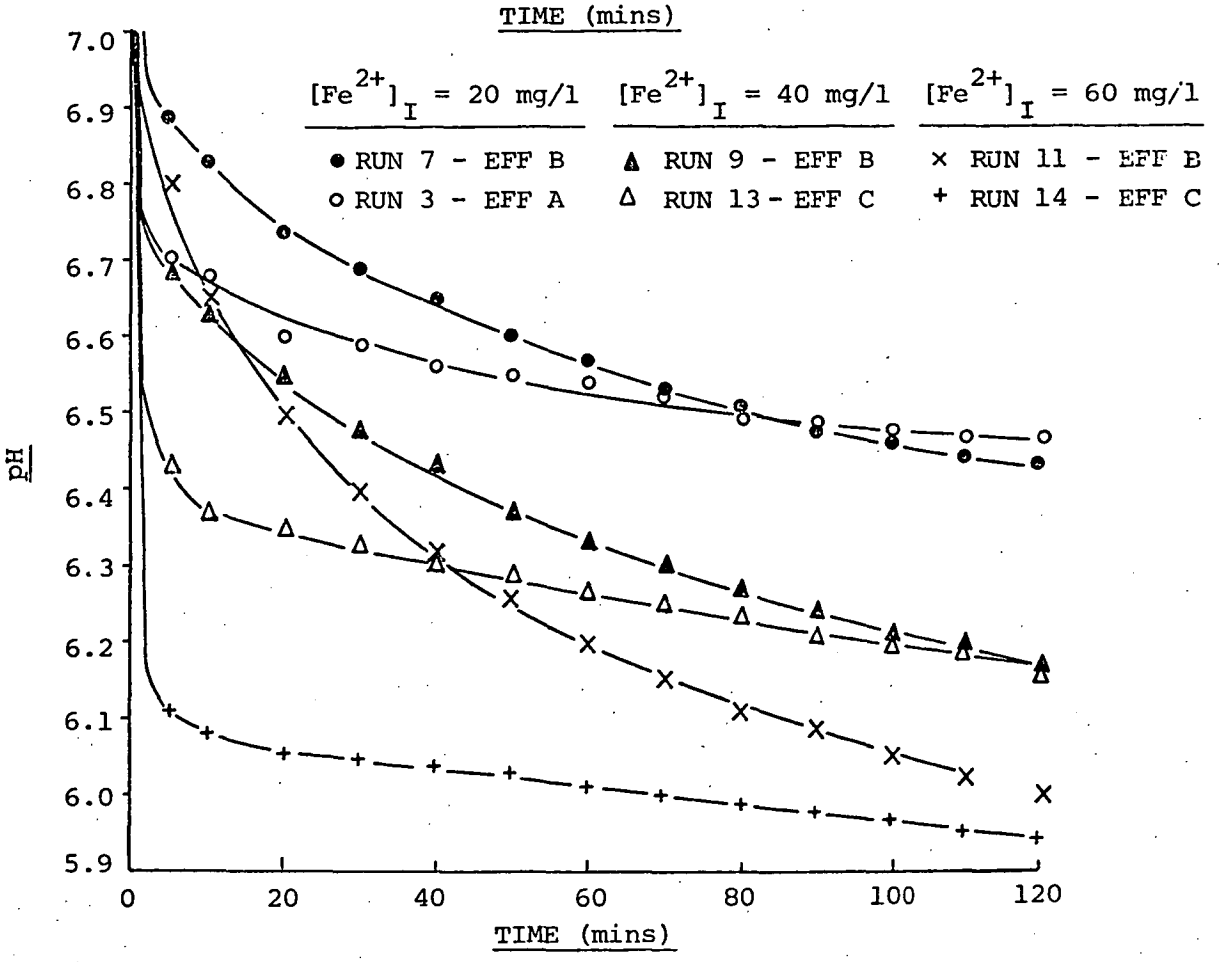

FIGURE 13 - pH VARIATION ON AN EXPANDED SCALE

FIGURE 14 - COMPAPISON OF OXYGEN CONSUMPTION CURVES FOR DIFFERENT EFFLUENTS @ 25°C.

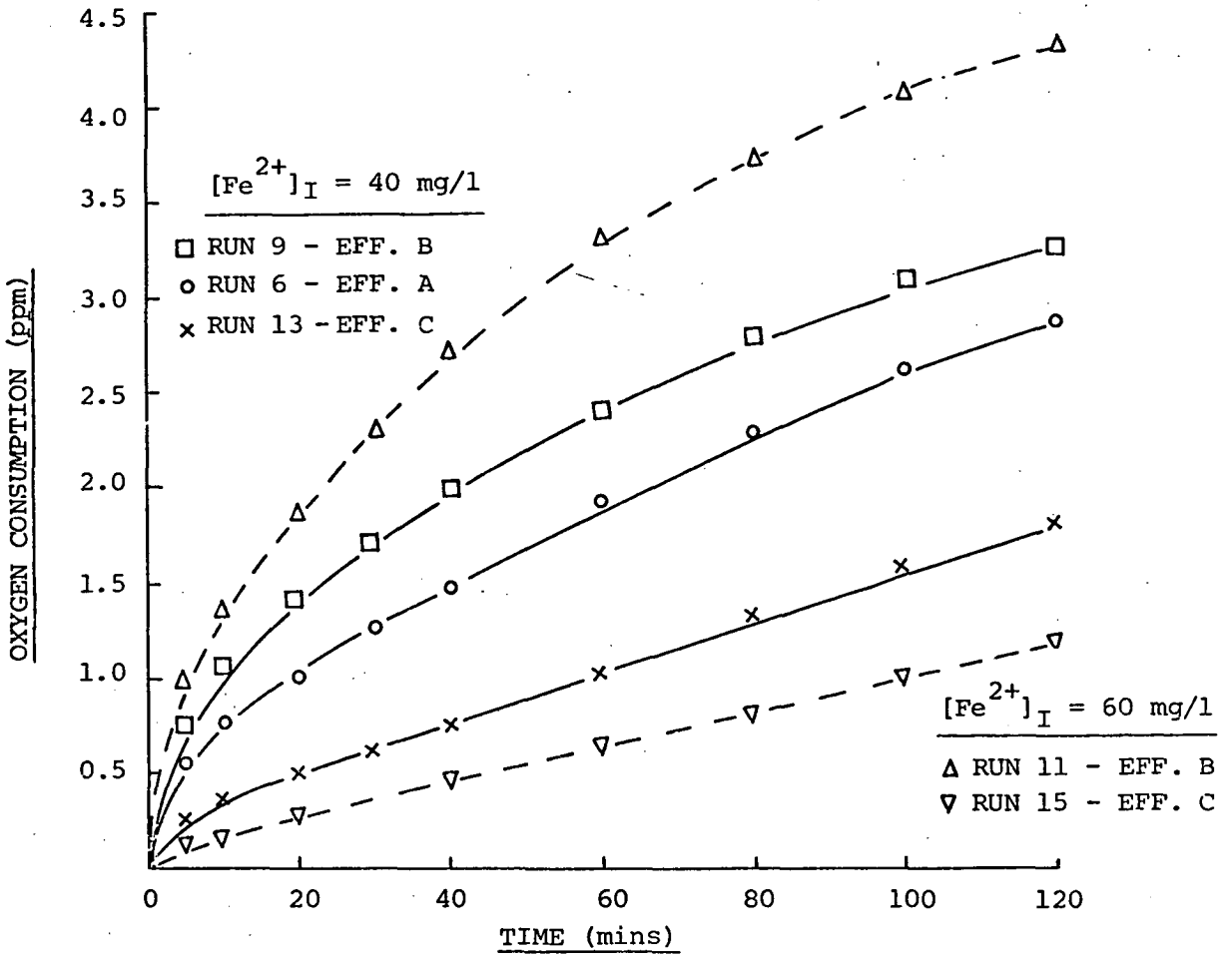

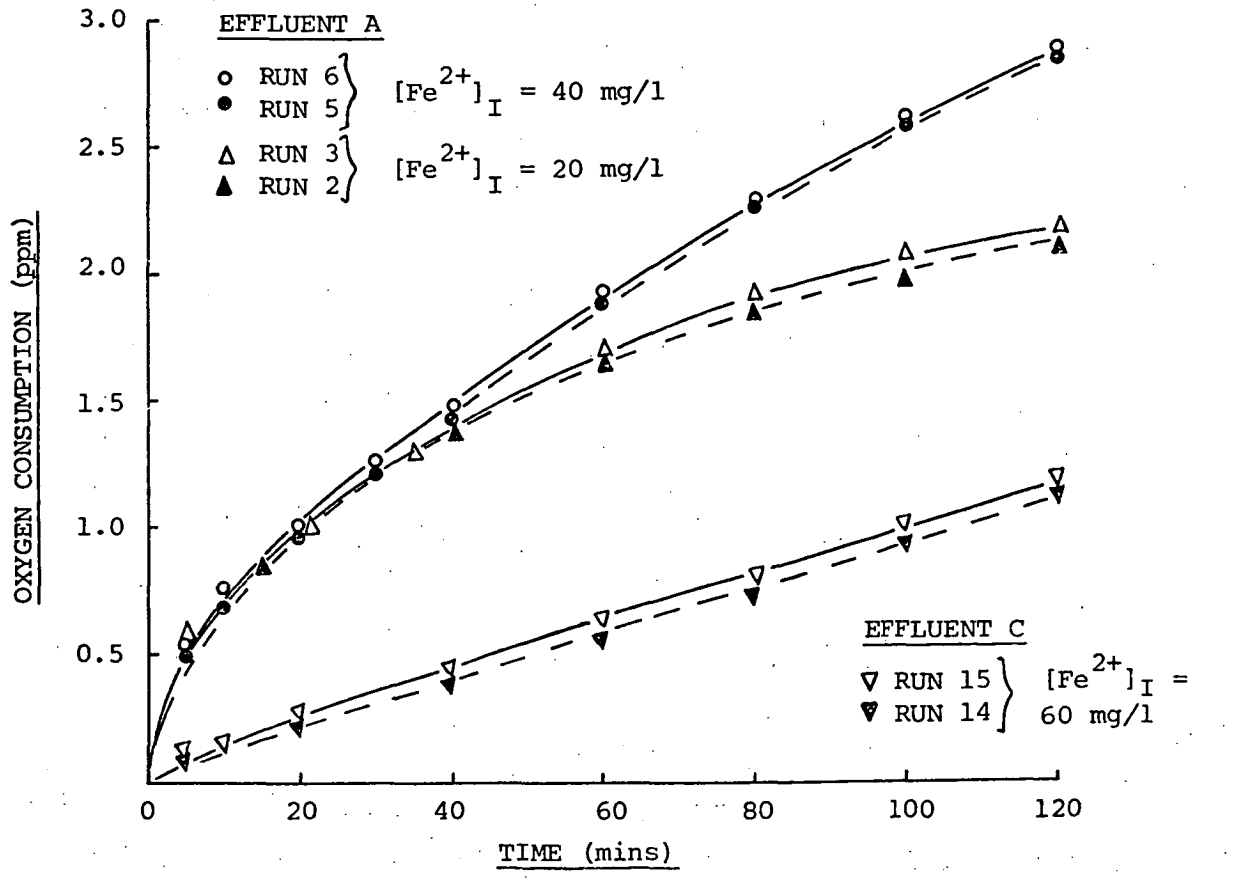

FIGURE 15 - REPRODUCIBILITY OF CLOSED KINETIC RUNS

increases. The lowest net consumption of dissolved oxygen recorded after two hours occurred with run 15, involving the most acidic effluent with $(Fe^{2+})_I$ = 60 mg/l. From the corresponding pH curve (Figure 12) we can thus state that at pH values below 6 the oxidation reaction is very greatly retarded, if not effectively quenched. This is in good agreement with the results of previous researchers investigating ferrous oxidation at low concentrations in low ionic strength bicarbonate waters ((14, 16) - and see figure 7).

A close examination of the "pH curves" representing the variation of pH in solution shows that they reflect the rate of ferrous oxidation taking place. A comparison of pH curves for runs of the same $(Fe^{2+})_I$ but involving effluents of different acidity is given in Figure 13. It must be remembered that the pH changes due to iron hydrolysis are small when compared to the initial large decrease due to the acid-buffer interaction, and that it is the latter that determines the "starting pH", as it were, for the bulk of ferrous iron oxidation.

From Figure 13 it can be seen that for constant $(Fe^{2+})_I$ the shape of the pH curve flattens out as effluent acidity increases. Both the starting pH for oxidation and the subsequent rate of decrease of pH are smaller in magnitude for the more acidic effluent. The negative slope of the pH curve is directly related to the amount of ferric hydrolysis and so to the rate of ferrous oxidation. Clearly, runs starting with the same $(Fe^{2+})_I$ but at a higher pH enjoy a more rapid oxidation, as already indicated in Figure 14. The greatest measured decrease in pH over the reaction period following the acid-buffer interaction occurred with run 11,which was carried out with the lowest acidity effluent (effluent B) at a $(Fe^{2+})_I$ of 60 mg/l. The nature of this run is discussed in detail later.

The experimental results, as illustrated in Figures 10-14, thus show that the rate of ferrous oxidation increases with increasing initial ferrous iron concentration and decreases with decreasing pH. This accords with the majority of previous ferrous oxidation studies carried out in other liquid media - see Sections 3.1 and 3.2. Before moving on to the kinetic analysis of the kinetic data several other points should be noted concerning the measured oxygen consumption curves.

Firstly, several runs were repeated to test the reproducibility of the results. The respective oxygen consumption curves are compared in Figure 15. It can be seen that the oxygen consumption curves are reproducible to within 0.1 ppm by the end of a run. This represents a good degree of reproducibility when it is remembered that individual oxygen readings are themselves accurate to ±0.02 ppm. In general, the Beckman oxygen sensor performed well during the experimental work. However, the kinetic data for several runs did have to be discarded due to erratic results. When this problem was encountered the sensor was dismantled, cleaned and the teflon membrane replaced, as recommended by the manufacturer. The "rejuvenated" sensor was then found to perform satisfactorily. It was found that the "life" of the sensor could be prolonged by leaving it (and particularly the membrane) immersed in distilled water when not in use.

Because of the dual nature of the effluent/artificial sea-water reaction, there was usually a "bump" or initial sharp jump in oxygen consumption immediately after effluent addition to the reaction vessel. This initial jump was the consequence of the initial alkaline pH of artificial sea-water (around 8.3), the small but finite time required to achieve complete dispersion of the effluent throughout the vessel and the time required for the completion of the acid-buffer interaction. Oxidation is extremely rapid above pH 7 (14) so, although the time

required for the pH to drop from 8.3 to below 7 was only of the order of a few minutes, a small degree of ferrous oxidation takes place at elevated pH values. Hence the initial jump in oxygen consumption. In general runs had "settled down" five minutes after effluent introduction and so the first five minutes of a run was designated as the initial mixing period.

Finally, a comment should be made on the percentage of introduced ferrous iron oxidised at the end of each monitored run. This can be calculated by noting that for each mg/l dissolved oxygen consumed, 7 mg/l Fe^{2+} will have been oxidised (see Section 3.3.1). From Figures 10 and 11 it can be seen that of the runs shown only Run 1, with $(Fe^{2+})_I$ = 10 mg/l, had proceeded to completion within two hours. For the others it can be calculated that the percentage of initial ferrous iron oxidised at the end of two hours varied from 74% for Run 7 ($(Fe^{2+})_I$ = 20 mg/l) to 51% for Run 11 ($(Fe^{2+})_I$ = 60 mg/l).

A two-hour period is thus sufficient in most cases to cover a majority of the total oxidation reaction. The greatest exception occurs with Run 15, run at a pH of around 6, where only 14% of the initial ferrous iron had been oxidised after two hours.

3.4.2 Kinetic Analysis of Closed Runs at 25°C

The oxygen consumption and pH curves recorded for the closed kinetic runs carried out at 25°C were analysed along the lines outlined in Section 3.3.4. The results of the kinetic analyses, in terms of the proposed rate constants k_A and k_B, are detailed in Tables 12 and 13. A comprehensive tabulation of monitored oxygen and pH values for all the kinetic runs undertaken is given, for reference, in Appendix 7.

Results show that the rate of ferrous oxidation is first order with respect to ferrous iron concentration and dissolved oxygen concentration. Calculated k_A values corresponding to the expression:

$$-\frac{d(Fe^{2+})}{dt} = k_A (Fe^{2+}) (O_2) \quad \text{.....} \quad (3E)$$

are given in Table 12. The appropriate logarithmic plots from which k_A values were estimated appear in Figure 16 and it can be seen that the results for each run fall on a very good straight line. The high degree of linearity achieved when the experimental results were plotted is reflected by the high values calculated for the linear correlation coefficients (Table 12), and shows that the rate of oxidation is very well empirically described by expression (3E). When the absolute value of the correlation coefficient is unity the corresponding points fall exactly on a straight line and the relationship is perfect (25). Calculations were made from t = 5 minutes to allow for the initial experimental mixing period in each run. The discrepancy between the initial value and later values due to this "unsteady-state" period when conditions are changing rapidly is illustrated in Figure 16. Errors in k_A were evaluated assuming an error of ±0.02 ppm in each oxygen reading and errors in $(Fe^{2+})_I$ as tabulated. The very high error in k_A for Run 1 can be attributed to the fact that in this case oxidation is all but complete after 65 minutes, and under these conditions the terms involved in calculating k_A (see equations (3G) and (3H)) become very sensitive to small changes in C and A values.

Although expression (3E) does describe the oxidation kinetics very well, the k_A values obtained, as shown in Table 12, are not constant within experimental error but vary dramatically according to the nature of the run carried out. A consideration of k_A values shows that they decrease for a particular effluent as initial ferrous iron

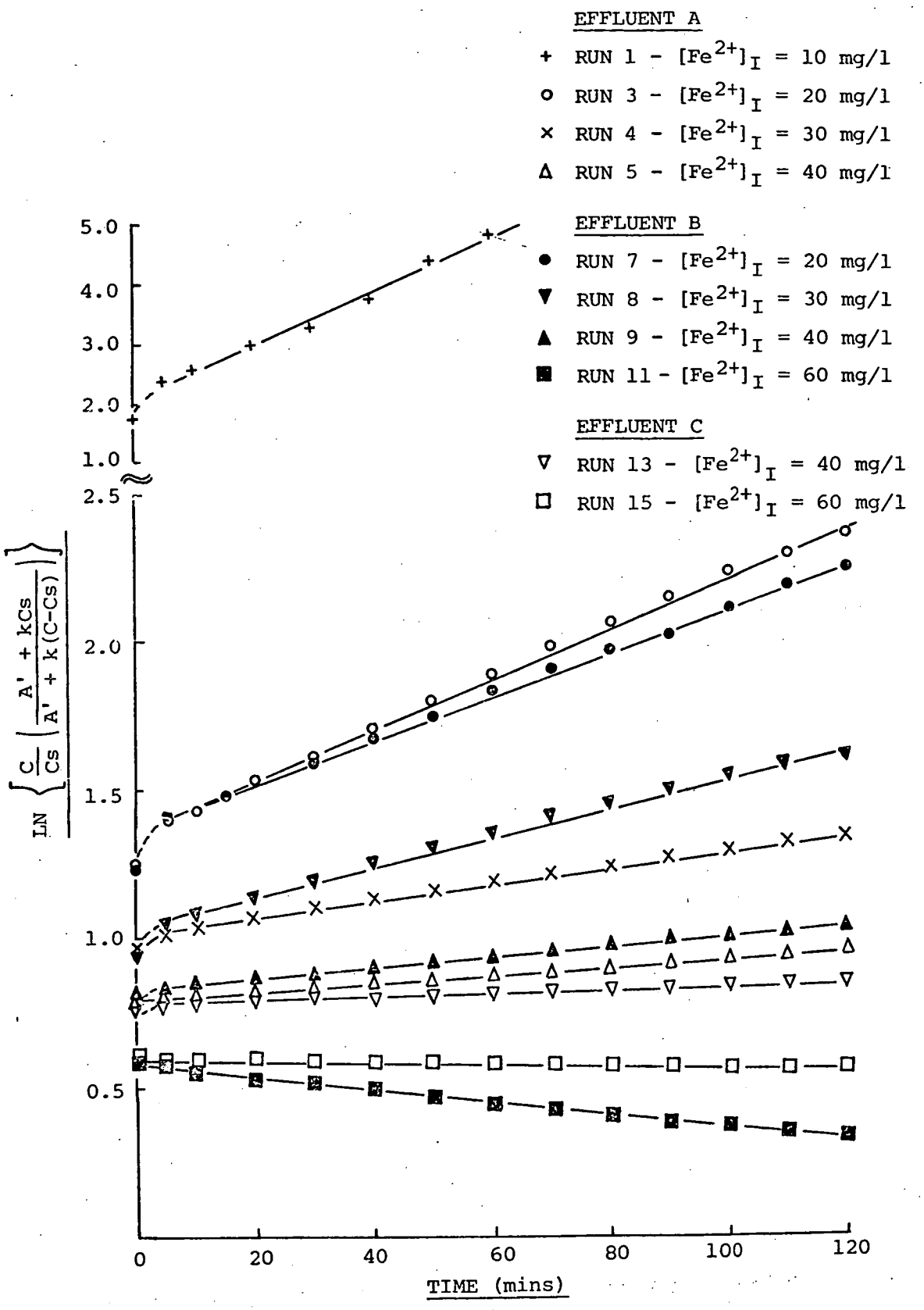

FIGURE 16 - KINETIC ANALYSIS OF CLOSED KINETIC RUNS

BASED ON EXPRESSION:

$$-\frac{d[Fe^{2+}]}{dt} = k_A[Fe^{2+}][O_2]$$

TABLE 12 - RESULTS OF THE KINETIC ANALYSIS OF RUNS BASED ON KINETIC EQUATION (3E)

Run Number	$(Fe^{2+})_I$ (mg/l)	Artificial Effluent	k_A (litre mole^{-1} min^{-1})	Error in k_A	Correlation Coefficient
1	10±0.2	A	260	±60	0.994
2	20±0.3	A	60	± 3	0.997
3	20±0.3	A	65	± 4	0.999
4	30±0.5	A	33.8	± 1.3	0.997
5	40±0.5	A	34.3	± 0.9	0.999
6	40±0.5	A	34.1	± 0.9	0.999
7	20±0.3	B	58	± 3	0.999
8	30±0.5	B	59	± 3	0.998
9	40±0.5	B	42.3	± 1.2	0.999
11	60±1	B	42.4	± 1.4	-0.999
13	40±0.5	C	16.9	± 0.4	0.998
14	60±1	C	5.6	± 0.2	-0.994
15	60±1	C	6.0	± 0.1	-0.998

concentration increases and decrease at a constant $(Fe^{2+})_I$ as effluent acidity increases. Both these trends are consistent with decreasing pH in solution and suggest that a pH term should be included in the ferrous oxygenation rate equation. Before considering a revised rate expression it is worth noting that k_A values for repeated runs (e.g. Runs 5 and 6) are very similar, again indicating that the results are reproducible to a good degree.

The above findings suggest that we should now test the kinetic data to see if it conforms to the rate expression:

$$-\frac{d(Fe^{2+})}{dt} = k_B (Fe^{2+}) (O_2) (OH^-)^n \quad \ldots\ldots \quad (3I)$$

where n is a set value yet to be determined and k_B is a new rate constant dependent only on temperature. Unfortunately, as shown in Figures 12 and 13, pH cannot be regarded as constant for the duration of a closed kinetic run as it gradually decreases, after the initial five minute mixing period, due to ferric hydrolysis.

This makes kinetic analysis difficult. In addition, on comparing expressions (3E) and (3I) we see that $k_A = k_B (OH^-)^n$. Now it has already been shown that, empirically, k_A can be taken to be a constant for each kinetic run. This suggests that as (OH^-) varies with time, then so must k_B and so expression (3I), at best, can only serve as an approximate description of the ferrous iron oxidation kinetics.

However, as discussed in Section 3.3.4, it is still possible to estimate an overall k_B value for each run (for a given value of n) by breaking down the run into separate five minute segments over which pH can be regarded as constant within experimental error. Individual calculated k_B values are then combined to give an estimated overall k_B for the run, the standard deviation of the individual values providing a measure of both experimental error and the tendency, if any, of values to vary with time. Such a procedure is worth carrying out as, with the qualifications expressed, it enables direct comparison of present kinetic results with those of previous workers such as Stumm and Lee (14). Also, as mentioned, there is a strong indication from the k_A values themselves that a (OH^-) term should be incorporated into the overall kinetic expression.

TABLE 13 - RESULTS OF THE KINETIC ANALYSIS OF RUNS BASED ON KINETIC EQUATION (3I)

Run Number	$(Fe^{2+})_I$ (mg/l)	Artificial Effluent	k_B VALUES n=1 (litre^2 mole^{-2} min^{-1}) /10^9	k_B VALUES n=2 (litre^3 mole^{-3} min^{-1}) /10^{16}
1	10±0.2	A	4.4±1.3	7.4±2.2
2	20±0.3	A	1.8±0.3	5.7±1.1
3	20±0.3	A	1.8±0.4	5.3±1.5
4	30±0.5	A	1.3±0.3	5.3±1.6
5	40±0.5	A	1.5±0.4	6.7±2.9
6	40±0.5	A	1.5±0.5	7.4±3.5
7	20±0.3	B	1.5±0.5	4.3±2.2
8	30±0.5	B	1.9±0.4	6.4±2.5
9	40±0.5	B	1.9±0.6	(9± 5)
11	60±1	B	2.6±0.8	(18±11)
13	40±0.5	C	0.9±0.3	5.2±2.2
14	60±1	C	0.5±0.2	5.6±2.7
15	60±1	C	0.6±0.2	6.6±2.6

Overall k_B values calculated from the experimental data are summarized in Table 13. Calculations were carried out assuming both a first-order and second-order oxidation rate dependence on hydroxyl ion concentration, i.e. with n=1 and with n=2. It can be seen that, as expected, there is a relatively large error associated with individual values. However, omitting the results of Runs 9 and 11, it can be seen that k_B values calculated with n=2 are all of the same order of magnitude. This is in stark contrast to the large scatter of the k_A values calculated for the same runs and suggests that the kinetic equation (3P), given below, is a more comprehensive description of the ferrous oxidation kinetics than equation (3E).

A comparison of k_B values shows that over the span of conditions covered by the experimental runs the oxidation kinetics are better described by a second order dependence on hydroxide ion concentration than by a first order dependence. The variation between k_B values for different runs is much less for n=2 than for n=1. In the former case, omitting Runs 9 and 11, the largest discrepancy between values corresponds to a factor of 1.7 and the difference is well within the range covered by the standard deviation of individual results. In contrast, k_B values for n=1 vary by up to a factor of 9 and values for runs involving effluent C differ markedly from those involving effluents A and B.

Thus, when the influence of pH is taken into account, we find that the kinetics of the ferrous oxidation reaction which takes place in artificial sea-water following the introduction of an acidic ferrous sulphate solution can be best empirically described by the equation:

$$-d\frac{(Fe^{2+})}{dt} = k_B\ (Fe^{2+})\ (O_2)\ (OH^-)^2 \qquad \ldots\ldots \qquad (3P)$$

The standard deviation associated with overall k_B values shown in Table 13 represents a combination of the following:

errors associated with the numerical integration technique (i.e. the assumption that pH for each run can be taken to be constant over separate five-minute intervals), experimental errors, and the tendency of k_B values to increase with time.

Half the error can be attributed to the first two factors.

This can be shown by a detailed consideration of the terms involved in calculating "five minute" k_B values (equation (3K)), assuming measurement errors of ±0.02 ppm in oxygen readings and ±0.02 pH unit in pH readings. The high sensitivity of k_B to small changes in pH accounts for the relatively large error involved. The tendency of k_B to increase in value with time thus accounts for the other half of the calculated standard deviation, and this gives an estimation of the magnitude of the trend. Given that two hours is sufficient time to cover the majority of the total oxidation in most cases, we will take the k_B values shown in Table 13 as representative of the average rate of oxidation achieved for each run. Combining the values shown (leaving out Runs 9 and 11), together with their respective errors, yields an overall average value for the rate constant k_B in equation (3P) of $5.7 \pm 0.6 \times 10^{16}$ litre^3 mole^{-3} min^{-1}. This value can now be used, for comparison purposes, to represent the net oxidation rate experimentally obtained in the present work.

Equation (3P), which has been found to give the best detailed empirical fit to the present experimental results, is the established kinetic expression describing the rate of ferrous iron oxidation in low ionic-strength bicarbonate waters, for ferrous concentrations lower than 2 mg/l (14, 15, 16). The present work indicates that the kinetic expression also describes the rate of ferrous iron oxidation in a high ionic-strength bicarbonate water, such as sea-water, and applies to soluble ferrous concentrations up to 60 mg/l. A comparison of experimentally determined rate constants at 25°C is given in Table 14. It can be seen that the estimated average value for k_B obtained in the present study compares very well with other reported values for k_B. Even allowing for the degree of "time variance" in the present results,

we can infer from this that the rate of oxidation of ferrous iron in artificial sea-water is basically of the same order as the rate of oxidation of ferrous iron in low ionic strength bicarbonate waters.

The suggested similarity between the rates of ferrous oxidation is surprising given the high ionic strength and low alkalinity (see Table 14) of artificial sea-water compared to other media studied. There is some theoretical basis for proposing that the rate of the ferrous oxidation reaction will be independent of ionic strength. The Brønsted equation (28) proposes that the influence of ionic strength on the rate of a reaction is dependent on the product of the ionic charges of the reactants. When the product is zero, as is the case with the reaction between Fe^{2+} and O_2 (soluble)(N.B. + 2 x 0 = 0), then the equation predicts that the kinetic rate will be independent of ionic strength.

As regards the low alkalinity of artificial sea-water (remembering that the alkalinity is the same as the true alkalinity of real sea-water),Ghosh (15) has found that the rate of ferrous oxidation is independent of alkalinity when the corresponding buffer capacity of the solution is less than 4×10^{-3} equiv/litre at $25^{o}C$. Buffer capacity is related to solution alkalinity and pH. In the case of artificial sea-water, the range of alkalinity and pH values spanned was such that a buffer capacity of 4×10^{-3} equiv/litre would not have been exceeded in any of the runs carried out. However, this does not apply for the other alkalinity ranges outlined in Table 14. On the basis of the results of Ghosh we could expect the ferrous oxidation rate in artificial sea-water to be as much as three times slower, other factors omitted, than the oxidation rate in solutions of alkalinity greater than 2×10^{-2} equiv/litre. Table 14 shows that this does not appear to be the case. This suggests that the oxidation

TABLE 14 - COMPARISON OF OXIDATION RATE CONSTANTS

@ 25°C (k_B - EQUATION (3P)) (15)

Alkalinity (eq/l)	k_B (litre^3 mol^{-3} min^{-1}) /10^{16}	Reference
1.0×10^{-3}-2.2×10^{-3}	5.7±0.6	Present Study
2.9×10^{-2}-3.9×10^{-2}	10.8±4.5	14
3×10^{-2}-5×10^{-2}	1.6±0.4	16
2.8×10^{-2}-4.1×10^{-2}	3.8	15
1.8×10^{-2}-3.2×10^{-2}	2.0-7.0	27

rate in artificial sea-water may, in fact, be enhanced by some ionic effect.

It is worth noting that in their original work Stumm and Lee (14) observed that k_B values tended to decrease as alkalinity decreased. This applied to alkalinity values down to 9×10^{-3} equiv/litre, the lowest they studied. All previous workers have carried out their experimental runs at constant pH and with a solution of constant alkalinity. However, in the present work, because pH changes during a run so does solution alkalinity. The variation of alkalinity with pH for artificial sea-water has already been calculated and is shown in Figure 4. It can be seen that in the pH range 6.8 - 5.9 (covered by the present work) the alkalinity drops sharply from 2.2×10^{-3} eq/l to 1.0×10^{-3} eq/l. If the results of Ghosh are not applicable to the high ionic-strength artificial sea-water matrix,then the fact that the sea-water alkalinity is not constant during a run, but decreases as the ferrous oxidation reaction proceeds, would tend to result in a decrease in k_B values with time. However, in fact, the

opposite trend is observed when fitting the experimental results to equation (3P) and so it is not possible to assess the applicability of Ghosh's findings.

Before moving on to a discussion of the effect of temperature on the oxidation reaction, a note should be made on the kinetic analysis of Runs 9 and 11. Looking back at Table 13 we see that, as already mentioned, k_B values for Runs 9 and 11 are in disagreement with those calculated for the other experimental kinetic runs. The reason for this is not immediately clear. However, these two runs were carried out with effluent B, the least acidic effluent, at high values of $(Fe^{2+})_I$. A comparison of the respective pH curves (Figure 13) with the ferrous iron solubility diagram (Figure 5) shows that, because of their nature, Runs 9 and 11 exceeded the calculated solubility limits for ferrous carbonate for the greatest length of time of any of the experimental runs carried out. In the case of Run 11 ($(Fe^{2+})_I$ = 60 mg/l) the solubility limit may have been exceeded for up to the first fifteen minutes of the reaction. This compares with less than five minutes for the majority of the other experimental runs.

Given the short time involved, the rapid change of conditions in the initial mixing period, and the fact that supersaturated solutions of ferrous carbonate often exist without precipitation (14), it is unlikely that any $FeCO_3$ would have been precipitated in any of the kinetic runs other than Runs 9 and 11. However, it is possible that a degree of precipitation may have occurred in the case of these latter two runs and this could explain the discrepancy in calculated rate constant (k_B) values. Ghosh et al (29) found that the kinetics of ferrous oxidation was disturbed by the precipitation of ferrous carbonate and the subsequent re-solution and oxidation of this species.

It is also worth mentioning that the recorded variation of pH, as oxidation proceeded, was greater for Run 11 than for any other run carried out (see Figure 13). This is due in part to the comparitively low acidity of effluent B. The numerical integration technique used to evaluate overall k_B values assumes that pH is constant over separate five-minute intervals. The error associated with this assumption is thus the greatest in the case of Run 11, and this helps explain the very large error in the estimated overall k_B value.

3.4.3 Closed Kinetic Runs at 12°C

The influence of temperature on the kinetics of the ferrous oxidation reaction was investigated by carrying out a series of runs using artificial sea-water and artificial effluent A at a temperature of 12°C. This temperature is probably a more realistic estimate of the temperatures likely to be found in the ocean waters pertinent to the present study, but the bulk of kinetic runs were carried out at 25°C to enable a comparison of results with the work of previous researchers and with theoretical solubility calculations.

The solubility of oxygen in sea-water increases with decreasing temperature. In a typical sea-water of salinity 35 ‰ oxygen solubility increases from 7.0 ppm to 8.8 ppm as the temperature decreases from 25°C to 12°C (21). In the case of the artificial sea-water matrix employed in the present work, measured saturated oxygen concentrations varied around 6.9 ppm at 25°C and around 8.5 ppm at 12°C. The good agreement of these values with those for a typical real sea-water is further indication that the artificial sea-water matrix can serve as a model for real sea-water in appropriate laboratory experiments.

The pH of artificial sea-water was also found to vary with

temperature, decreasing from an average of 8.38 at 25°C to an average of 8.27 at 12°C. This can be attributed to the effect of temperature on the various ionic equilibria describing the bicarbonate buffer system. Both pH values lie well within the range measured in real surface ocean waters (21).

Results of the runs carried out at 12°C are illustrated in Figure 17. Tabulated values of oxygen concentration and pH are given in Appendix 7. Oxygen consumption curves can be compared directly with those shown in Figure 10 and it can be seen that the rate of oxygen consumption (and thus ferrous oxidation) is substantially decreased by lowering the temperature from 25°C to 12°C. Comparing runs involving the same effluent (effluent A) at the same initial ferrous iron concentration, we see that the oxygen consumed at 12°C after four hours is less than that consumed at 25°C after two hours. For example, for $(Fe^{2+})_I$ = 20 mg/l the respective oxygen consumptions are 1.7 ppm (12°C - 4 hrs) and 2.1 ppm (25°C - 2 hrs), and for $(Fe^{2+})_I$ = 40 mg/l, 1.6 ppm (12°C - 4 hrs) and 2.9 ppm (25°C - 2 hrs). It can also be seen that whereas the amount of oxygen consumed at 25°C after two hours increases directly with $(Fe^{2+})_I$ up to 40 mg/l, this is not the case at 12°C after four hours, though the shape of the oxygen consumption curves indicates that such a relationship will be attained eventually.

The lower oxidation rate at 12°C corresponded to an observed slower rate of colour development in the reaction vessel. It was decided to monitor the 12°C runs over a four hour period to cover at least a sizeable proportion of the total oxidation reaction. For the purposes of kinetic analysis it was sufficient to divide the runs into separate ten-minute periods, as pH could be regarded as constant over

FIGURE 17 - OXYGEN CONSUMPTION CURVES FOR EFFLUENT A @ 12°C.

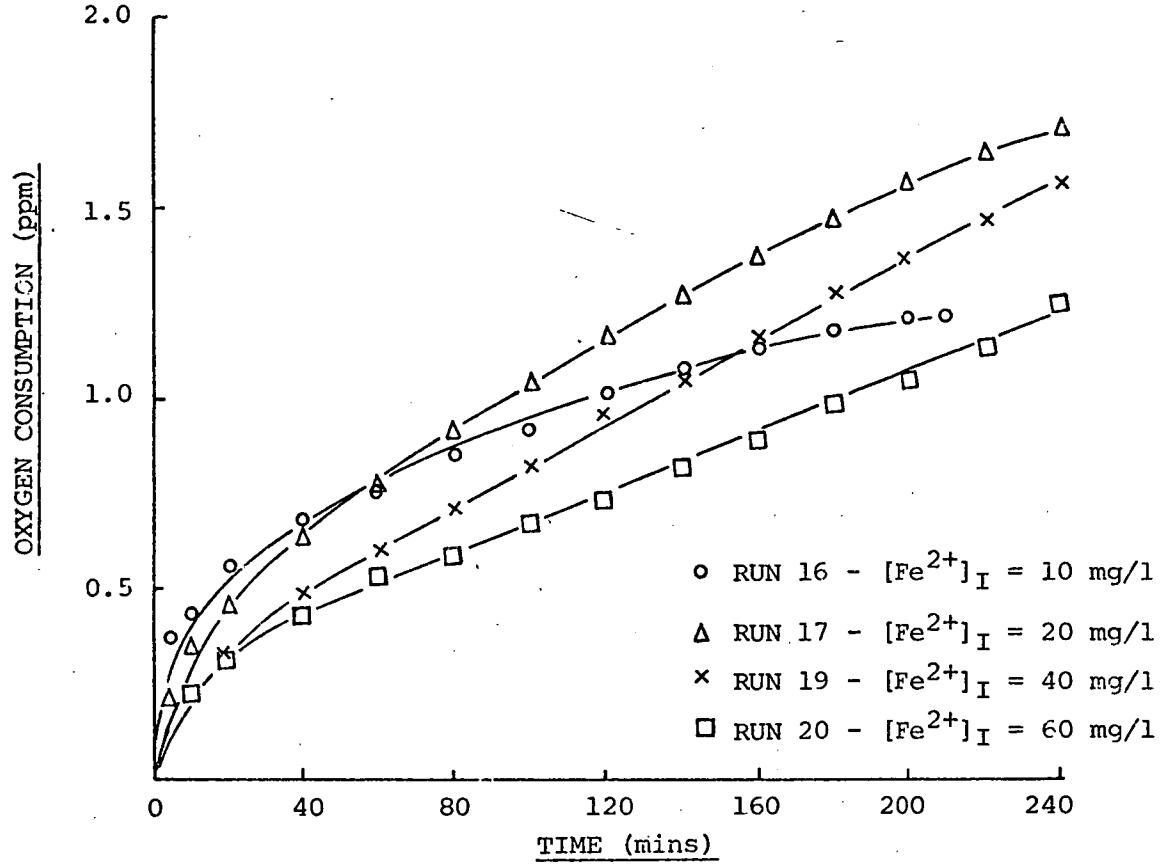

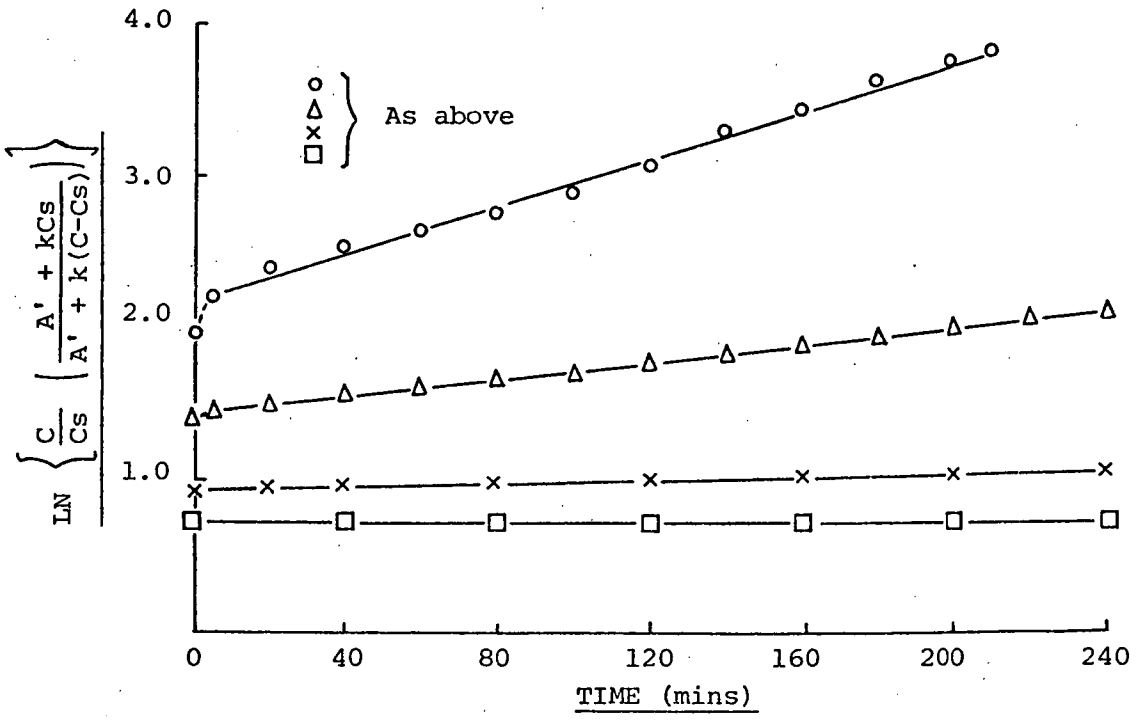

FIGURE 18 - KINETIC ANALYSIS OF RUNS @ 12°C BASED ON EQUATION (3E)

TABLE 15 - RESULTS OF THE KINETIC ANALYSIS OF CLOSED RUNS AT 12°C

Run Number	$(Fe^{2+})_I$ (mg/l)	Artificial Effluent	k_A (litre mole^{-1} min^{-1})	Correlation Coefficient	k_B (litre^3 mole^{-3} min^{-1}) /10^{16}
16	10±0.2	A	35.2±4.3	0.998	1.1±0.4
17	20±0.3	A	15.3±0.6	0.999	1.5±0.5
18	40±0.5	A	6.1±0.1	0.999	0.8±0.3
19	40±0.5	A	5.0±0.1	1.000	1.1±0.3
20	60±1	A	2.2±0.1	0.995	0.8±0.3

N.B. $$-d\frac{(Fe^{2+})}{dt} = k_A (Fe^{2+}) (O_2) \quad \ldots\ldots \quad (3E)$$

$$-d\frac{(Fe^{2+})}{dt} = k_B (Fe^{2+}) (O_2) (OH^-)^2 \quad \ldots\ldots \quad (3P)$$

this increment of time. The results of the kinetic analysis of the runs, in terms of the proposed rate constants k_A (expression (3E)) and k_B (expression (3P)), are given in Table 15. Run 18 was carried out at the same $(Fe^{2+})_I$ as Run 19 but at a higher pH due to the higher initial pH of the artificial sea-water solution used (see Appendix 7). Deviations in initial pH values were due to such factors as human error in solution preparation and differences in aeration time.

The kinetic analysis of the 12°C closed runs yields the same conclusions as those drawn from the 25°C closed runs and shows that the kinetic expressions describing the oxidation reaction apply equally well at both temperatures. Logarithmic plots from which k_A values at

$12^{o}C$ were estimated are given in Figure 18. As was the case in Figure 16, it can be seen that the experimental results for each run fall on a very good straight line, reflecting the ability of expression (3E) to empirically describe the oxidation kinetics. Correlation coefficients for each plot appear with k_A values in Table 15. However, although each k_A value qualifies a run, it can be seen that k_A values for different runs vary widely and show the same trend as before of decreasing as the pH of solution decreases. Once again this indicates that a (OH^-) term should be included in (3E) to give a more comprehensive kinetic expression.

When the term $(OH^-)^2$ is included in the kinetic expression (equation 3P) then it can be seen from Table 15 that the corresponding overall rate constants, k_B, exhibit only a minimal variance between different runs and this variance is within the error estimated for separate values. Again, however, it was found that in the numerical integration calculation of overall k_B values individual "ten-minute" k_B values within a run exhibited a tendency to increase with time. With this qualification we can state that equation (3P) gives a good empirical description of the ferrous oxidation kinetics at $12^{o}C$, with the k_B values of Table 15 giving an average oxidation rate for each run.

As k_B values are independent of solution pH they provide a basis on which to compare the ferrous oxidation rates at different temperatures. Comparing Tables 13 and 15, we see that the net oxidation rate at $25^{o}C$ is roughly six times greater than the net oxidation rate at $12^{o}C$. Values in Table 15 can be combined to give an overall average value for k_B for the kinetics at $12^{o}C$ of $1.0 \pm 0.1 \times 10^{+16}$ $litre^3\ mole^{-3}\ min^{-1}$. This compares with the average value at $25^{o}C$

of $5.7 \pm 0.6 \times 10^{+16}$ litre^3 mole^{-3} min^{-1}. As both these values are averages taken over roughly equivalent periods of the oxidation reaction (as regards degree of oxidation) then their ratio should be comparatively independent of time. By substituting the ratio into a form of the Arrhenius equation we can obtain an estimation for the activation energy, Ea, for the reaction. The calculations are outlined in Appendix 5 and the estimated activation energy for the ferrous oxidation reaction in artifical sea-water is $9.6 \pm 1.3 \times 10^4$ joules/mole (23 ± 3 kcal/mole).

The above obtained value for Ea is in excellent agreement with the value of 9.6×10^4 joules/mole (no error quoted) established by Stumm and Lee (14) for the oxidation of ferrous iron in low ionic-strength bicarbonate waters, and the similarity between the values points to the validity of the present work. The value compares with an activation energy of 7.5×10^4 joules/mole for the oxygen oxidation of acidic ferrous sulphate solutions (30).

3.4.4 Closed Runs at 25°C Using Samples of Real Sea-Water & Industrial Effluent

The oxidation reaction resulting on the introduction of an industrial acidic ferrous iron solution to sea-water has thus far been simulated in the laboratory by the use of simplified "artificial" solutions. To assess the applicability of the kinetic results found using artificial solutions to the real situation, a series of closed runs were undertaken at 25°C using real sea-water samples and samples of Tioxide industrial effluent.

Initially, to compare the influence of real sea-water as opposed to artificial sea-water, a few runs were carried out using real sea-water samples and an artificial effluent. On aeration real sea-water samples were found to have an average pH at 25°C of 8.26 and an average saturated oxygen concentration of 6.8 ppm. This compared with values of 8.38 and 6.9 ppm for the simulated artificial sea-water. Because of the slightly lower pH in the real sea-water samples and the strong dependence of the oxidation kinetics on the pH of solution, it was decided to use a new artificial effluent, effluent D, in the required real sea-water runs. The acidity of this effluent (given in Table 11) was designed so that, at a given $(Fe^{2+})_I$, the pH variation with time in a real sea-water sample would be similar to that recorded for effluent A in artificial sea-water. This would enable the respective oxygen consumption curves to be compared directly.

Oxygen consumption curves recorded in real sea-water at $(Fe^{2+})_I$ values of 20 mg/l and 40 mg/l are shown in Figure 19, and compared with those recorded for similar runs using effluent A and artificial sea-water. The corresponding pH curves are given in Figure 20. Tabulated values for the runs appear in Appendix 7. The 20 mg/l run was repeated to assess the ability to reproduce results in samples of real sea-water. As can be seen, the results were reproduced to an excellent degree, but it should be kept in mind that both sea-water samples involved came from the one bulk sample so that the reproducibility attained reflects on the accuracy of the experimental technique rather than on the effect of differences in sea-water composition on the oxidation reaction.

From the oxygen consumption curves given in Figure 19 we see that although there appears to be a difference in the initial response, with time runs carried out in real sea-water samples do not differ too

FIGURE 19 - COMPARISON OF OXYGEN CONSUMPTION IN REAL AND ARTIFICIAL SEA-WATER @ 25°C.

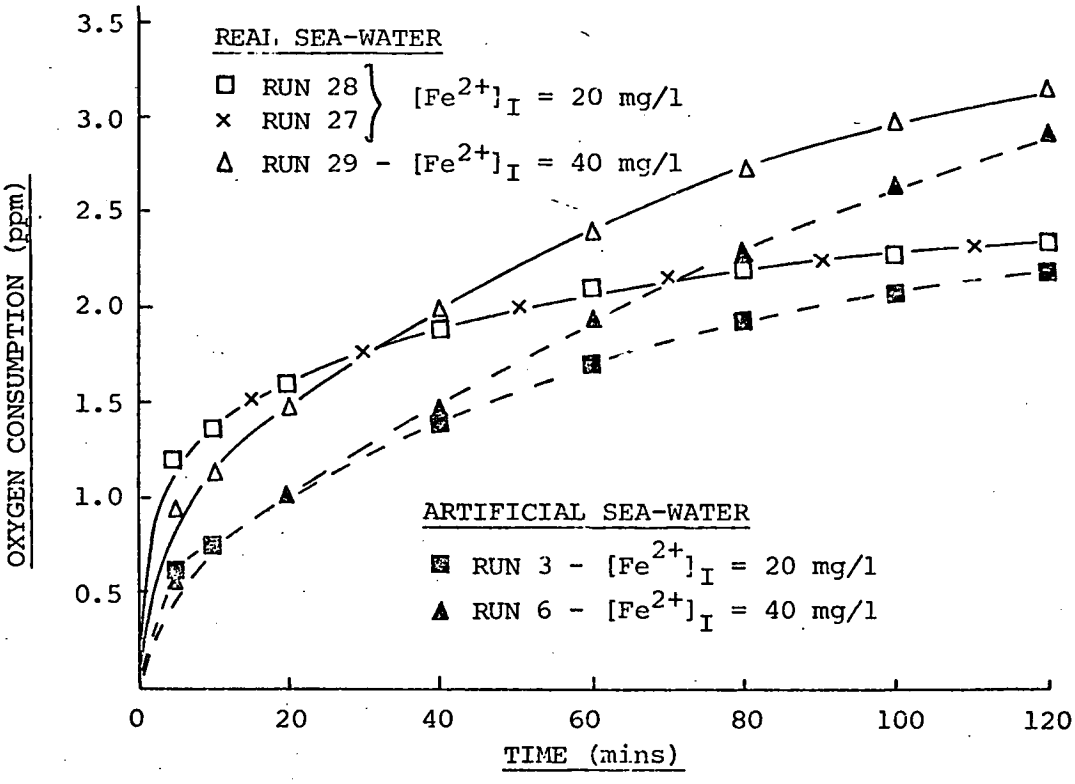

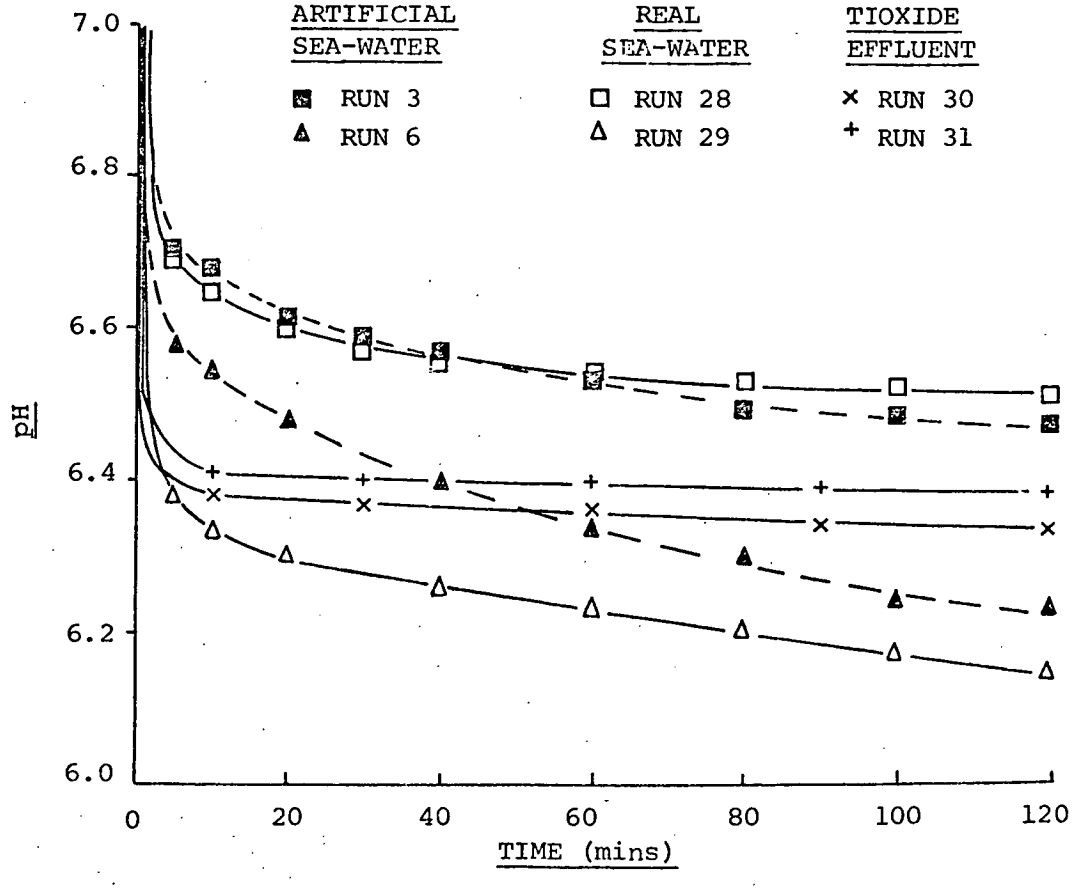

FIGURE 20 - COMPARISON OF pH VARIATIONS (EXPANDED SCALE)

greatly from those carried out in artificial sea-water. The oxygen consumption in both cases tends to a single value determined by the initial ferrous iron concentration, and the rate of the oxidation reaction is of the same magnitude in both solutions. The curves corresponding to a $(Fe^{2+})_I$ of 20 mg/l can be compared directly due to the similarity of the respective pH curves (Figure 20). However, at a $(Fe^{2+})_I$ of 40 mg/l the pH curves differ by roughly 0.1 pH unit and kinetic analysis of the data is required in order to be able to quantitatively compare ferrous oxidation rates.

Kinetic analysis of the real sea-water/artificial effluent runs carried out reinforces the finding that differences between real sea-water and the artificial sea-water used to simulate it cause comparatively minor differences in the rate of ferrous oxidation. Kinetic analysis results are compared in Table 16. It can be seen that at $(Fe^{2+})_I$ = 20 mg/l values for the rate constants k_A and k_B, for runs in real and artificial sea-water, are in excellent agreement. The initial catalytic effect observed in the real sea-water samples, but not in artificial sea-water (see Figure 19), does not substantially alter the computed values for the two overall rate constants but is reflected by the lower correlation coefficients corresponding to the "k_A" logarithmic plots for the real sea-water runs.

In the case of the real sea-water run carried out at $(Fe^{2+})_I$ = 40 mg/l, the rate constant k_A is in good agreement with the corresponding value found in artificial sea-water. However, when the influence of pH is included the k_B value calculated is anomalous and on the basis of previous results would appear to be too high. One explanation could be an experimental error in the measured pH curve causing it to be depressed. The good agreement obtained between pH curves for real and artificial sea-water runs carried out at $(Fe^{2+})_I$ = 20 mg/l suggests

TABLE 16 - COMPARISON OF REAL SEA-WATER AND ARTIFICIAL SEA-WATER RUNS

Run Number	Effluent	Nature of Sea-water	$(Fe^{2+})_I$ (mg/l)	k_A (litre $mole^{-1}$ min^{-1})	Corr. Coefft.	k_B (litre^3 $mole^{-3}$ min^{-1})/10^{16}
3	A	Artificial	20±0.3	65±4	0.999	5.3±1.5
27	D	Real	20±0.3	70±6	0.989	5.5±1.6
28	D	Real	20±0.3	70±6	0.988	5.3±1.3
6	A	Artificial	40±0.5	34±1	0.999	7.4±3.5
29	D	Real	40±0.5	38±1	0.999	13.2±2.6

that this may be so, but it remains to be shown by further experimental work.

Overall, the results of the runs carried out in real sea-water accord with the previous findings made using the artificial sea-water matrix. This suggests that the latter has provided a good basis for an initial investigation into the kinetics of the ferrous oxidation reaction in sea-water. It also suggests that the concentrations of the more common minor elements found in sea-water are such that they have little significant effect on the magnitude of the oxidation kinetics.

Up to date the ferrous iron oxidised has been introduced into the sea-water matrix in the form of an artificial ferrous sulphate/sulphuric acid solution. To compare this artificial effluent with a real titanium dioxide industrial acid-iron effluent, several closed kinetic runs were undertaken using samples of Tioxide effluent. Two bulk effluent samples were obtained from the company and relevant details concerning the samples and the runs in which they were used are

TABLE 17 - RUNS INVOLVING TIOXIDE EFFLUENT SAMPLES

Effluent Sample	When Sampled	Estimated Ferrous Content (prior to use)
1(A)	2/10/75	28.2±0.3 gms/l
2	12/ 5/76	22.3±0.2 gms/l

Run Number	Effluent Sample	Nature of Sea-water	Dilution Factor	$(Fe^{2+})_I$ (mg/l)
30	1	Real	1:1500	18±0.5
31	2	Real	1:1500	14±0.5
32	2	Artificial	1:1500	14±0.5
33	2	Real	1:3000	7±0.3

given in Table 17.

The ferrous content of the effluent samples was determined by titration with potassium permanganate solution, as discussed in Section 2.6.2.

Tioxide effluent is much more acidic than the artificial effluents used in the present study. Whereas the acid/iron ratio in the most acidic artificial effluent used, effluent C, was 0.9 (Table 11), the ratio in Tioxide effluent is greater than 2 (Section 1.2). This limits the dilution range that can be studied by the present experimental method. Kinetic runs at dilution factors less than 1:1500 were not attempted because the oxidation reaction has already been shown to be extremely slow at pH values less than 6. At the other extreme, at dilution factors greater than 1:3000, the amount

of ferrous iron introduced into solution is too small to obtain a meaningful oxygen consumption for kinetic analysis. The span of $pH/(Fe^{2+})_I$ values covered on the dilution of Tioxide effluent 1(A) in real sea-water has already been investigated in Section 2.6 and is shown in Figure 5.

Oxygen consumption curves for the Tioxide effluent closed kinetic runs undertaken are given in Figure 21, and compared with the oxygen consumption curves for artificial effluent runs of roughly equivalent initial ferrous iron concentration. Details of all the runs shown, together with kinetic analysis results in terms of the estimated rate constant k_B (equation (3P)), are given in Table 18. Tabulated values of oxygen concentration and pH are given, for reference, in Appendix 7.

From Figure 2i it can be seen that the rate of oxygen consumption in all the Tioxide effluent runs undertaken was much slower than for the equivalent artificial effluent runs. Tioxide runs were monitored for up to 7 hours to obtain a reasonable degree of oxygen consumption in solution. In determining an overall k_B value for each run, pH could be regarded as constant over increments of 30 minutes. The shape of the oxygen consumption curves indicates that in the Tioxide effluent runs of highest $(Fe^{2+})_I$, the oxidation reaction was retarded over a lengthy initial period, as evidenced by an observed lack of colour development in the reaction vessel in the first three hours.

In comparing oxygen consumption curves note has to be taken of both initial ferrous iron concentration and the solution pH. Tioxide effluent runs were undertaken at lower pH than the equivalent artificial effluent runs. This can be seen by comparing the pH curves shown in Figure 20. The pH curves for Runs 30 and 31 are roughly 0.3 pH unit lower than those for Runs 3 and 28 at the onset of oxidation.

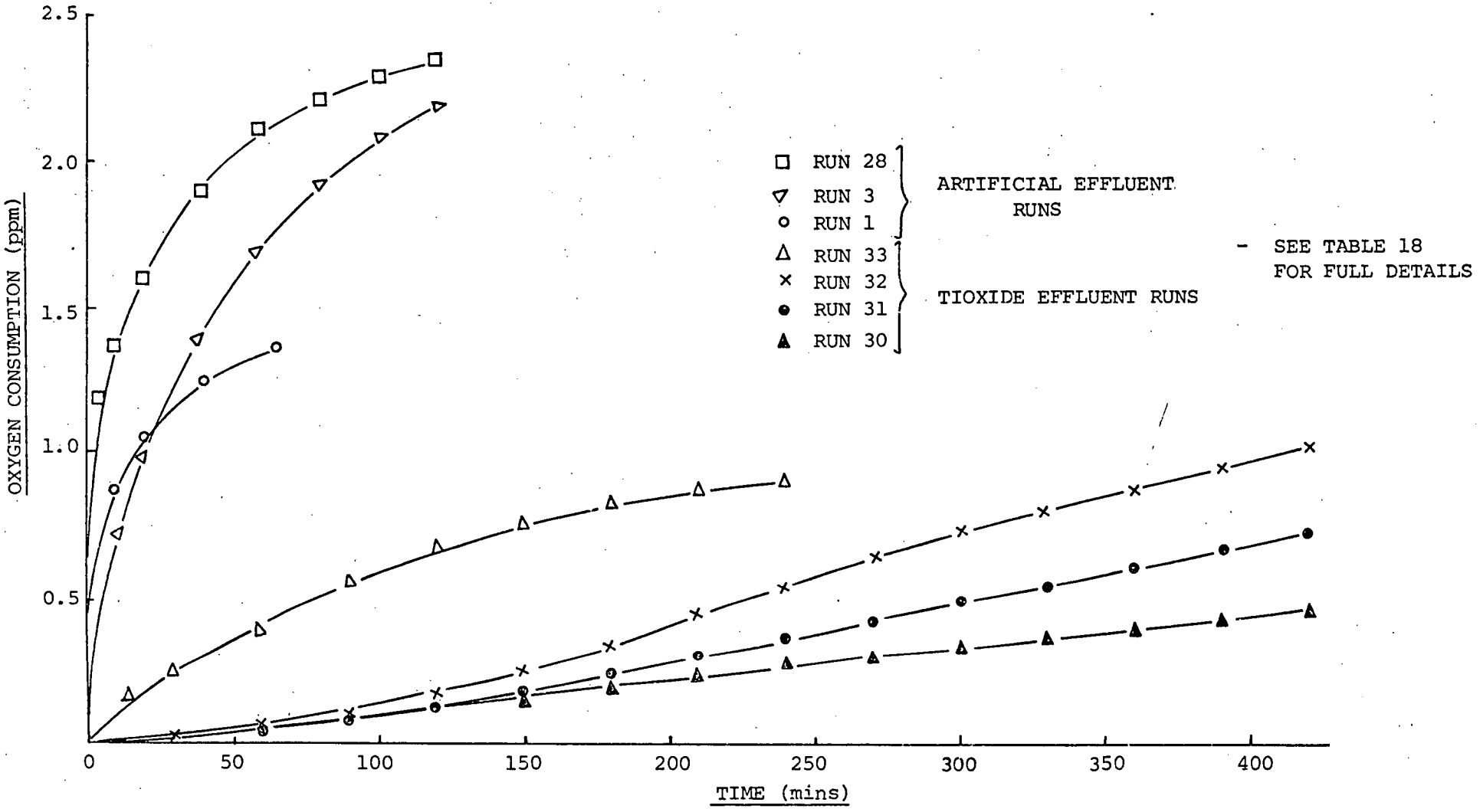

FIGURE 21 - COMPARISON OF OXYGEN CONSUMPTION CURVES AT 25°C FOR ARTIFICIAL EFFLUENT AND TIOXIDE INDUSTRIAL EFFLUENT

TABLE 18 - COMPARISON OF ARTIFICIAL EFFLUENT AND TIOXIDE EFFLUENT RUNS (See Figure 21).

Run Number	Nature of Effluent	Nature of Sea-Water	$(Fe^{2+})_I$ (mg/l)	Estimated Rate Constant k_B (litre^3 mole^{-3} min^{-1}) /10^{16}
28	Artificial	Real	20	5.3±1.3
3	Artificial	Artificial	20	5.3±1.5
1	Artificial	Artificial	10	7.4±2.2
33	Real	Real	7	1.7±0.6
32	Real	Artificial	14	3.0±1.5
31	Real	Real	14	1.2±0.5
30	Real	Real	18	0.5±0.1

The slow rate of ferrous oxidation in the Tioxide effluent runs is reflected by the near horizontal nature of the respective pH curves over the initial two-hour period.

However, pH is taken into consideration when calculating values for the overall rate constant k_B. Comparing the values given in Table 18, it is clear that, in fact, in all the runs undertaken with Tioxide effluent the rate of oxidation of ferrous iron is substantially lower than found previously. This applies to runs using both real and artificial sea-water. The difference between k_B values for artificial effluent runs and Tioxide effluent runs is too great to be explained by any limitations in the method of determining the rate constants.

As has already been discussed, results of runs undertaken with artificial effluent (e.g. compare Runs 3 and 28) show that differences between real sea-water and the artificial sea-water used to simulate it do not greatly affect the kinetics of the ferrous oxidation reaction. The difference in the sea-water matrices thus does not explain the observed damping of the oxidation reaction in the Tioxide effluent runs. It appears, therefore, that ferrous oxidation is retarded by some component or speciation of the Tioxide effluent, though the retardation may be greater in real sea-water than in artificial sea-water (Runs 31 and 32). An explanation for these findings will require a detailed analysis of the nature of the industrial effluent and an investigation of the effect of trace elements, such as manganese and titanium, on the ferrous oxidation reaction. This work is left as a suggestion for a future research programme.

3.4.5 Open Kinetic Runs at 25°C

In the real situation, ferrous oxidation may take place in surface ocean waters with an accompanying transfer of oxygen from the atmosphere into solution to replace deplenished dissolved oxygen. It was thus of interest to repeat several of the previous closed kinetic runs under open conditions. The experimental method has been given in Section 3.3.3. It was also of interest to see if a model could be proposed describing the resultant rate of oxygen consumption in sea-water. The net rate and extent of oxygen decrease is of importance in considering the effect of ferrous iron disposal at sea on marine life.

The kinetic analysis of open kinetic runs is discussed in Section 3.3.4. A model describing the rate of transfer of oxygen across the air-solution interface has been proposed and tested, and appears to be valid as a first approximation (see Figure 9). From the re-aeration runs carried out, the rate of oxygen transfer into solution has been described in terms of a "re-aeration constant", k_R, which is directly dependent on the rate of the stirrer speed in the reaction vessel. Combining the expression for oxygen transfer from the atmosphere with the expression for the rate of oxygen consumption due to the ferrous oxidation reaction (as determined in the closed kinetic runs), yields an overall relationship predicting the net oxygen consumption recorded in the open kinetic runs (see Appendix 4).

The above overall relationship is expressed in terms of the constants k_R and k_A. Thus, using the determined values for k_R from the re-aeration runs, it is possible, by trial and error, to obtain a value for the oxidation rate constant k_A (equation (3E)) from the data of each open kinetic run. If values are in agreement with k_A values found from the corresponding closed kinetic runs then we can conclude that the open situation has been satisfactorily modelled.

Oxygen consumption curves obtained in open kinetic runs are compared with those for equivalent closed kinetic runs in Figures 22A and 22B. All runs were carried out using artificial sea-water. Tabulated values of oxygen concentration are given in Appendix 7. Because equivalent runs used artificial effluents of the same acidity, comparisons can be made directly without considering pH. It can be seen that the open kinetic run curves have an inherent different shape to the closed kinetic run curves, as the result of oxygen diffusing into solution from the atmosphere. Present results indicate that the amount of oxygen transferred into solution becomes substantial above

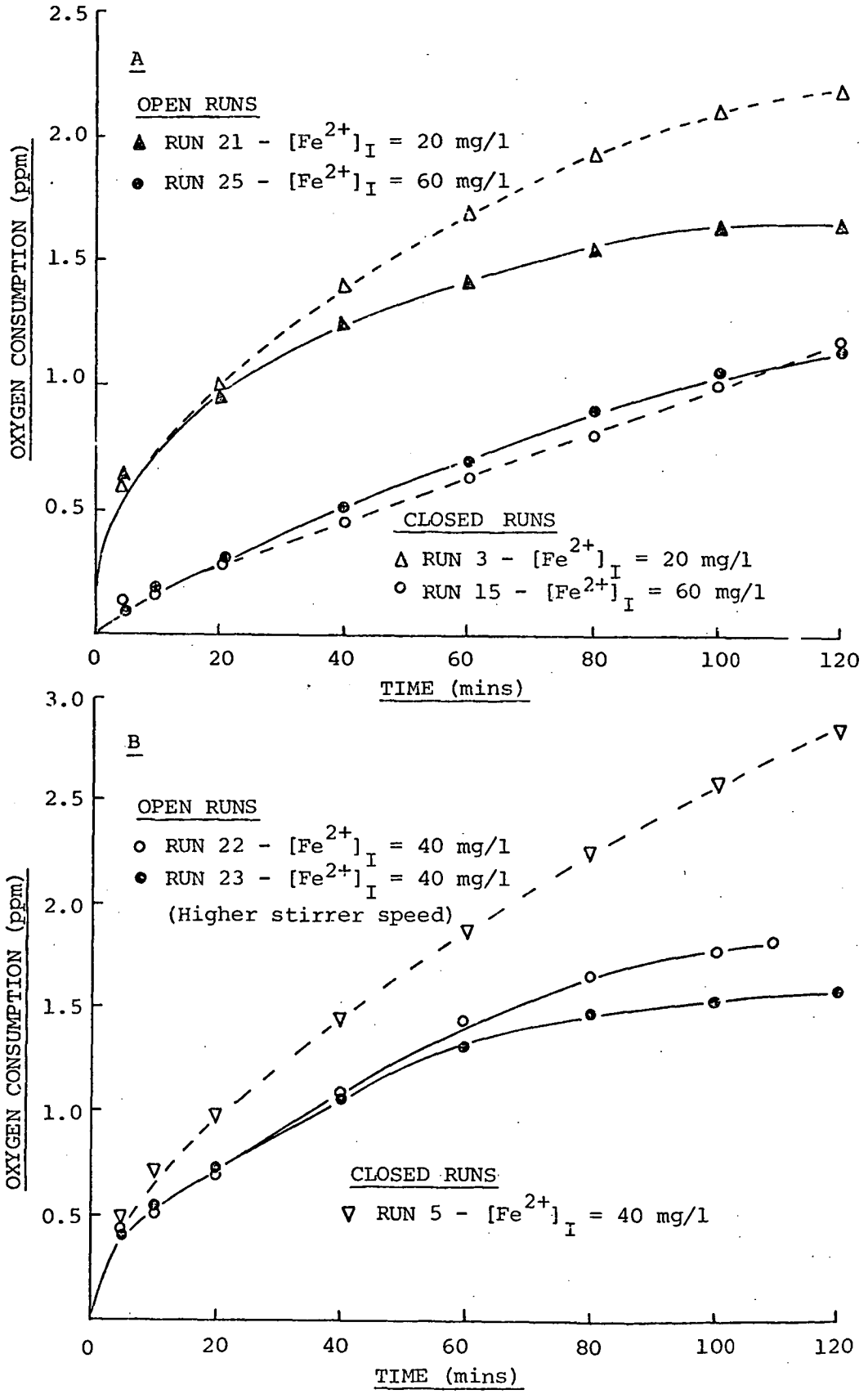

FIGURE 22 - COMPARISON OF OXYGEN CONSUMPTION CURVES FOR CLOSED AND OPEN KINETIC RUNS AT 25°C.

an oxygen consumption value of 1.0 ppm, though this is somewhat dependent on the actual experimental set-up. It is clear, however, that the rate of oxygen transfer between the air and the simulated sea-water solution is rapid enough to increasingly offset the oxygen consumed in the ferrous oxidation reaction.

The amount of oxygen transferred into solution depends in the present situation on the stirrer speed in the reaction vessel. Two different stirrer speeds were employed in the open kinetic runs carried out. The influence of the stirrer speed on the obtained oxygen consumption curve is illustrated in Figure 22B. As could be expected, the net oxygen consumption recorded in the artificial sea-water decreases for a given run as stirrer speed increases. At the top stirrer speed there was a vortex in the vessel of approximately 1 cm depth, but there was no entrainment of air into the solution. Downing and Truesdale(26) have found that the rate of solution of oxygen in saline water increases with increasing wind velocity, stirring, wave height and temperature.

Results of the kinetic modelling of the open kinetic runs are shown in Figures 23A and 23B. The corresponding estimated rate constant (k_A) values are given in Table 19, and compared with those calculated for equivalent closed kinetic runs. If allowance is made for an initial mixing period in each run, then Figure 23 shows that for a given k_A value, and using the previously estimated k_R values, a reasonable agreement is obtained between predicted and measured oxygen consumptions for each run. From the respective k_A values compared in Table 19 it can be seen that values obtained from the open runs are of the same order as calculated in the corresponding closed runs. The results thus indicate that we have been able to model, with

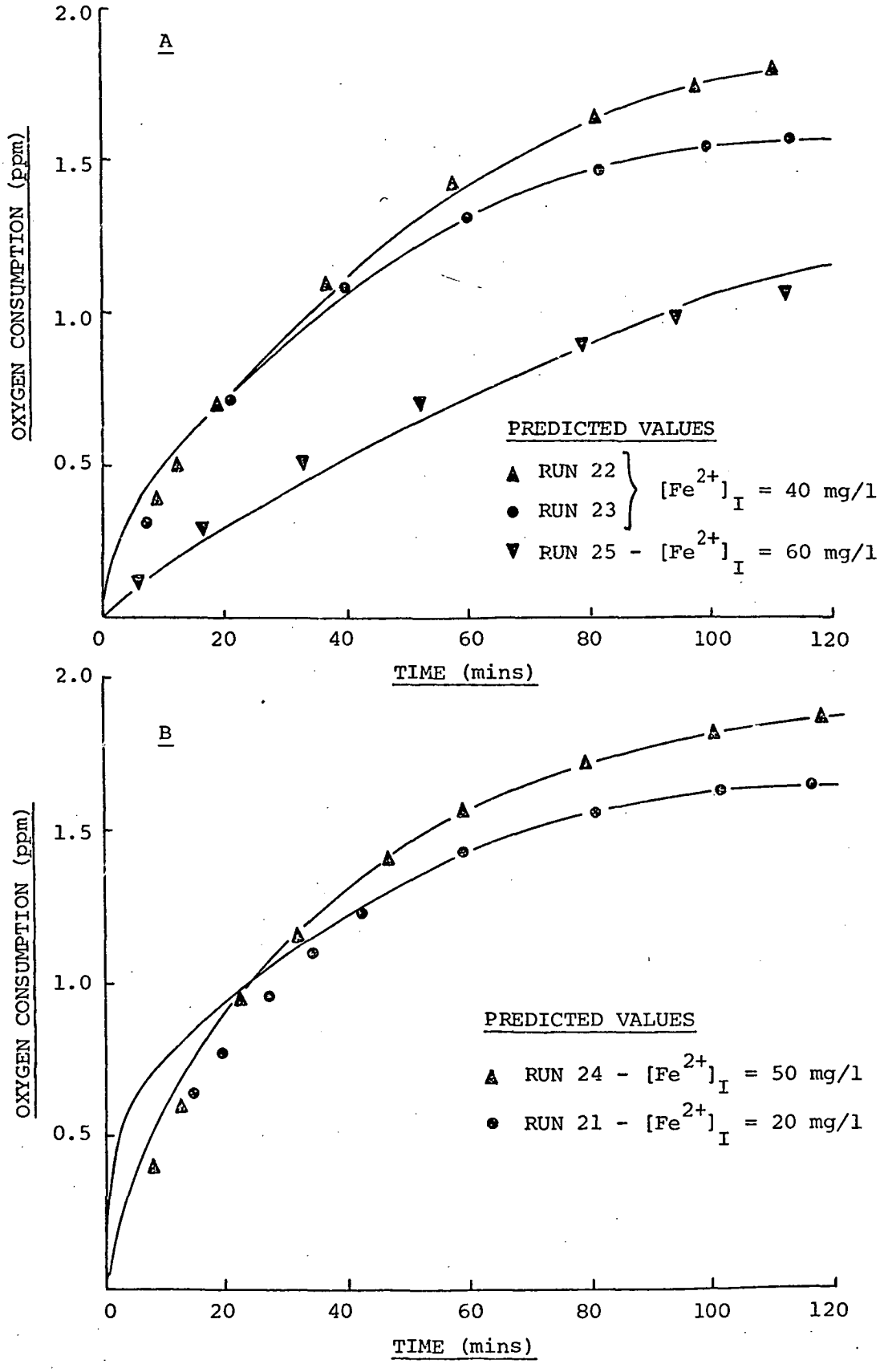

FIGURE 23 - SIMULATION OF OPEN KINETIC RUNS

(SOLID LINES GIVE EXPERIMENTAL CURVES)

N.B. SEE TABLE 19 FOR MORE DETAILS.

TABLE 19 - COMPARISON OF OPEN AND CLOSED KINETIC RUNS

Run Number	Nature of Run	Artificial Effluent	$(Fe^{2+})_I$ (mg/l)	Assumed Re-Aeration Constant $k_R(min^{-1})$	Estimated k_A (litre mole^{-1} min^{-1})
3	Closed	A	20±0.3	-	65±4
21	Open	A	20±0.3	0.010	86±4
5	Closed	A	40±0.5	-	34±1
22	Open	A	40±0.5	0.010	35±1
23	Open	A	40±0.5	0.014	34.5±1
24	Open	A	50±0.75	0.014	38±1
15	Closed	C	60±1	-	6.0±0.1
25	Open	C	60±1	0.010	10±1

a fair degree of success, the net oxygen consumption resulting from ferrous iron oxidation in a simulated sea-water sample open to the air.

Whether or not the open kinetic runs give a more realistic picture than the closed kinetic runs of the oxidation reaction following the introduction of acidic ferrous sulphate effluent to the sea, depends on the method of disposal of the effluent and such factors as effluent temperature and density. Whenever the effluent is dispersed at or near the ocean surface (e.g. following barge disposal) then the open situation, with oxygen transferring across the air-sea interface, would be the more relevant. However, whenever the effluent is dispersed near the sea-bed (e.g. following discharge from a submarine pipeline as in the Tioxide practice) then the subsequent reaction takes place in what can be regarded as a closed system and is simulated by the closed kinetic runs carried out.

3.5 REFERENCES

(1) Tamura H., Goto K. & Nagayama M. - Shikizai Kyokaishi, 45(11),629 (1972) (Japan).

(2) Klinghoffer O. - Pr. Nauk. Inst. Chem.Nieorg. Metal. Pierwiastkow., Rzadkich Politech. Wroclaw.,21, 79 (1974) (Polish).

(3) Astanina A.N. & Rudenko A.P. - Russian Jour. Phys. Chem., 45(2), 191 (1971).

(4) Pound J. R. - J. Phys. Chem., 43, 955 (1939).

(5) George P. - J. Chem. Soc. , 4, 4349 (1954).

(6) Cornelius R. J. & Woodcock J. T. - Proc. Aust. Inst. Min. Met., No. 185, 65 (1958).

(7) Mathews C. T . & Robins R.G. - Proc. Aust. Inst. Min. Met., No. 242, 47 (1972).

(8) Macejevskis B. & Liepina L. - Laturjas PSR Zinatnu Akad. Vestis.,10, 19 (1960) (Russian).

(9) Huffman R.E. & Davidson N. - J. Am.Chem.Soc.,78,4836(1956).

(10) Hine F. & Yasuda M. - Zairyo,23 (251), 654 (1974) (Jap).

(11) Saprygin A.F. & Gusar L.S. - Zh. Prikl. Khim. (Leningrad), 47 (8), 1690 (1974) (Russian).

(12) Lacey D.T. & Lawson F. - "A New Method for Treating and Regenerating Spent Sulphuric Acid Pickle Liquor", Dept. of Chem. Eng., Monash University, 1971.

(13) Just G. - Zeitschrift fuer Physikalische Chemie, 63, 385 (1908).

(14) Stumm W. & Lee G.F. - Industrial and Engineering Chemistry, 53, 143 (1961).

(15) Ghosh M.M. in "Aqueous Environ. Chem. Met." (Ann Arbor Science, Michigan, 1974)ed. Rubin A.J.-Chapter 5.

(16) Schenk J. E. and Weber W. J. Jr. - Jour. A.W.W.A.,60 (2), 199 (1968).

(17) Jobin R. and Ghosh M.M.- Jour. A W.W.A., 64 (9), 590 (1972).

(18) Whitfield M. - Limnol. Oceanog.,19(2), 235 (1974).

(19) Ngo Van Suc - Hoc Ky Thuat,(1), 17 (1974) (Vietnamese).

(20) Goto K., Tamura W. & Nagayama M. - Inorg.Chem.,9 (4), 963 (1970).

(21) Horne R.A. - "Marine Chemistry" - (John Wiley & Sons, 1969).

(22) Weichart G. -Mar. Pollut. Sea Life, FAO, 186 (1972).

(23) Kester D. R. et al. - Limnol. Oceanog., 12, 176 (1967).

(24) Gordon and Ford - "The Chemist's Companion: A Handbook of Practical Data, Techniques and References" (John Wiley & Sons, 1972).

(25) Davies O.L. & Goldsmith P.L. - "Statistical Methods in Research and Production" (Oliver & Boyd, 1972).

(26) Downing A.L. & Truesdale G.A. - J. Appl. Chem., 5,570 (1955).

(27) Morgan J.J. & Birkner F.B. - J. San. Eng. Div.,ASCE, 92, 137 (1966).

(28) Capellos & Bielski - "Kinetic Systems"(John Wiley & Sons, 1974).

(29) Ghosh M.M.,O'Connor J.T. & Engelbrecht R.S. - Jour.A.W.W.A., 59(7), 897 (1967).

(30) Mathews C.T. & Robins R.G. - Proc. Aust. Inst. Min. Met., 242, 47 (1972).

CHAPTER 4

THE PRODUCT OF FERROUS IRON OXIDATION

4.1 IRON OXIDATION AND HYDROLYSIS PRODUCTS

The results of the calculations undertaken in Chapter 2 indicate that ferric iron has a very low solubility in sea-water and that the solubility is controlled by ferric hydroxide. The calculated solubility of $Fe(OH)_3$ in sea-water has been found to be highly pH dependent with a value of about 10^{-8} moles Fe/l at pH 8 (see Figure 3). It can thus be predicted that the bulk of ferric iron produced in sea-water by the oxidation of introduced ferrous iron will precipitate as a form of ferric hydroxide. Horne suggests that $Fe(OH)_3$ in sea-water is suspended as a colloid (1).

The term "ferric hydroxide" is used to represent a range of hydrated iron-oxide compounds, namely the different crystalline forms of hydrated ferric oxide and hydrated ferric oxyhydroxide:

$Fe(OH)_3$	≡	$Fe_2O_3 \cdot 3H_2O$	≡	$FeOOH \cdot H_2O$
Ferric hydroxide		Hydrated ferric oxide		Hydrated ferric oxyhydroxide

The oxides and oxyhydroxides of iron have long been used as commercial pigments and α-Fe_2O_3 also as a polishing powder (rouge). More recently these compounds have found application as catalysts and as coatings for magnetic tapes. Consequently the chemistry of iron salt solutions has been the subject of innumerable investigations for over one hundred years. By carefully controlling the conditions it has

been found possible to form the ferric oxides α-Fe_2O_3, γ-Fe_2O_3 and Fe_3O_4, and the ferric oxyhydroxides α-FeOOH, β-FeOOH, γ-FeOOH and δ-FeOOH from iron solutions and suspensions. The crystal structures of the oxides and hydrous oxides are now known (2,3). In general, the different iron hydrated oxides are formed either by the controlled hydrolysis of ferric iron salt solutions or by the controlled oxidation of ferrous suspensions and solutions.

An excellent review of the hydrolysis of iron (III) has been given recently by Sylva (2). Of the known iron oxides and oxyhydroxides α-FeOOH, β-FeOOH, γ-FeOOH and α-Fe_2O_3 have been obtained by the hydrolysis of ferric salts (4,5). Kiyama and Takada(6) have suggested a mechanism of hydrolysis on the basis of the spectrophotometric and magnetic properties of the ferric complexes present in the solution prior to the formation of precipitates. The product formed when a ferric salt solution is heated or made alkaline depends on the temperature of preparation and the anion present in solution (2).

Of interest to the present work is the fact that the hydrolysis precipitate formed in the presence of chloride (Cl^-) ions is normally β-FeOOH. Ferric chloride solutions hydrolyse to give β-FeOOH, in contrast to ferric nitrate solutions which give α-FeOOH or α-Fe_2O_3 (depending on the hydrolysis temperature) and ferric sulphate solutions which give α-FeOOH or a basic sulphate (depending on the pH) (6). Ferric perchlorate solutions yield γ-FeOOH or α-FeOOH depending on the amount of base added to solution (5).

In relevance to the sea-water situation, and emphasizing the influence of the chloride ion on the nature of the product formed, the precipitate resulting from the hydrolysis of ferric iron in 0.5M NaCl is also β-FeOOH. This precipitate has been studied by X-ray diffraction and electron microscopy (8) and its actual composition has

been determined to be $Fe(OH)_{2.7}Cl_{0.3}$ (9). In marine environments the corrosion products of steel have been found to contain 20-30% β-FeOOH (7).

The effect of the anions in producing different compounds is almost certainly associated with the formation or otherwise of anion-iron (III) complexes (2). In the case of β-FeOOH, chloride co-ordinates strongly to ferric iron and it is likely that the species which adds to the growing crystal nuclei is a chloro complex. This is supported by the fact that β-FeOOH samples prepared by the hydrolysis of $FeCl_3$ solutions always contain a certain amount of Cl, the content varying with the conditions of preparation and subsequent treatment (10). The mechanism of β-FeOOH formation on the slow addition of alkali to a very dilute $FeCl_3$ solution has been investigated by Feitknecht et al (11). Ishikowa and Inouye (3) have studied the influence of Cl content on the reactivity of the crystal surface of β-FeOOH.

Many reports have been published on the formation of the iron compounds δ-FeOOH, α-FeOOH, γ-FeOOH and Fe_3O_4, by the oxidation of aqueous suspensions of ferrous precipitates such as hydroxide, carbonate and basic-sulphate. The particular ferric compound formed depends on the speed of oxidation, the pH, the temperature and the kind of anion present (4). Detournay et al have determined the conditions required for the formation of α-FeOOH from ferrous hydroxide suspensions and have studied the kinetics of formation and the influence of temperature and various foreign ions (12, 13). Kiyama has determined the optimum conditions for the formation of Fe_3O_4 by the air oxidation of $Fe(OH)_2$ (4).

It is known that if oxidation of $Fe(OH)_2$, in a ferrous salt solution with a pH of about 7, is carried out slowly by passing air into

the suspension then γ-FeOOH can be obtained by selecting the proper oxidizing conditions. In this case a dark green compound, called a "green rust", is always formed before the formation of γ-FeOOH (14). The structure of this oxidation intermediate has been investigated by Misawa et al (15). It was thought that the presence of green rust was indispensable for the formation of the ferric oxyhydroxide γ-FeOOH, but Kiyama and Takada have shown that γ-FeOOH can also be formed directly, by the slow oxidation of acidic ferrous salt solutions under the proper conditions (14).

Several other workers have reported the formation of γ-FeOOH from ferrous suspensions. Feitknecht (16) found that γ-FeOOH was formed by the aerial oxidation of ferrous hydroxide at high pH in the presence of chloride ions. Schwertmann (17) found that the oxidation of $Fe(OH)_2$ with oxygen, in the absence of CO_2, at room temperature, resulted at pH 4-5 in a highly disordered γ-FeOOH with X-ray amorphous fractions and between pH 5-8 in crystalline γ-FeOOH. However, he found that in the presence of carbon dioxide the formation of γ-FeOOH was depressed in favour of α-FeOOH. Krause (18), in one of the few reported studies of the oxidation of ferrous carbonate suspensions, found that at pH 4 the oxidation products were γ-FeOOH and "$Fe(OH)_3$". The rate of oxidation of the $FeCO_3$ suspension was retarded by the addition of small amounts of SiO_3^{2-} and AsO_2^- (19).

Although there exists a large volume of literature on the oxidation of ferrous iron suspensions, little can be found describing the formation of iron compounds by the oxidation of ferrous salt solutions in which no ferrous precipitate is present. Kiyama and Takada (14) have studied the products resulting from the atmospheric oxidation of ferrous iron solutions at low pH (<2) and 70°C.

α-FeOOH was formed from $FeSO_4$ solution initially and then converted to a basic sulphate. β-FeOOH was predominantly formed from $FeCl_2$ solution. Kiyama and Takada also found that γ-FeOOH was present in the oxidation products formed from $FeBr_2$ solution. The amount of γ-FeOOH produced depended on the time of aeration and the solution temperature.

Few other studies concerning the products of the oxidation of ferrous iron solutions have been reported. Kalaczkowski (20) found that at pH 6 an aqueous solution of "$Fe(HCO_3)_2$" was easily oxidized to yellow α-FeOOH by atmospheric oxygen. It is worth noting here that Stumm and Lee (21) state that the frequently made statement,"ferrous iron is soluble as ferrous bicarbonate",is misleading and incorrect. Schwertmann and Taylor (22) prepared γ-FeOOH samples by bubbling O_2 slowly through $FeCl_2$ solutions at pH 7-7.5.

In the present work we are interested in identifying the nature of the precipitate formed when a ferrous sulphate/sulphuric acid solution is added to sea-water. So far we have considered the iron precipitates known to be formed from the hydrolysis of ferric iron solutions and from the oxidation of ferrous iron suspensions and solutions. The results of the literature survey suggest that the sea-water precipitate is likely to be one of the compounds α-FeOOH, β-FeOOH, γ-FeOOH or α-Fe_2O_3, probably with associated water of hydration. Kaneko et al (23) have recently used dielectric behaviour to investigate the mechanism of water adsorption by iron oxyhydroxides. Further support for the above choice of possibilities comes from a consideration of the known composition of natural iron ores.

Of the four polymorphs of the oxyhydroxide so far known, α-FeOOH (goethite), β-FeOOH (akaganite) and γ-FeOOH (lepidocrocite) occur naturally as minerals and as the corrosion products of iron (23).

α-Fe_2O_3 (haematite) is the most commonly found ferric oxide mineral and has been identified in some marine sediments (24).

In the formation of marine sedimentary iron ores the source material is regarded to be ferrous iron leached from clay minerals in sea basins. If deposition occurs in the O_2 zone of the sea, that is in well oxygenated waters, then limonite is predominantly formed (25). The term "limonite" is used to describe hydrated oxides of iron with poorly developed crystalline character. X-ray analysis has shown that most limonites are generally composed of goethite of very small crystal size, though some may consist of lepidocrocite or a mixture of the two crystalline forms (26). If ore deposition occurs in a CO_2 zone of the sea, a region of decreased oxygen content and increased CO_2 content, then the most typical sediment is siderite ($FeCO_3$). Iron deposits associated with submarine volcanoes and hydrothermal springs are generally in the form of non-crystalline hydroxides and of poorly crystalline goethite (27).

Thus natural marine deposits of "ferric hydroxide" consist mainly of poorly crystalline α-FeOOH and occasionally of poorly crystalline γ-FeOOH. As previously mentioned, β-FeOOH and α-Fe_2O_3 are also found in the marine environment (7,24). The fact that these four compounds have been found to form in contact with sea-water re-inforces their use as a basis for identifying the precipitates formed in the kinetic runs described in Chapter 3. Having delineated the required reference iron hydrated oxides it was necessary to prepare a sample of each so that their characteristic spectra and X-ray diffraction patterns could be recorded. It was also of interest to prepare a sample of ferrous carbonate. The methods of preparation of the required iron compounds are described in the following section.

4.2 PREPARATION OF REFERENCE COMPOUNDS

The required reference iron compounds were prepared as follows:

α-FeOOH (goethite) - 0.84M ferric sulphate solution was hydrolyzed at 50°C for 30 hours, the pH being adjusted to 13 with 1M KOH. The product was washed with distilled water till no sulphate ion was detected (with dilute Ba $(NO_3)_2$) and was then dried at 100°C for 3 hours (28). The crystals obtained were light brown in colour.

β-FeOOH (akaganite) - 500 ml 0.1M $FeCl_3$ containing 30 gms urea was heated to 90°C within 1 hour and then kept at this temperature for an additional 5 hours. The product was washed by decantation with distilled water till no chloride ion was detected (with dilute $AgNO_3$), collected by centrifugation, and then dried at 100°C for 3 hours (28). Dark brown crystals were obtained.

γ-FeOOH (lepidocrocite) – The following mixed solution was warmed at 60°C for 50 minutes in a stream of nitrogen:
500 ml 0.2M $FeCl_2$, 100 ml 2M hexamethylenetetramine, 13.5 ml 5M HCl and 100 ml 1M $NaNO_2$. The product was washed with distilled water till no chloride ion was detected (with dilute $AgNO_3$) and then dried at 60°C for 10 hours (28). The final product was orange/brown in colour.

α-Fe_2O_3 (haematite) - As for β-FeOOH except that the solution was heated above boiling and gently refluxed for 5 hours (29). A sample of commercial haematite was also obtained for reference. Both products consisted of dark, reddish-brown crystals.

$FeCO_3$ (siderite) - Under a stream of nitrogen 1M Na_2CO_3 solution (deoxygenated) was slowly added to a 0.1M $FeSO_4$ solution (deoxygenated) to pH 7 (30). A white gelatinous precipitate was formed. When exposed to air, during filtration, this precipitate was observed to rapidly turn green. The original white precipitate also turned green when left in oxygenated water. The green product contained a lot of entrained water, gave rapid effervescence with dilute sulphuric acid, and was deemed to be partially oxidised $FeCO_3$ (31). An attempt to dry the green partially oxidised product under nitrogen was unsuccessful.

Because in the present work we are concerned with the possible presence of ferrous carbonate in oxygenated waters, several samples of the green intermediate oxidation product were washed with distilled water and then treated as follows:

(a) Dried at 60°C for 18 hours.

(b) Allowed to dry in air.

(c) Placed under water for six weeks and then collected.

In all cases the final product obtained was orange/brown in colour, indicating that the original $FeCO_3$ had been fully oxidised to a ferric compound or compounds.

After preparation the different reference iron compounds, together with the iron precipitates obtained in the kinetic runs of Chapter 3 and in the dilution experiments of Chapter 2, were examined as outlined in the next section. The formation of the "kinetic" and "dilution" precipitates has already been described. At the end of the respective runs the resulting precipitates were collected by decantation and filtration, were well-washed with distilled water and then dried at 60°C for 3 hours.

4.3 INVESTIGATION OF PRECIPITATES

4.3.1 Examination of Samples

Prepared iron compounds and obtained iron precipitates were examined by infrared spectroscopy, by X-ray diffraction and by electron microscopy. Infrared absorption spectra were recorded on a Perkin-Elmer 577 spectrophotometer using KBr discs and Nujol mulls. No attempt was made to remove adsorbed water from the dried precipitates because of the suggestion that this can cause changes in the internal particle structure (29). X-ray diffraction patterns were obtained by the powder method with a Philips automatic diffractometer, using CuK_α radiation (40 kV, 20 mA). Patterns were identified using the 1973 ASTM Powder Diffraction Data File.

Electron micrographs were taken using a JEOL scanning electron microscope. Samples for examination were prepared by drying small drops of dilute aqueous suspension on thin glass slides with the aid of a non-ionic detergent, Triton X-100, to reduce surface tension.

4.3.2 Estimation of Crystallite Size

The hydrated iron oxides of interest in the present work are composed of very tiny crystals, or "crystallites", which are so small that in general they can only be seen by means of an electron microscope. Crystallites smaller than about 10^{-7}m in diameter cause a broadening in recorded X-ray diffraction lines (32,33). The fact that line broadening depends on crystallite size has naturally led to a method for determining the latter.

The Scherrer Formula (34) relates the true width of a powder diffraction line to the crystallite size of the sample under investigation:

$$\beta = K\lambda / L\cos\theta \quad \ldots\ldots \quad (4A)$$

where β = true diffraction width of line (radians)

K = Scherrer constant

λ = radiation wavelength

L = apparent or average crystallite size

θ = Bragg angle

To estimate the true width of a powder diffraction line it is necessary to first obtain an estimate of the instrumental broadening. This can be obtained from the diffraction pattern of a sample of equivalent absorption coefficient to the one under study but known to be composed of crystals greater than 10^{-7}m in size. In the present work instrumental broadening was estimated using a sample of commercial grade haematite (comparison of its spectrum with that of a silicon reference crystal showed it to have crystals of the required size). Once instrumental broadening has been measured the true diffraction width of a line can be obtained from the measured width by using one of the graphical correction procedures devised by Jones (34,35).

In practice a "line" on a powder diffraction pattern has the shape of an arc or peak (33). If the width of a peak is taken to be its integral breadth, in other words the area under the curve divided by its height, then the Scherrer constant in equation (4A) has a value of between 1.0 and 1.3 depending on the geometry of the crystallites under study. Recommended values for K when the crystallite shape is not known vary from 1.08 (36) to 1.15 (33). In the present work a value of 1.1 has been used.

Examples of crystallite size calculations undertaken in the present study are given in Appendix 6. An average apparent crystallite size was calculated, where possible, for each iron compound of interest from the estimated integral breadths of the compound's three principal X-ray powder diffraction lines. A table of estimated crystallite sizes is also given in Appendix 6 and the results are discussed in Section 4.4.2.

Although no great accuracy can be expected in work of this sort (33), it is useful in determining trends within a group of similarly prepared compounds. Jones (35) states that the difference between the true mean size and the estimated mean crystallite size is unlikely to be greater than 30%. Care has to be taken in comparing crystallite sizes determined from X-ray diffraction patterns when the compounds involved have been prepared under different conditions. This is because broadening of diffraction lines is due not only to the dimension of the crystallites under study but also to any internal strains in the latter, such as are produced by the incorporation of hetero-elements into the crystal lattice (32). Derie et al (37) found that the X-ray diffraction lines of goethite (α-FeOOH) containing 1.6% Cu were much broader than those of goethite with 2.6% Cr, although both samples had comparable specific surface area. The discrepancy was attributed to the fact that the octahedron of co-ordination around Cu^{2+} is strongly distorted by the Jahn-Teller effect.

4.4 RESULTS AND DISCUSSION

4.4.1 Infra-Red Spectroscopy

Each of the four reference iron compounds was found to have a characteristic infra-red spectrum, thus providing an easy and positive method for identification. The different recorded infra-red spectra are shown in Figure 24. Peaks at 2900 cm^{-1}, 1460 cm^{-1}, 1380 cm^{-1} (strong) and 720 cm^{-1} (weak) which appear in all the spectra are due to the Nujol mulling agent used. The characteristic peaks which differentiate between the individual compounds appear in the region 1200-300 cm^{-1} and their recorded positions are detailed in Table 20.

The infra-red spectra of various iron oxides and oxyhydroxides have been discussed by Kauffman and Hazel (29). As can be seen in Figure 24 all the oxyhydroxides have a very broad strong adsorption in the region 3500-3200 cm^{-1}. This is due to the fact that the oxyhydroxides contain large amounts of absorbed water which cannot be removed without changes in structure, and the infra red adsorption is attributed to O-H stretching. The broad very weak adsorption found at about 1630 cm^{-1} is due to H-O-H scissoring (38).

The characteristic peaks of the iron compounds, as shown in Table 20, are found in the region 1100-650 cm^{-1}, corresponding to O-H....O bending vibrations and in the region 650-350 cm^{-1}, corresponding to lattice vibrations. The latter normally result in two broad peaks and are discussed by Waldron (39). The OH deformation (bending) vibrations of β-FeOOH are affected by the Cl content of the compound. Ishikawa and Inouye (3) found that the adsorption bands shifted to higher frequencies and their adsorption increased as Cl content increased.

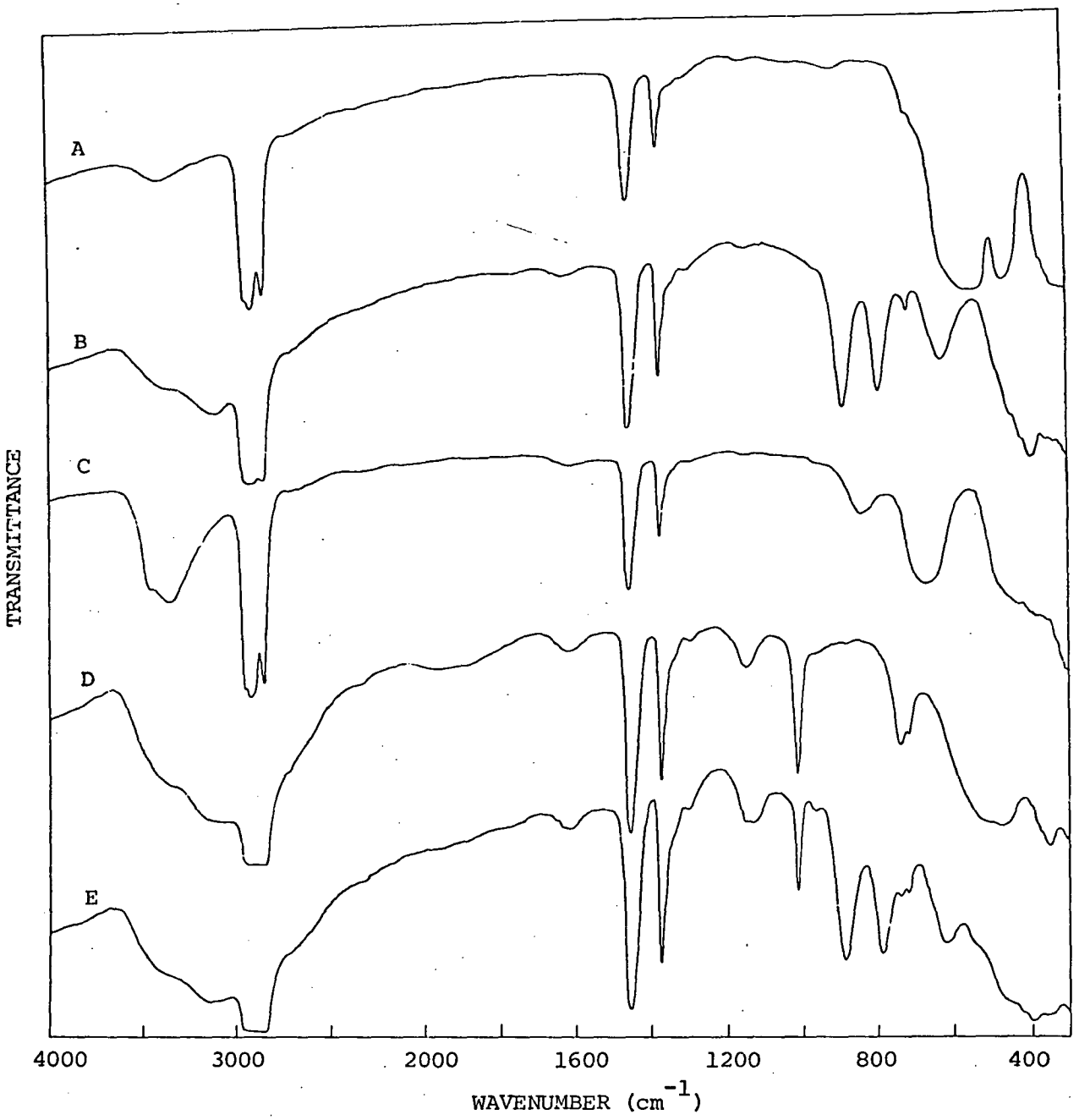

FIGURE 24 - INFRA-RED SPECTRA OF REFERENCE IRON COMPOUNDS

A - α Fe_2O_3

B - α FeOOH

C - β FeOOH

D - γ FeOOH

E - $FeCO_3$ oxidation product

(Nujol mull, KBr discs)

TABLE 20 - INFRA-RED SPECTRA - POSITION OF CHARACTERISTIC PEAKS

	Region 1100-650 cm^{-1}	Region 650-350 cm^{-1}	Other
α-FeOOH	890(ss) 795(ss)	635(mb) 400(wb)	-
β-FeOOH	840(wb) 675(mb)	425(wb)	-
γ-FeOOH	1020(ss) 745(ms)	480(sb) 360(wb)	1155(wb)
α-Fe_2O_3	-	560(sb) 470(sb)	-

Code: s - strong, m - moderate, w - weak; s - sharp, b-broad

In general, peak positions recorded in the present work are in very good agreement with those presented in the literature (3,29). γ-FeOOH was found to have an additional broad weak peak at 1155 cm^{-1} to which no reference has been found and which proved useful in the identification of oxidation precipitates. The γ-FeOOH peak at 745 cm^{-1} was commonly observed as a shoulder due to the presence of a Nujol peak at 720 cm^{-1}. All the spectra shown in Figure 24 are distinct from those of potassium jarosite and basic iron sulphate which have been recorded by Powers et al (40).

Spectrum E in Figure 24 is that of the orange/brown oxidation product obtained from ferrous carbonate after each of the different methods of treatment (see Section 4.2). A comparison with spectra B and D clearly shows that the product is a mixture of α-FeOOH and γ-FeOOH. The results indicate that at around pH 7 ferrous carbonate is unstable in oxygenated waters and is oxidised

to this mixture of iron oxyhydroxides. As already mentioned, at pH 4 Krause (18) found that ferrous carbonate was oxidised to γ-FeOOH and "$Fe(OH)_3$".

Figure 25 shows the infra-red spectra of the precipitates obtained at the completion of several selected kinetic runs. The particular runs chosen span the full range of experimental conditions employed in the present study. As can be seen, all the precipitates have the same infra-red spectrum indicating that the same ferrous oxidation product has been formed. A comparison with the reference spectra of Figure 24 shows that the product is γ-FeOOH. This oxyhydroxide is most clearly identified by the presence of a sharp peak in its infra-red spectrum at 1020 cm^{-1}.

Lepidocrocite (γ-FeOOH) was detected by infra-red analysis in all the precipitates obtained in the kinetic runs and dilution experiments carried out, although the characteristic peaks were not very strong (relatively) in some cases indicating that the product concerned had a poorly crystalline nature. The same oxidation product was obtained with artificial solutions as was obtained using Tioxide effluent and real sea-water, another indication that the results of the laboratory modelling of the ferrous oxidation process are applicable to the real situation. The results of infra-red analysis thus indicate that over the pH range 5.5 to 7.5, with initial ferrous iron concentrations varying from 7 mg/l to 75 mg/l, the product of ferrous iron oxidation in sea-water is composed of lepidocrocite, γ-FeOOH.

The fact that γ-FeOOH was the sole crystalline oxidation product identified over the range of ferrous oxidation conditions employed in the present work is somewhat surprising, given the high

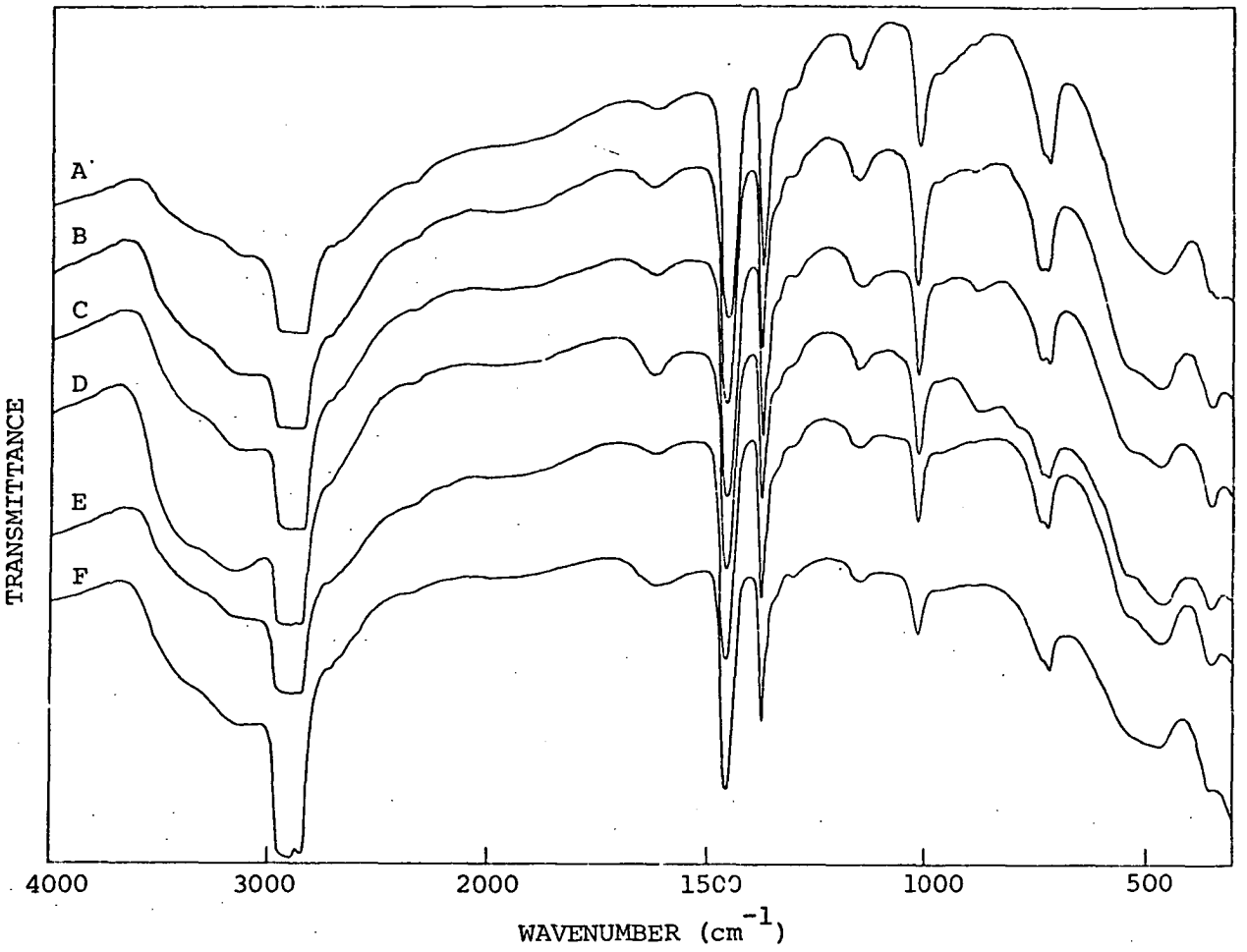

FIGURE 25 - INFRA-RED SPECTRA OF VARIOUS FERROUS OXIDATION PRECIPITATES

SPECTRUM	RUN NUMBER	$[Fe^{2+}]_I$ (mg/l)	DETAILS OF RUN
A	1	10	CLOSED, 25°C. EFFLUENT A, ASW*
B	9	40	CLOSED, 25°C. EFFLUENT B, ASW
C	14	60	CLOSED, 25°C. EFFLUENT C, ASW
D	19	40	CLOSED, 12°C. EFFLUENT A, ASW
E	21	20	OPEN, 25°C. EFFLUENT A, ASW
F	30	≃ 18	CLOSED, 25°C. TIOXIDE EFFLUENT/ REAL SEA-WATER

(*ARTIFICIAL SEA-WATER)

Cl^- concentration in the sea-water matrices and the fact that the presence of Cl^- commonly favours the formation of β-FeOOH. However, the result is consistent with the indication from literature (25) that β-FeOOH is not commonly found in natural marine sedimentary iron ores.

Schwertmann and Taylor (22) note that lepidocrocite (γ-FeOOH) is less stable than its polymorph goethite (α-FeOOH) and can easily be converted to goethite in the presence of alkali hydroxide or ferrous sulphate solutions. They studied the transformation of γ-FeOOH to α-FeOOH in highly alkaline solutions. At 20°C, at pH 13, the half conversion time for a particular preparation of lepidocrocite was 65 days. No variation in crystalline character was detected by infra-red analysis in γ-FeOOH oxidation precipitates left in artificial sea-water solutions for 70 days. If conversion of γ-FeOOH to α-FeOOH does in fact occur in sea-water then the process is extremely slow, as could be predicted from the low alkaline character of sea-water (pH 8). Söderquist and Jansson (8), in studying precipitates of β-FeOOH formed by the hydrolysis of iron (III) in 0.5M NaCl, found that preparations that had been aged in the mother liquid at 25°C for up to one year did not show any detectable change in crystalline character or crystallite size.

As has been shown in Chapter 2, the solubility of ferrous iron in sea-water is controlled by the solubility of siderite, $FeCO_3$. If enough ferrous iron is added to sea-water then ferrous carbonate can be expected to precipitate. The relative rate of ferrous precipitation as compared to the rate of ferrous oxidation is mostly dependent on the pH of the oxygenated water. If ferrous carbonate precipitation takes place in sea-water then the final oxidation products will include any oxidation products of ferrous carbonate. It has

been suggested that the oxidation of siderite in a natural water is extremely slow and, in fact, may not occur at all (41). Present results do not agree with this view. The oxidation of $FeCO_3$ under water exposed to the air has been found to be relatively rapid, the product being a mixture of α-FeOOH and γ-FeOOH. However, as already mentioned, no α-FeOOH has been detected in any of the real and artificial sea-water ferrous oxidation precipitates formed in the present work. This indicates that under the conditions spanned by the experimental kinetic runs $FeCO_3$ oxidation was not part of the overall oxidation process.

Solubility calculations carried out in Chapter 2 predict that $FeCO_3$ could have been precipitated in only one or two, at most, of the kinetic runs undertaken. This has been discussed in detail in Section 3.4.2. Analysis of the oxidation products formed thus supports the solubility predictions. For those runs in which $FeCO_3$ precipitation could possibly have taken place, the fact that no α-FeOOH was found in the final oxidation product indicates that, if indeed $FeCO_3$ precipitation did occur, then the precipitate was not oxidised directly but redissolved in the solution as the oxidation reaction proceeded.

4.4.2 X-Ray Diffraction and Crystallite Size

The four reference iron compounds gave X-ray diffraction patterns in excellent agreement with those tabulated for α-FeOOH, β-FeOOH, γ-FeOOH and α-Fe_2O_3 respectively, thus proving that the preparations described in Section 4.2 had been successful. The characteristic X-ray diffraction patterns are shown in Figure 26. The

DETAILS OF X.R.D. PATTERNS - FIGURE 26

	COMPOUND	INSTRUMENTAL RANGE* (y-AXIS)
A	α-Fe_2O_3	400
B	α-FeOOH	200
C	β-FeOOH	200
D	γ-FeOOH	200

(*Other instrument settings equivalent)

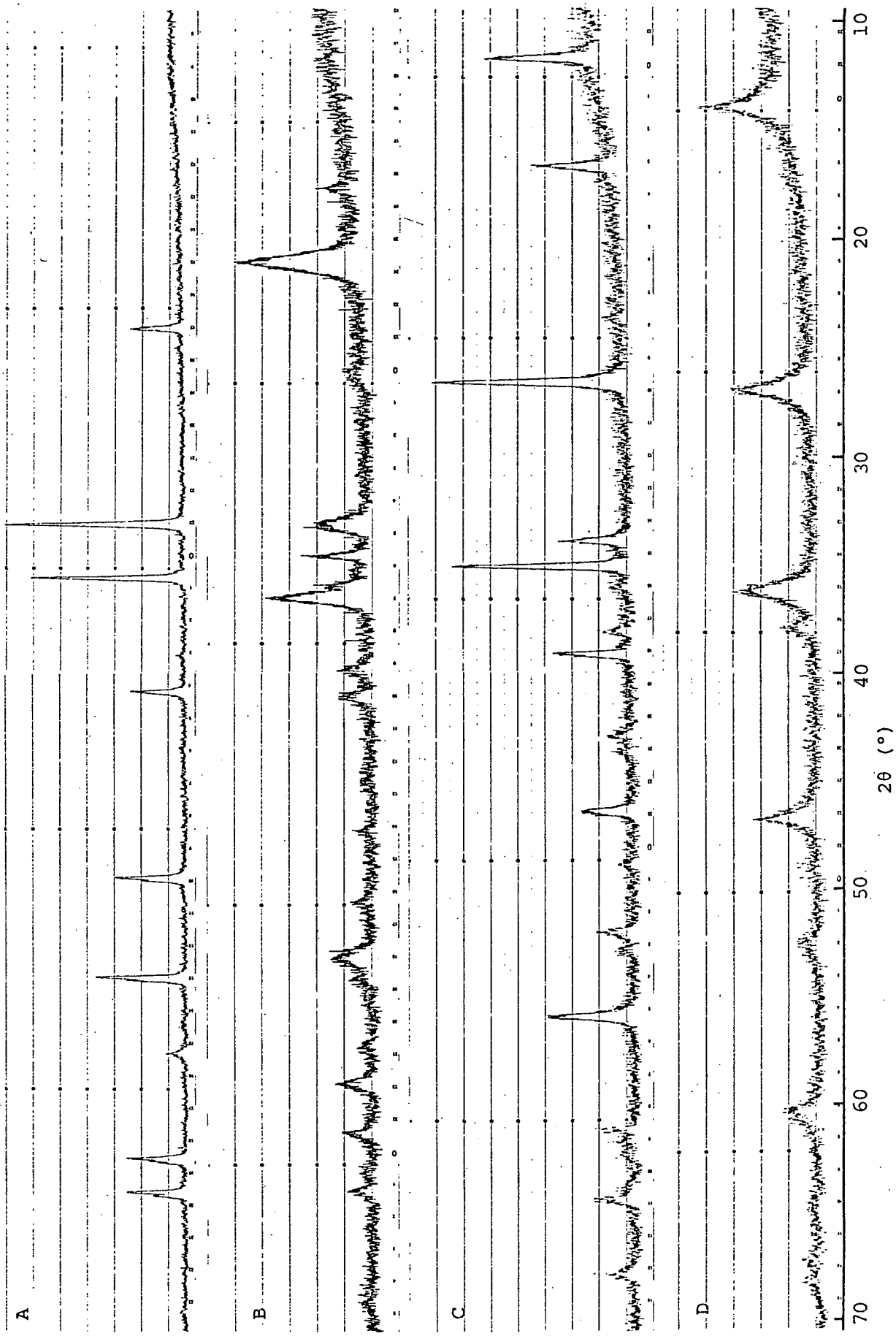

FIGURE 26 - X-RAY DIFFRACTION PATTERNS OF REFERENCE IRON COMPOUNDS

(For details see opposite)

width of the diffraction peaks reflects the size of the component crystallites in each compound, the greater the broadening the smaller the crystallites. It can be seen that the sample of α-Fe_2O_3 prepared had a greater crystalline character than any of the oxyhydroxide samples, though the peaks shown are broader and less pronounced than those of the commercial haematite used to estimate instrumental broadening. Of the oxyhydroxide samples the β-FeOOH proved to be the most crystalline. Diffraction peaks ("lines") of both α-FeOOH and γ-FeOOH are broadened appreciably, reflecting the fact that these preparations were composed of very small crystallites.

Estimated crystallite sizes for each compound are shown in Table 21 and compared with values quoted in the literature. Sizes were calculated by the Scherrer formula from the integral breadth of the three principal X-ray diffraction lines (see Appendix 6). Crystallite size is a variable parameter dependent on the method of sample preparation (26) and the temperature to which a sample is heated (3). The actual value obtained also depends on the method of application of the Scherrer formula (36). However, it is worth comparing values shown in Table 21 because the compounds were prepared by the same method in each case (see Section 4.2), with the exception of α-Fe_2O_3 which in reference (3) was obtained from β-FeOOH by heating to 400^{o}C rather than by boiling in water. The good agreement between the experimental and literature crystallite size values for the iron oxyhydroxides indicates that the present method of estimating crystallite size from X-ray diffraction patterns is consistent with that of other workers and that the preparations of Kaneko and Inouye (28) have been successfully reproduced.

In the present work each of the reference iron compounds prepared had a characteristic colour. In particular, the sample of α-FeOOH

TABLE 21 - CRYSTALLITE SIZE OF REFERENCE IRON COMPOUNDS

Compound	Estimated Crystallite Size ($\mathring{A}$ = $x10^{-10}m$)	Literature Values ($\mathring{A}$ = $x10^{-10}m$)		
		Ref (28)	Ref (23)	Ref (3)
α-FeOOH	180	210	280	-
β-FeOOH	450	470	550	750
γ-FeOOH	120	63	110	-
α-Fe_2O_3	1140	-	-	700

was light brown, that of β-FeOOH dark brown and γ-FeOOH orange/brown. All experimental oxidation precipitates collected were orange/brown in colour thus suggesting that they were all composed of γ-FeOOH, a fact confirmed by infra-red analysis. Bunn (42) states that the oxy-hydroxides possess characteristic colours, colour being a structure-sensitive property, although some modification of depth of colour may be attributable to particle size. The variation of sample colour with particle size is clearly illustrated in the work of Knight and Silva (5). Goethite (α-FeOOH) precipitates formed by the hydrolysis of ferric nitrate solutions were found to vary in colour from dull yellow at low base additions (larger crystallite size) to dark brown at high base additions (smaller crystallite size).

In the X-ray diffraction patterns shown in Figure 26 it can be seen that there is a degree of background or "scatter" associated with each spectra, especially in the case of the three iron oxyhydrox-ides. This is due in part to the poor crystalline nature of the

compounds (c.f. small crystallite size) which means a relatively high machine sensitivity is needed to obtain the required X-ray diffraction patterns. More importantly, the spectra are affected by iron fluorescence. Söderquist and Jansson (8) found similar interference due to Fe fluorescence radiation when taking powder diffraction photographs of β-FeOOH with CuK_α radiation. As in the present case, the interference made estimation of line breadths somewhat uncertain. Schwertmann's (17) diffraction patterns of α-FeOOH and γ-FeOOH have a similar scattered appearance to those in Figure 26, indicating that this type of background interference is commonly obtained with poorly crystalline iron oxyhydroxides.

The X-ray diffraction patterns given by sea-water ferrous oxidation precipitates support the findings of infra-red analysis. Only one type of pattern was obtained from the oxidation products formed in the present study, though the breadth and height of the peaks varied as the crystalline nature of the precipitate varied. Comparison of the peak positions with those of the reference iron compounds (Figure 26) showed that the only crystalline material contained in the oxidation products was γ-FeOOH (lepidocrocite). Some of the products contained a very high proportion of amorphous ferric hydroxide. As before, X-ray diffraction showed that the same ferrous oxidation product was obtained with artificial solutions as was with Tioxide effluent and real sea-water.

Typical X-ray diffraction patterns given by the kinetic run precipitates are shown in Figure 27 and a comparison with Figure 26D clearly identifies the crystalline phase as γ-FeOOH. The different patterns correspond to runs carried out over the range of conditions

DETAILS OF X.R.D. PATTERNS - FIGURE 27

PATTERN	RUN NUMBER	$[Fe^{2+}]_I$ (mg/l)	DETAILS OF RUN (All at 25°C)	ESTIMATED CRYSTALLITE SIZE (Å ≡ 10^{-10} m)
A	11	60	CLOSED, EFF. B, ASW*	140 ± 10
B	6	40	CLOSED, EFF. A, ASW	130 ± 10
C	22	40	OPEN, EFF. A, ASW	115 ± 10
D	31	≃ 14	TIOXIDE EFF./REAL S.W.	110 ± 10
E	3	20	CLOSED, EFF. A, ASW	75 ± 10

(* ARTIFICIAL SEA-WATER)

N.B. All patterns recorded at the same instrumental range (Y-axis).

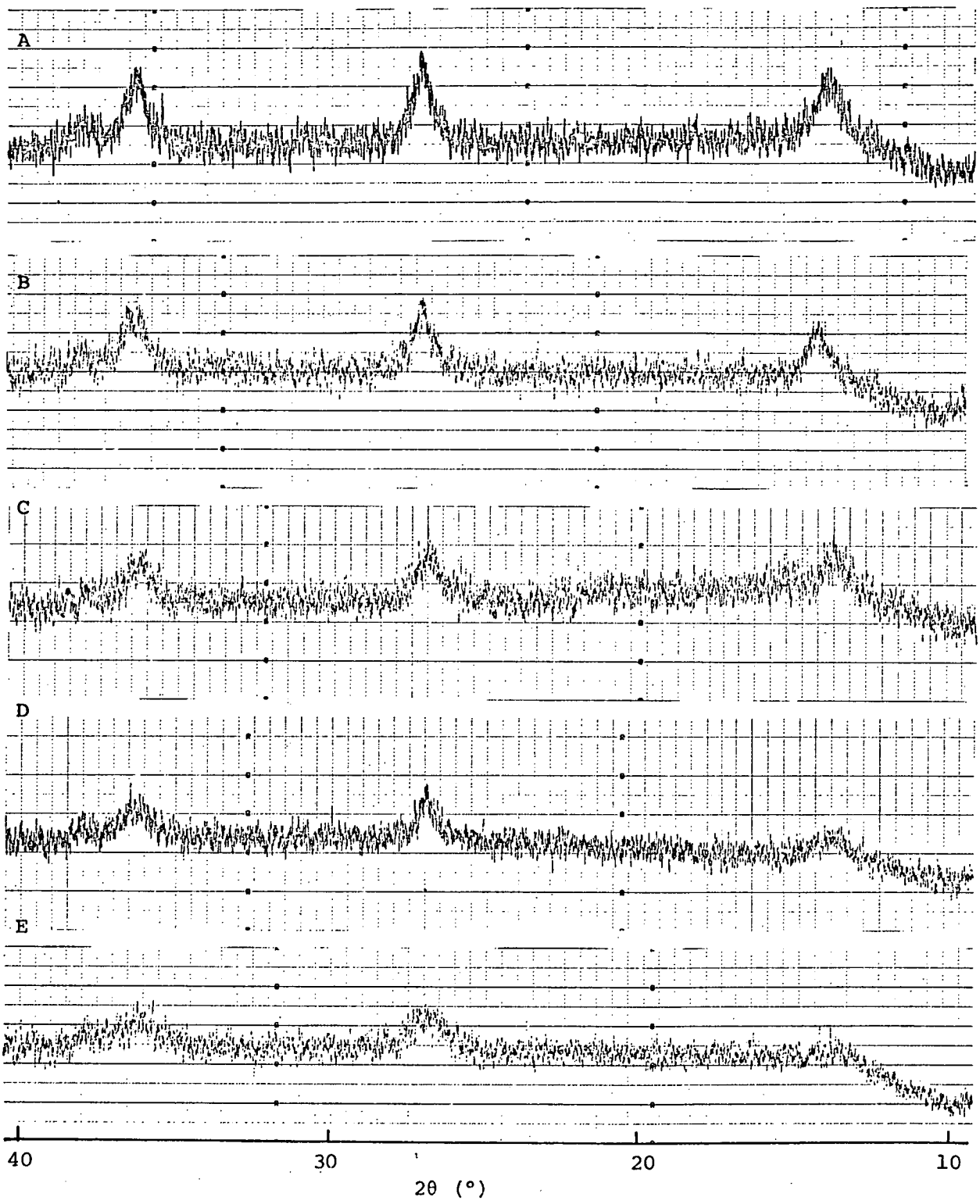

FIGURE 27 - X-RAY DIFFRACTION PATTERNS OF VARIOUS FERROUS OXIDATION PRECIPITATES, ILLUSTRATING THE RANGE OF CRYSTALLITE SIZE FORMED

(For details see opposite)

employed in the present study, and it can be seen that the same product is formed in each case but that the crystallite size varies. As the precipitate becomes more amorphous (i.e. as crystallite size decreases) the γ-FeOOH diffraction peaks at 14^{o}, 27^{o} and 36.3^{o} (as 2θ) decrease in height and broaden. At estimated crystallite sizes below 100 Å (10 nm) the peak at 14^{o} effectively disappears.

In spite of the high background interference obtained in the patterns (presumed to be due to both iron fluorescence and the high machine sensitivity employed), it was still possible to estimate a value for crystallite size for most of the oxidation products obtained. A table of values is given in Appendix 6. For those runs undertaken at $[Fe^{2+}]_I$ values of less than 10 mg/l insufficient precipitate was collected to enable an X-ray diffraction pattern to be run. However, as has been mentioned, there was enough precipitate for infra-red analysis to identify the presence of γ-FeOOH in the oxidation product.

Figure 27 clearly illustrates that in some kinetic runs the oxidation conditions were more favourable to the development of a crystalline precipitate than in others. The estimated average crystallite size of the ferrous oxidation product varied over the different runs carried out from 140 Å (14 nm) to 55 Å (5.5 nm). The values are in good agreement with crystallite sizes previously estimated for samples of γ-FeOOH (see Table 21), although individual values have a high associated error due to the uncertainty involved in determining the integral breadths of the diffraction peaks. Values corresponding to the X-ray diffraction patterns in Figure 27 indicate that, leaving out the Tioxide effluent run, crystallite size has a tendency to decrease with decreasing initial ferrous iron concentration over the range of oxidising conditions spanned by the present work.

Estimated crystallite size is plotted against initial ferrous iron concentration, for kinetic runs involving the use of an artificial effluent, in Figure 28. Values plotted correspond to oxidation products formed in both closed and open runs and in runs at $25^{o}C$ and at $12^{o}C$.

It can be seen that over this range of oxidising conditions (corresponding to pH 6-7) the crystallite size of the ferrous oxidation product shows a definite trend to decrease with decreasing $[Fe^{2+}]_I$.

In the oxidation process soluble ferrous iron is first oxidised to soluble ferric iron which then precipitates because the solubility product of ferric hydroxide is exceeded. As the oxidation proceeds the continued formation of ferric hydroxide precipitate can occur by either the formation of new crystal particles or by the growth of existing crystal particles. Both processes may well take place simultaneously. If the growth of crystal particles is part of the mechanism of ferric hydroxide formation then the longer the oxidation process proceeds, the greater the size of the final crystal particles obtained.

In the case of the present series of experimental runs undertaken with artificial effluents there is a general overall trend, in spite of the slower oxidation rate at $12^{o}C$ as compared to $25^{o}C$, for the time required for complete ferrous oxidation to increase proportionally with the initial ferrous iron concentration. The observed overall trend shown in Figure 28, for the oxidation product crystallite size to increase with $[Fe^{2+}]_I$, is thus consistent with a mechanism of ferric hydroxide formation which includes the slow growth of crystal particles. In a study of the mechanism of ferric hydroxide precipitation in hydrolysed iron (III) solutions, Knight and Sylva (5) state that pre-

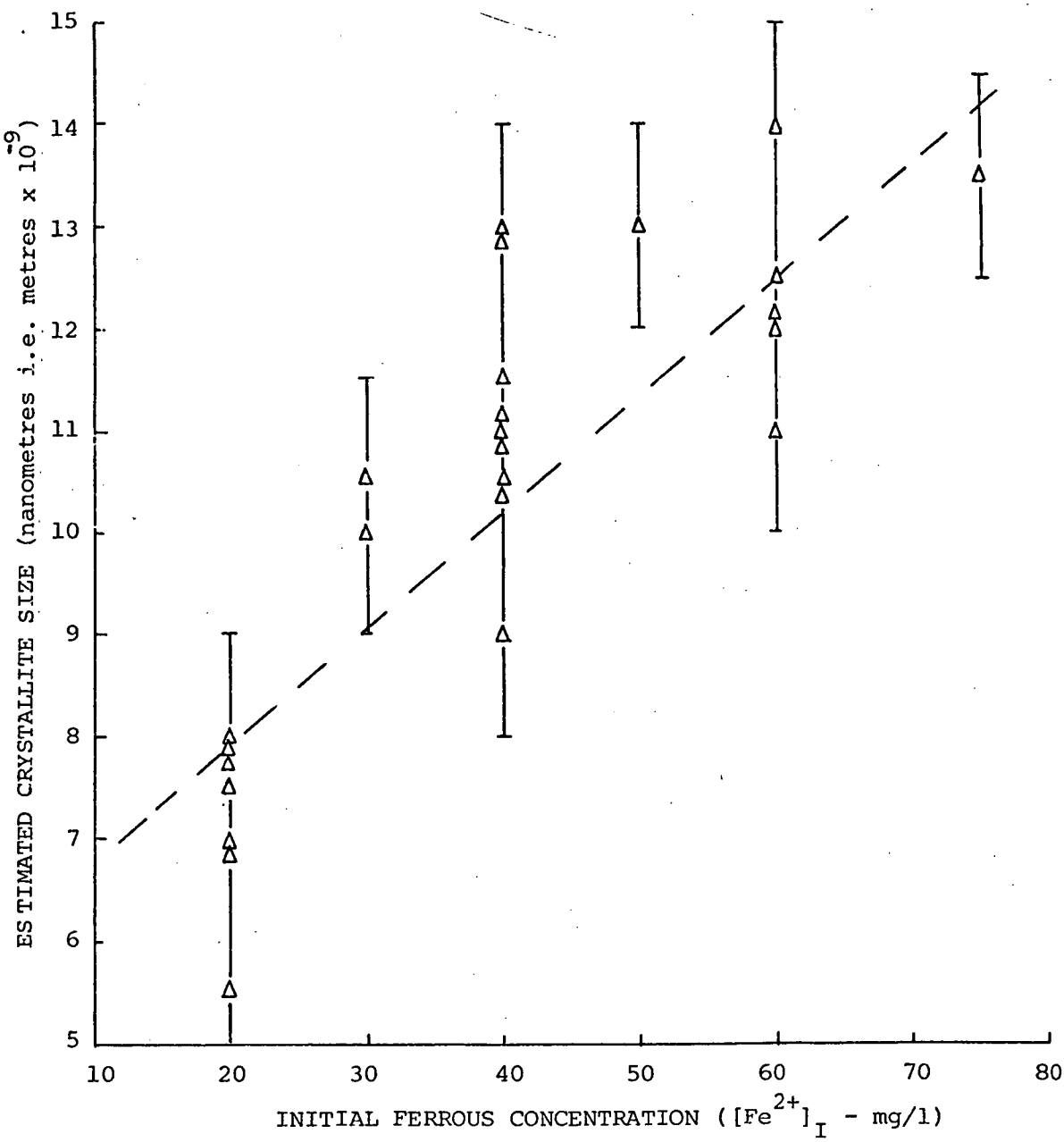

FIGURE 28 - TREND OF CRYSTALLITE SIZE WITH INITIAL FERROUS IRON CONCENTRATION

(ARTIFICIAL EFFLUENTS, pH 6-7,
TEMPERATURE 12-25°C)

cipitate formation must occur by the step-wise addition of low molecular weight species to growing nuclei. The species $Fe(OH)_2^+$ was suspected to be the likely precursor of the crystalline phase.

The estimated crystallite sizes of the final oxidation products obtained in the Tioxide effluent runs are greater than those for artificial effluent runs of roughly equivalent $[Fe^{2+}]_I$ (e.g. 12 nm for $[Fe^{2+}]_I$ = 18 mg/l and 11 nm for $[Fe^{2+}]_I$ = 14 mg/l). As has been discussed in Chapter 3, the rate of oxidation was much slower in the Tioxide runs than in the equivalent artificial effluent runs. The greater crystallite sizes found are thus further indication that the time required for oxidation is important in determining the crystalline nature of the ferrous oxidation product, lepidocrocite (γ-FeOOH).

4.4.3 Electron Microscopy

Because of their small size and characteristic shape crystals of iron oxides and oxyhydroxides are often examined under an electron microscope. It has been established that α-FeOOH particles are thin rectangular plates ("needle-like"), β-FeOOH particles are long square rods and γ-FeOOH particles are very thin rectangular plates (23). Haematite particles, α-Fe_2O_3, by contrast, have a round hexagonal shape (43). Electron microscopic examination not only allows the morphology of a sample to be determined but proves useful in sample identification (4,29).

Unfortunately, in the present work the use of electron microscopy did not prove successful. Scanning electron microscope pictures of prepared samples of both the iron reference compounds and ferrous oxidation products were indistinct and did not reveal

characteristic crystal shapes. This may have been due to the limitations of the instrument (lack of resolving power) and/or to the thickness of the prepared samples. A sample of α-FeOOH did have a thin rod-like composition but the presumed crystals were of a much greater size than reported elsewhere.

Electron microscopic examination did reveal that the product of ferrous oxidation in artificial sea-water (shown by infra-red spectroscopy and X-ray diffraction to be poorly crystalline γ-FeOOH) was composed of large agglomerates (very roughly 100μ x 60μ in size) of very small particles. This agglomeration of the oxidation product may well be due to the high ionic strength of the sea-water matrix and helps explain the ability of the product to settle on standing and then be collected by filtration. In contrast, the sample of β-FeOOH, with larger sized crystallites, tended to stay in suspension and had to be collected by prolonged centrifugation.

4.5 REFERENCES

(1) Horne R. A. - "Marine Chemistry" - (John Wiley and Sons,1969).

(2) Sylva R. N. - Rev. Pure & Appl. Chem., 22,115 (1972).

(3) Ishikawa T. & Inouye K.- Bull. Chem. Soc. Japan, 48(5), 1580 (1975).

(4) Kiyama M. - Bull. Chem. Soc. Japan, 47(7), 1646 (1974).

(5) Knight R. J. & Sylva R.N. - Jour. Inorg. Nucl. Chem., 36, 591 (1974).

(6) Kiyama M. & Takada T. - Bull.Chem.Soc. Japan, 46(6),1680 (1973)

(7) Keller V.P. -Werkstoffe u. Korrosion, 20,102 (1969)

(8) Soderquist R. & Jansson S. - Acta. Chem. Scand., 20(5), 1417 (1966).

(9) Biedermann G. & Chow J.T. - Acta. Chem. Scand., 20(5), 1376 (1966).

(10) Weiser H.B. & Milligan W.O. - J. Amer.Chem. Soc., 57, 238 (1934).

(11) Feitnecht W. et al - Helv. Chim. Acta., 56(8), 2847 (1973).

(12) Detournay J., Ghodsi M. & Derie R. - Ind. Chim. Belg., 39, 695 (1974).

(13) Detournay J., Ghodsi M. & Derie R. - Z. anorg. allg.Chem., 412, 184 (1975).

(14) Kiyama M. & Takada T. - Bull. Chem. Soc. Japan, 45(6), 1923 (1972).

(15) Misawa T., Hasimoto W., & Shimodaira S. - J.Inorg. Nucl. Chem., 35 (12), 4159 (1973).

(16) Feitknecht W . - Z. Elektrochem., 63, 34 (1959).

(17) Schwertmann U. - Z. anorg. allg. Chem., 298, 337 (1959).

(18) Krause A. - Monatsh. Chem., 96(2), 682 (1965).

(19) Krause A. & Skupinova W. - Monatsh. Chem., 96(6), 1809 (1965).

(20) Kolaczkowski St. & Byczynski H. - Z. anorg. allg. Chem., 342, 103 (1966).

(21) Stumm W. & Lee G.F. - Schweiz. Zeitsch. Fur. Hydrol., 22, 295 (1960).

(22) Schwertmann U. & Taylor R.M. - Clays and Clay Minerals, 20, 151 (1972).

(23) Kaneko K. et al - Bull. Chem. Soc. Japan, 48 (6), 1764 (1975).

(24) Lebedev T.S. - Geofiz. Sb. (Kiev), 57, 58 (1974) (Russian).

(25) Borchert H. - "Formation of Marine Sedimentary Iron Ores", in J.P. Riley and G. Skirrow, eds "Chemical Oceanography" Vol. 2, Chap. 18 (Academic Press, London, 1965).

(26) Brown G. - "The X-Ray Identification and Crystal Structures of Clay Minerals", (Jarrold & Sons Ltd., Norwich, 1961).

(27) Bonatti E. et al - "Classification and Genesis of Submarine Iron-Manganese Deposits" - P.B. 226,001, NTIS (U.S.A.), November 1972.

(28) Kaneko K. & Inouye K. - Bull. Chem. Soc. Japan, 47(5), 1139 (1974).

(29) Kauffman K. & Hazel F. - J. Inorg. Nucl. Chem., 37, 1139 (1975).

(30) Markichev N.A. & Kirillov I.P. - Izv. Vyssh. Ucheb. Zaved., Khim. Khim. Tekhnol., 14(10), 1603 (1971) (Russian).

(31) Sidgwick N.V. - "Chemical Elements and Their Compounds. Vol. II" - (Oxford University Press, 1951).

(32) D'Eye R.W.M. & Wait E. - "X-Ray Powder Photography in Inorganic Chemistry" - (Butterworths, 1960).

(33) Bunn C.W. - "Chemical Crystallography" -(Oxford University Press, 1961).

(34) James R. W. - "The Crystalline State - Vol. II: The Optical Principles of the Diffraction of X-Rays" (G. Bell & Sons Ltd., London, 1948).

(35) Jones F.W. - Proc. Roy. Soc., A166, 16 (1938).

(36) "X-Ray Diffraction by Polycrystalline Materials", Peiser H.S., Rooksby H.P. & Wilson A.J.C. (editors) - (The Institute of Physics, London, 1955).

(37) Derie R., Ghodsi M. & Hourez R.J. -Jappl. Chem. Biotechnol., 25, 509 (1975).

(38) Silverstein R.M. & Bassler G. C. - "Spectrometric Identification of Organic Compounds" - (John Wiley & Sons, 1967).

(39) Waldron R. D. - Phys. Rev., 99, 1727 (1955).

(40) Powers D.A. et al - Journ. Solid State Chemistry , 13,1 (1975).

(41) Olson L.L. & Twardowski Jr. C.J. - Jour. AWWA, 67(3), 150 (1975).

(42) Bunn C.W. - J. sci. Instr., 18, 70 (1941).

(43) Atkinson R.J. - J. Inorg. Nucl. Chem., 30, 2371 (1968).

CHAPTER 5

SUMMARY AND CONCLUSIONS

5.1 THE INTERACTION OF AN ACIDIC FERROUS SULPHATE EFFLUENT WITH SEA-WATER

The problem of disposing of large quantities of acidic ferrous sulphate effluent is one that has plagued the titanium pigment industry for many years. The effluent is the spent solution remaining at the end of the production of titanium dioxide by the so-called "sulphate process", the first stage of which is the dissolution of the raw ore, ilmenite ($FeO \cdot TiO_2$), in concentrated sulphuric acid. At present, because of the lack of an economic alternative, most "sulphate process" titanium pigment plants dispose of their effluent by dumping it at sea, either by barging or by pumping through direct submarine pipelines.

On disposal at sea the sulphuric acid in the effluent is neutralized and the ferrous iron content is oxidised and precipitated as hydrated ferric oxide (1). The latter causes immediate visual discolouration of the sea and on aggregation forms flakes which float above the sea-bed with little or no permanent deposition. The present project has investigated several aspects of the chemical interaction that takes place when an acidic ferrous sulphate solution is added to sea-water. In particular, work has been carried out to determine the theoretical solubility of both ferrous iron and ferric iron in sea-water, the kinetics of the ferrous iron oxidation process and the exact nature of the oxidation product formed.

Ferric iron is the dominant form of iron in sea-water, ferrous iron being thermodynamically unstable under the mildly oxidative conditions present in normal oxygenated waters. Solubility calculations along the lines of Kester and Byrne (2) have shown that the solubility of ferric iron in sea-water is controlled by the solubility of ferric hydroxide, but that the actual calculated solubility varies appreciably according to whether or not the proposed soluble undissociated molecular complex of ferric hydroxide, $Fe(OH)_3$ (d), is included in the calculations. When this species is included the calculated solubility is relatively constant over the pH range 5 to 9 and is in better agreement with experimentally measured values of soluble iron concentration in sea-water.

The solubility of ferrous iron in sea-water is controlled, as it is in low ionic strength bicarbonate waters (3), by the solubility of ferrous carbonate. Solubility calculations require a knowledge of the pH-dependent distribution of the bicarbonate buffer system. Detailed calculations, based on available thermodynamic data at $25^{o}C$ and one atmosphere pressure, have shown that ferrous iron interacts primarily with the carbonate and chloride ions in sea-water. Like other divalent metal ions (4) soluble ferrous iron is highly complexed in the sea-water matrix, present results indicating that up to 80% is complexed at the average sea-water pH 8.1. Because of its apparent ability to form soluble chloride complexes the calculated solubility of ferrous iron in sea-water is much greater than the calculated solubility in natural ground waters.

Results show that ferrous solubility has a strong dependence on solution pH, increasing dramatically as pH decreases. It has been estimated that at pH 8.1, at $25^{o}C$, the solubility of ferrous iron in sea-water is approximately 4.5×10^{-5} mole/litre, though it must be remembered that in oxygenated waters ferrous iron is unstable so that

this figure is only applicable to a temporary non-equilibrium situation. The greater sea-water solubility of ferrous iron, as compared to ferric iron, over the pH range 4 to 9 covered in the present work, accords with the observed precipitation of ferric hydroxide following the oxidation of an acidic ferrous sulphate solution introduced to the sea.

The interaction of an acidic ferrous sulphate solution with sea-water can be considered to consist of two separate stages. Firstly, there is the rapid reaction between the sulphuric acid in the effluent and the bicarbonate buffer of sea-water. Secondly, there is the subsequent oxidation of the introduced ferrous iron (and accompanying precipitation of $Fe(OH)_3$) at the pH resulting from the first reaction. A series of dilution experiments have been carried out with samples of a typical titanium dioxide industrial waste (Tioxide effluent) and samples of real sea-water. Calculations have shown that, given the effluent acidity and the sea-water pH and alkalinity, the pH resulting from the initial rapid sulphuric acid-bicarbonate buffer reaction can be predicted to a good degree of accuracy.

Because of the slow rate of transfer of carbon dioxide between sea-water and the atmosphere (5) the inorganic carbon content of sea-water can be regarded as remaining constant in the period immediately following the acid-buffer reaction. Ferrous solubility calculations have been made on this basis. Using the results of the dilution experiments the ferrous concentration/pH range spanned in sea-water following the dilution of Tioxide effluent (prior to ferrous oxidation but after the acid-buffer reaction) has been superimposed on the calculated ferrous solubility diagram. At no stage of dilution does the locus intercept the region of ferrous carbonate precipitation. It can thus be concluded that because of the high acid/iron ratio of the effluent there is little, if any, possibility of ferrous carbonate being precipitated on the disposal of

this effluent at sea. A consideration of the values involved suggests that this conclusion is valid over the temperature range encountered in coastal waters.

It was of interest to determine the conditions (and thus effluent composition) required for the precipitation of ferrous carbonate in sea-water because of the suggestion (6) that ferrous carbonate (siderite) precipitates as large separate crystalline particles which are then, under water, relatively stable to subsequent oxidation. A precipitate of siderite might thus be expected to settle to the sea-bed, in contrast to the very fine suspended precipitate of ferric hydroxide which is observed to form following the disposal of titanium pigment effluent at sea and which gives rise to the visual and other pollution problems encountered. However, studies with a prepared sample of ferrous carbonate have shown that in oxygenated waters this precipitate is not stable but is oxidised to a mixture of ferric hydroxides. There would thus seem to be no advantage to be attained in altering the acid/iron ratio of the industrial effluent so as to achieve ferrous carbonate precipitation in sea-water.

The kinetics of the ferrous oxidation reaction that takes place following the introduction of an acidic ferrous sulphate solution to sea-water has been studied using artificial effluents and an artificial sea-water. The latter, a solution of sodium chloride and sodium bicarbonate, provided a reproducible medium of known composition for use in the kinetic studies. Solubility calculations show that the pH dependent solubility of both ferrous iron and ferric iron is basically the same for the artificial sea-water matrix as for real sea-water. Kinetic results found using the artificial sea-water are applicable to real sea-water as shown by the results of several comparative kinetic runs. The fact that differences between real sea-water and the simplified matrix used to simulate it cause only minor differences in the measured rate of ferrous oxidation indicates that the concentrations of the more common

minor elements found in sea-water are such that they have little significant effect on the magnitude of the oxidation kinetics. The results also show that a simplified medium can be used successfully in laboratory experiments to model the behaviour and salient characteristics of real sea-water.

It has been found that the rate of ferrous iron oxidation in the artificial sea-water increases with increasing initial ferrous iron concentration and decreases with decreasing pH. Below pH 6 the oxidation reaction is effectively quenched. Kinetic analysis of oxygen consumption curves measured in solutions closed to the atmosphere at 25°C shows that the rate of ferrous oxidation is of first order with respect to ferrous iron concentration and dissolved oxygen concentration. Consideration of the empirical rate constants shows that a pH term should also be included in the overall rate expression. The pH of a sea-water solution does not remain constant after the addition of a set volume of acidic ferrous sulphate effluent and completion of the rapid sulphuric acid - bicarbonate buffer interaction, but gradually decreases due to ferric hydrolysis.

When the influence of pH is taken into account the kinetics of the ferrous iron oxidation reaction in the artificial sea-water conform to the expression:

$$-\frac{d(Fe^{2+})}{dt} = k_B\ (Fe^{2+})\ (O_2)\ (OH^-)^2 \quad \ldots \quad (5A)$$

where the rate constant k_B has an estimated value of $5.7 \pm 0.6 \times 10^{16}$ $litre^3\ mole^{-3}\ min^{-1}$ at 25°C. Equation (5A) is the established kinetic expression describing the rate of ferrous iron oxidation in low ionic-strength bicarbonate waters, for ferrous concentrations lower than 2 mg/l

(7). The present work carried out has thus extended the work of Stumm and Lee (7) and has shown that equation (5A) also describes the rate of ferrous iron oxidation in a high ionic - strength bicarbonate water, such as sea-water, and applies to soluble ferrous concentrations up to 60 mg/l. The estimated value for k_B obtained in the present study is of the same order of magnitude as k_B values found in simulated ground-waters (8). The results thus suggest that in spite of the lower alkalinity and higher ionic-strength of sea-water, as compared to low ionic - strength natural waters, the net rate of ferrous oxidation in both is basically the same.

Kinetic runs undertaken at 12^oC show that the rate of ferrous iron oxidation in sea-water is highly temperature dependent. Analysis of the kinetic data shows that the same rate expression applies at 12^oC as does at 25^oC, and the rate constant k_B (expression (5A)) has an estimated value of $1.0 \pm 0.1 \times 10^{16}$ litre^3 mole^{-3} min^{-1} at the lower temperature. The oxidation rate thus decreases by roughly a factor of 6 with a decrease in temperature of 13^oC. From the k_B values at the two different temperatures the activation energy of the ferrous oxidation reaction in the artificial sea-water is calculated to be $9.6 \pm 1.3 \times 10^4$ joules/mole.

Titanium pigment effluent is disposed of at sea either near the ocean surface (barge dumping) or near the sea-bed (discharge from submarine pipeline). The closed kinetic runs carried out simulate the latter situation. Open kinetic runs carried out suggest that where oxidation takes place near the surface, the rate of oxygen transfer from the air into solution is rapid enough to increasingly offset the oxygen consumed in the ferrous iron oxidation reaction. The net rate of oxygen consumption in the open situation has been successfully modelled for the experimental arrangement employed in present work. In the real situation the rate of oxygen dissolution in saline water depends on both the degree of oxygen depletion in solution and such factors as wind velocity, wave height and

temperature (9).

Under the experimental conditions employed in the present study the quantity of dissolved oxygen consumed by ferrous oxidation, even in the open runs undertaken, was substantial. In practice, due to the continuing dilution of an industrial effluent in sea-water, one would expect only a minor depletion of dissolved oxygen in the waters involved. The net oxygen consumption in surface waters will be correspondingly less than that in waters near the sea-bed, due to the rate of oxygen transfer across the air-sea interface. The actual time required for the oxygen concentration to return to normal will depend on the rate of effluent dilution. To give an example of in-situ measurements, Weichart (10) found that immediately after the release of a titanium pigment effluent into surface ocean waters the sea-water pH was 6 and the initial ferrous iron concentration 40 mg/l. Two hours later the oxygen concentration and pH had nearly returned to normal. The majority of the present experimental work has been carried out within these indicated boundary conditions.

If adequate dilution of an effluent is not achieved, especially in the case of pipeline disposal, then a sizeable percentage of the sea-water dissolved oxygen can be consumed. For example, present work shows that at $12^{o}C$, at an initial ferrous iron concentration of 10 mg/l (artificial effluent) and with pH roughly constant at 6.7, ferrous oxidation consumes 12% of the dissolved oxygen in two hours. These values correspond to a stagnant 1:2000 dilution in sea-water of an effluent with roughly the same ferrous iron concentration as Tioxide industrial effluent.

To compare Tioxide effluent with the artificial effluents used in the majority of kinetic studies several runs have been carried out with the industrial effluent and samples of real sea-water. Because of

the experimental method used runs were limited to the dilution range 1:1500 to 1:3000. Below a dilution of 1:1000 oxidation of the ferrous iron in this industrial effluent has been found to be quenched, the resulting sea-water pH being less than 6. At dilution ratios above 1:4000 the ferrous iron concentration in solution is less than 5 mg/l, too small for a significant consumption of oxygen. In all the runs undertaken with Tioxide effluent the rate of oxidation of ferrous iron has been found to be substantially lower than the rate found using artificial effluents. This damping of the ferrous oxidation reaction is not due to differences between real sea-water and the artificial sea-water used to simulate it. It can thus be concluded that the ferrous oxidation reaction in sea-water is retarded by some minor component, yet to be identified, in the Tioxide effluent.

Following ferrous oxidation the ferric iron produced in sea-water precipitates as ferric hydroxide. The term "ferric hydroxide" covers the crystalline forms of hydrated ferric oxide and hydrated ferric oxyhydroxide. By preparing the three naturally found iron oxy-hydroxides and haematite it has been shown that these four compounds can be differentiated by means of their infra-red spectra. Crystallite sizes can be estimated from the line widths obtained in X-ray diffraction patterns by means of the Scherrer formula. For the samples prepared the order of crystallite size was calculated to be α-Fe_2O_3 > β-FeOOH > α-FeOOH > γ-FeOOH. The ordering of the oxyhydroxides agrees with values determined by previous workers for similarly prepared samples (11).

The "ferric hydroxide" formed following the oxidation of ferrous iron in both real and artificial sea-water has been shown by infra-red spectroscopy and X-ray diffraction to be poorly crystalline lepidocrocite, γ-FeOOH. Lepidocrocite was identified in all the oxidation

products formed in the present work and the precipitate showed no signs of conversion to other crystalline forms when left under solution for ten weeks. Electron microscopic examination of precipitate samples showed them to be composed of large agglomerates of very small particles. It is surmised that the agglomeration of the fine particles is due to the high ionic-strength of the sea-water matrix. The agglomerates are of low density, in accordance with the observation that ferric hydroxide precipitated in sea-water forms loose flakes which do not tend to settle but float above the sea-bed (1).

The fact that the same oxidation product was obtained with the artificial solutions as was with Tioxide effluent and real sea-water is further indication that the relevant sea-water oxidation reaction has been successfully modelled in the laboratory. It can be concluded from the series of experiments carried out that lepidocrocite, γ-FeOOH, is the crystalline product formed from the oxidation of ferrous iron in sea-water over the pH range 5.5 to 7.5 and for initial ferrous iron concentrations ranging from 7 mg/l to 75 mg/l.

The formation of lepidocrocite following the oxidation of ferrous iron in sea-water is consistent with the natural formation of the sedimentary iron ore limonite, although the majority of limonites are composed of goethite, α-FeOOH, rather than γ-FeOOH. There was no evidence of the formation of β-FeOOH although this oxyhydroxide is known to be formed in the presence of chloride ions (12).

Average crystallite sizes estimated for the ferrous oxidation products formed in the different kinetic runs carried out vary from 140 Å (14 nm) to 55 Å (5.5 nm). For the runs involving artificial effluents there is a trend for the average crystallite size of the oxidation product to increase with increasing initial ferrous iron concentration. This trend has been shown to be consistent with a

mechanism of lepidocrocite formation involving the slow growth of crystal particles.

Finally, the product of ferrous carbonate oxidation in oxygenated waters has been shown by infra-red spectroscopy to be a mixture of α-FeOOH and γ-FeOOH. Because no α-FeOOH has been detected in any of the oxidation precipitates formed in both real and artificial sea-water, it can be concluded that under the conditions spanned in the present work ferrous carbonate precipitation and oxidation is not part of the overall oxidation process. This conclusion agrees with the results of the solubility calculations carried out early in the project.

Thus overall it can be stated that the work carried out has been successful in achieving its objectives. In particular, the solubility and speciation of ferrous iron in sea-water at $25^{o}C$ have been determined, according to the best available thermodynamic data, and the calculated solubility has been related to the disposal of acidic ferrous sulphate effluent at sea; the kinetics of the oxidation of ferrous iron in sea-water has been established, extending the results of previous workers for ferrous oxidation in low ionic-strength bicarbonate waters; and the crystalline nature of the ferric hydroxide formed following ferrous oxidation in sea-water has been determined. As in most research there are several aspects of the present work that require further investigation. These are suggested as suitable areas for a future research programme.

5.2 SUGGESTIONS FOR FURTHER WORK

The rate of ferrous iron oxidation in sea-water following the addition of Tioxide industrial effluent has been found to be retarded compared to the rate achieved following the addition of a synthetic sulphuric acid/ferrous sulphate solution. However the same oxidation product is formed in both cases. An explanation is required for these findings. It is suggested that, following an analysis of the Tioxide effluent, a study be made of the influence of the trace components in the effluent, such as manganese and titanium species, on the kinetics of ferrous iron oxidation. An investigation into the precise ionic form of the ferrous iron as present in the low pH Tioxide effluent should also be undertaken. The study could be extended to investigate the effect on the oxidation kinetics and the oxidation product formed of additions of selected trace elements, such as copper, to the effluent.

As a follow-up to the present work an in-situ sample of the oxidation product that results from industrial effluent disposal at sea should be collected, if possible, and examined by infra-red spectroscopy and X-ray diffraction. Also, it would be of interest to study the kinetics of the ferrous oxidation reaction at initial ferrous iron concentrations below 5 mg/l, corresponding to much higher effluent dilution ratios than employed in the present study. It is suggested that this could be achieved by undertaking open kinetic runs using the method of Stumm and Lee (7), in other words by following the rate at which the soluble ferrous iron concentration decreases rather than the rate of depletion of dissolved oxygen in a closed solution. Preliminary investigations have shown that the ferrous iron concentration in the artificial sea-water

matrix at a given time can be determined by a slight modification to the 1, 10 - phenanthroline analytical method of Tamura et al (13). In this spectrophotometric technique high concentrations of ferric iron are masked by the addition of fluoride ions.

Two other possible areas of research have suggested themselves to the author. Firstly, concern has been expressed that heavy metals can be taken up and thus concentrated by ferric hydroxide particulates suspended above the sea-bed, creating a pollution hazard. It is therefore suggested that a study be made of the adsorption of heavy metals by lepidocrocite (γ-FeOOH) suspensions. Secondly, on a theoretical note, it would be of interest to undertake a study of the soluble ferrous-ferric species present in the sea-water matrix prior to precipitate formation. These could be investigated by means of electronic and Raman spectroscopy (14).

5.3 REFERENCES

(1) Rachor E. - Mar. Pollut. Sea Life, FAO, 390 (1972).

(2) Kester D.R. & Byrne R.H. Jr. - "Chemical Forms of Iron in Sea Water" - see ref. (20), Chapter 2.

(3) Stumm W. & Lee G.F. -"The Chemistry of Aqueous Iron"- Schweiz. Zeitsch. Fur. Hydrol., 22 , 295 (1960).

(4) Zirino A. & Yamamoto S. - Limmol. Oceanog., 17 (5), 661 (1972).

(5) Harvey H. W. - "Biological Chemistry and Physics of Sea-Water" (Cambridge University Press, 1928).

(6) Olson L .L. & Twardowski C.J. Jr. - Jour. A.W.W.A., 67(3), 150 (1975).

(7) Stumm W. & Lee G.F. - Industrial and Engineering Chemistry, 53, 143 (1961).

(8) Jobin R. & Ghosh M.M.- Jour. A.W.W.A., 64(9), 590 (1972).

(9) Downing A.L. & Truesdale G.A. - J. Appl. Chem., 5, 570 (1955).

(10) Weichart G. - Mar. Pollut. Sea Life, FAO, 186 (1972).

(11) Kaneko K. & Inouye K.- Bull. Chem. Soc. Japan, 47 (5), 1139 (1974).

(12) Ishikawa T. & Inouye K.- Bull. Chem. Soc. Japan, 48(5), 1580 (1975).

(13) Tamura H. et al - Talanta, 21, 314 (1974).

(14) Misawa T. et al - J. Inorg. Nucl. Chem., 35, 4159 (1973).

APPENDIX 1

Calculation of Ferric Iron Solubility in Sea-Water

The total ferric iron solubility is given by the sum of the concentrations of the soluble ferric complexes.

i.e. $(Fe(III)) = (Fe^{3+}) + (Fe(OH)^{2+}) + (Fe(OH)_2^{+}) + (Fe(OH)_4^{-})$

$(+ (Fe(OH)_3(d)))$

Applying the method of Kester and Byrne (20) as outlined in section 2.4.1 and employing the data of tables 2, 3 and 4 we find:

A. For Real Sea-Water

$$(Fe(III)) = (Fe^{3+}) \left(1 + \frac{2.02 \times 10^{-3}}{(H^+)} + \frac{2.33 \times 10^{-8}}{(H^+)^2} + \frac{1.34 \times 10^{-22}}{(H^+)^4} \left(+ \frac{9.39 \times 10^{-13}}{(H^+)^3} \right) \right)$$

where $(Fe^{3+}) = 3.09 \times 10^5 \times (H^+)^3$ (as controlled by the solubility of $Fe(OH)_3$ (s))

B. For 'Artificial' Sea-Water

$$(Fe(III)) = (Fe^{3+}) \left(1 + \frac{1.45 \times 10^{-3}}{(H^+)} + \frac{1.42 \times 10^{-8}}{(H^+)^2} + \frac{1.34 \times 10^{-22}}{(H^+)^4} \left(+ \frac{5.64 \times 10^{-13}}{(H^+)^3} \right) \right)$$

where $(Fe^{3+}) = 5.15 \times 10^5 \times (H^+)^3$

These equations were evaluated, by means of a computer programme, over a pH range from 4 to 9. The results are plotted in Figure 3.

APPENDIX 2

2A - Calculation of the pH-Dependent Distribution of the Carbonate System in Artificial Sea-Water at 25°C and Constant C_T

The distribution is described by the following set of relationships:-

(A2.1): $C_T = (H_2CO_3) + (HCO_{3_T}^-) + (CO_{3_T}^{2-}) = 0.0027$

(A2.2): $Alk = (HCO_{3_T}^-) + 2(CO_{3_T}^{2-}) + (OH^-) - (H^+)$

(A2.3): $H_2CO_3 \rightleftharpoons HCO_{3_F}^- + H^+ ; \quad K = 4.45 \times 10^{-7}$ (6)

(A2.4): $HCO_{3_F}^- \rightleftharpoons CO_{3_F}^{2-} + H^+ ; \quad K = 4.8 \times 10^{-11}$ (6)

(A2.5): $Na^+ + HCO_{3_F}^- \rightleftharpoons NaCO_3^- + H^+ ; \quad K = 6.5 \times 10^{-10}$ (16)

(A2.6): $Na^+ + H_2CO_3 \rightleftharpoons NaHCO_3^o + H^+ ; \quad K = 1.8 \times 10^{-7}$ (16)

(A2.7): $(HCO_{3_T}^-) = (HCO_{3_F}^-) + (NaHCO_3^o)$

(A2.8): $(CO_{3_T}^{2-}) = (CO_{3_F}^{2-}) + (NaCO_3^-)$

To aid in the calculations the assumption is made that

$$Na^+_{complexed} \ll Na^+_{total}$$

so that $(Na^+) = 0.42$ moles/litre (N.B. it can be shown that at pH 7 only 0.06% of the sodium is complexed). Then, by applying the relevant activity coefficients, rewriting the equilibrium expressions in terms of $(HCO_{3_F}^-)$ and substituting into equation A2.1 we find:

$$\left(\frac{(H^+) \times (HCO_{3_F}^-)}{6.1 \times 10^{-7}}\right) + 1.124(HCO_{3_F}^-) + \left(\frac{3.97 \times 10^{-10}(HCO_{3_F}^-)}{(H^+)}\right) = 0.0027$$

$$\Longrightarrow \text{(A2.9)}: (HCO_{3_F}^-) = 0.0027 \Big/ \left(\frac{(H^+)}{6.1 \times 10^{-7}} + 1.124 + \frac{3.97 \times 10^{-10}}{(H^+)}\right)$$

A similar substitution gives the corresponding expression for alkalinity. Values for alkalinity, as well as for the required carbonate species, were calculated over a pH range from 4 to 9 by means of a computer programme and are plotted in Figure 4.

2B - Calculation of Ferrous Iron Solubility in Sea-Water

The total ferrous iron solubility is given by the sum of the concentrations of the soluble ferrous complexes.

A/ For Real Sea-Water

$$(Fe(II)) = (Fe^{2+}) + (Fe(OH)^{+}) + (Fe(OH)_2^{o}) + (Fe(OH)_3^{-}) + (FeCl^{+}) + (FeCl_2^{o}) + (FeF^{+}) + (FeSO_4^{o}) + (FeCO_3^{o}) + (Fe(HCO_3)^{+})$$

Applying the method of Kester and Byrne to the data of tables 5, 6 and 7, and rewriting carbonate equilibrium terms in terms of bicarbonate concentration, we find:

$$(Fe(II)) = (Fe^{2+}) \left(1 + \frac{1.17 \times 10^{-9}}{(H^+)} + \frac{3.5 \times 10^{-20}}{(H^+)^2} + \frac{2.46 \times 10^{-33}}{(H^+)^3} + 1.28 + 0.79 + 3.6 \times 10^{-4} + 0.114 + \frac{8.56 \times 10^{-6}}{(H^+)} (HCO_{3_F}^{-}) + 62.3 (HCO_{3_F}^{-}) \right)$$

where i/ if solubility is controlled by $Fe(OH)_2(s)$,

$$(Fe^{2+}) = 4.59 \times 10^{13} \times (H^+)^2$$

ii/if solubility is controlled by $FeCO_3(s)$,

$$(Fe^{2+}) = 1.88 \times (H^+) / (HCO_{3_F}^{-})$$

and $(HCO_{3_F}^{-})$ is obtained via the data of Whitfield (16).

B/ For 'Artificial' Sea-Water

$$(Fe(II)) = (Fe^{2+}) + (Fe(OH)^{+}) + (Fe(OH)_2^{o}) + (Fe(OH)_3^{-}) + (FeCl^{+}) + (FeCl_2^{o}) + (FeCO_3^{o}) + (Fe(HCO_3)^{+})$$

whence, as before:

$$(Fe(II)) = (Fe^{2+}) \left(1 + \frac{9.94 \times 10^{-10}}{(H^+)} + \frac{2.9 \times 10^{-20}}{(H^+)^2} + \frac{2.09 \times 10^{-33}}{(H^+)^3} + 0.96 + 0.44 + \frac{7.93 \times 10^{-6}}{(H^+)} (HCO_{3_F}^{-}) + 56.9(HCO_{3_F}^{-}) \right)$$

where i/if solubility is controlled by $Fe(OH)_2(s)$,

$$(Fe^{2+}) = 5.47 \times 10^{13} \times (H^+)^2$$

ii/if solubility is controlled by $FeCO_3(s)$,

$$(Fe^{2+}) = 2.09 \times (H^+) \; / \; (HCO_{3_F}^{-})$$

and $(HCO_{3_F}^{-})$ is given by expression (A2.9) in Appendix 2A.

The preceding equations were evaluated, by means of a computer programme, over a pH range from 5.5 to 9. The results are plotted in Figure 5.

APPENDIX 3

CALCULATION OF pH RESULTING FROM ACID-BUFFER INTERACTION AT 25°C.

Case A - Buffer Capacity Not Exceeded

In this case, equation (2M) is relevant

$$\text{i.e. } (H^+)_{End} = K \left(\frac{(H^+)_{Init} \times (Alk) \times K^{-1} + (H^+)_{Add}}{(Alk) - (H^+)_{Add}} \right)$$

Substituting in the values:

$(H^+)_{Init} = 8.32 \times 10^{-9}$ m/l (pH 8.08)

$(Alk) = 2.33 \times 10^{-3}$ m/l

$K_{25^oC} = 7.39 \times 10^{-7}$ (corrected with sea-water activities)

we have: $$(H^+)_{End} = 7.39 \times 10^{-7} \left(\frac{2.62 \times 10^{-5} + (H^+)_{Add}}{2.33 \times 10^{-3} - (H^+)_{Add}} \right)$$

Thus, for example, at a dilution of 1:2,000 (given effluent acidity of 1.3 m/l),

$$(H^+)_{Add} = {}^{1.3}/_{2,000} = 6.5 \times 10^{-4} \text{ m/l}$$

and so we find:

$$(H^+)_{End} = 3.02 \times 10^{-7}{}_{m/l} \Rightarrow pH = 6.52$$

The above calculation was repeated for dilutions ranging from 1:50,000 to 1: 1,000 and values appear in Table 9.

Case B - Buffer Destroyed

In this case, $(H^+)_{Add} > 2.33 \times 10^{-3}$ m/l. At the point when $(H^+) = 2.33 \times 10^{-3}$ m/l we have effectively a 2.33×10^{-3}M solution of H_2CO_3 with a calculated pH of 4.38 (using equation 2A). Excess acid can thus be regarded as having been added to

this solution. Because of the weak acidity of carbonic acid a negligible amount will be ionised in the presence of excess acid.

Let the excess acid be M molar H_2SO_4; then the dissociation steps are:-

$$H_2SO_4 \longrightarrow H^+ + HSO_4^-$$

M moles → M moles, M moles

$$HSO_4^- \rightleftharpoons H^+ + SO_4^{2-} \quad ; \quad K_{a_{25^oC}} = 3.9 \times 10^{-2}$$

(corrected with sea-water activities)

(M-X moles) → X moles, X moles

Thus at equilibrium: $\frac{(M+X)X}{(M-X)} = 3.9 \times 10^{-2}$

and X can be found by solving the quadratic. The final pH is then given by: $(H^+)_{End} = M + X$

For example, at a dilution of 1:500,

$$(H^+)_{Add} = {}^{1.3}/_{500} = 2.6 \times 10^{-3} \text{m/l}$$

Excess acid = $(2.6 \times 10^{-3} - 2.33 \times 10^{-3})/2 = 1.35 \times 10^{-4}$ m/l as H_2SO_4

Solving the quadratic, we find $X = 1.34 \times 10^{-4}$ m/l

$$\Rightarrow (H^+)_{End} = (1.35 + 1.34) \times 10^{-4} = 2.7 \times 10^{-4} \text{ m/l} \Rightarrow \text{pH} = 3.57$$

The calculation was repeated for dilutions of 1:50 and 1:100 and values are given in Table 9.

APPENDIX 4

RATE ANALYSIS OF OPEN KINETIC RUNS

The net rate of oxygen consumption recorded in the open kinetic runs is given by equation (3L):

$$-\frac{d(O_2)}{dt_N} = -\frac{d(O_2)}{dt_R} - \frac{d(O_2)}{dt_A}$$

Substituting in the relevant expressions corresponding to the assumptions described in Section 3.3.4 we have:

$$-\frac{d(O_2)}{dt_N} = \frac{k_A}{4}(Fe^{2+})(O_2) - k_R((O_2)_{SAT} - (O_2)) \quad .... \quad (A4.1)$$

Equation A4.1 can be rewritten in terms of measured oxygen concentration, C, as follows:

$$-\frac{dC}{dt} = \frac{k_A}{4}(A-4k(C_s-C))C - k_R(C_s-C) \quad .... \quad (A4.2)$$

where relevant nomenclature is given in the text. We now require to integrate this expression. This is achieved as outlined below.

Firstly, equation A4.2 can, by re-arrangement, be expressed in the form:

$$-\frac{dC}{dt} = aC^2 + bC + d \quad .... \quad (A4.3)$$

where $a = k_A k$, $b = Ak_A/4 + k_R - k_A k \times C_s$, $d = -k_R C_s$

Now the general solution to this differential equation is obtained by completing the square and then using partial fractions. Given that at

$t = 0$, $C = C_s$, the solution can be expressed in the form:

$$\ln \left(\frac{C + b/2a + E}{C + b/2a - E} \right) - \ln \left(\frac{C_s + b/2a + E}{C_s + b/2a - E} \right) = 2Eat$$

where $E = \sqrt{(b^2/4a^2 + d/a)}$ .... (A4.4)

Thus, on making the relevant substitutions, equation A4.4 describes the modelled oxygen concentration in solution as a function of time. The unknown in the expression is the ferrous oxidation rate constant, k_A. A computer programme was designed to accept a given k_A and compare the corresponding calculated oxygen consumption/time curve with that actually experimentally obtained. The procedure was repeated until a k_A value was found that gave theoretical results in best agreement with the experimental data.

APPENDIX 5

ESTIMATION OF ACTIVATION ENERGY

The Arrhenius equation states that:

$$K = Ae^{-Ea/RT} \quad \ldots \quad (A5.1)$$

where A = constant

K = rate of reaction

Ea = activation energy for reaction

R = universal gas constant

T = temperature at which reaction proceeds

When we have two recorded rates of reaction, measured for the same reaction at different temperatures, equation (A5.1) gives the relations hip:

$$\frac{K_1}{K_2} = e^{-Ea(1/T_1 - 1/T_2)/R} \quad \ldots\ldots \quad (A5.2)$$

Re-arranging:

$$Ea = \ln\left(K_1/K_2\right) \Big/ \left(1/R\,(1/T_2 - 1/T_1)\right) \quad \ldots\ldots \quad (A5.3)$$

In the present case we have that:

(a) At $T_1 = 25.00 \pm 0.05^{o}C$, $k_{B_1} = 5.7 \pm 0.6 \times 10^{16}$ litre^3 mole^{-3} min^{-1}

(b) At $T_2 = 12.0 \pm 0.1^{o}C$, $k_{B_2} = 1.0 \pm 0.1 \times 10^{16}$ litre^3 mole^{-3} min^{-1}

Substituting values into equation (A5.3), and using the given errors in T and k_B, we get as an estimation of the activation energy for the ferrous iron oxidation reaction in artificial sea-water:

$$\underline{Ea = 9.6 \pm 1.3 \times 10^4 \text{ joules/mole}}$$

$$(23 \pm 3 \text{ kcal/mole})$$

APPENDIX 6

6A-CALCULATION OF CRYSTALLITE SIZE FROM X-RAY DIFFRACTION PATTERNS

Crystallite sizes were estimated by the application of the Scherrer formula to the three principal X-ray diffraction lines obtained for each sample. Re-arranging the Scherrer formula (4A), with values of 1.1 for the Scherrer constant and 1.54 $\mathring{A}$ for the wavelength of CuK_α radiation, we have:

$$L = 1.69/\beta \cos\theta \quad .... \quad (A\ 6.1)$$

where L = apparent crystallite size ($\mathring{A}$)

β = true integral breadth of the diffraction line (radians)

θ = Bragg angle

For the particular experimental arrangement employed, 1^o $(2\theta) \equiv 20$ mm. Rewriting (A6.1) for β in units of millimetres:

$$L = 1941/\beta \cos\theta \quad .... \quad (A\ 6.2)$$

The integral breadth of each required diffraction peak was calculated by using a series of triangles to approximate the area beneath each curve and then dividing the resultant calculated area by the overall peak height. Because of the poorly crystalline nature of most of the samples (which meant a high sensitivity was required to obtain the different diffraction patterns), the small size of the crystallites and the presence of iron fluorescence radiation, integral breadths had a high associated error (see Section 4.4.2 and Figures 26 and 27).

Having obtained the integral breadth (B) for a particular peak, the ratio $b/_B$ was calculated where b is the estimated machine broadening at the same Bragg angle (given by the integral breadths of the peaks of the commercial haematite diffraction pattern - see Section 4.3.2.) The use of the Jones correction curve (curve (a) Fig. 197, p. 543 (34)) then allows β, the true integral breadth of the peak, to be calculated. The substitution of β with associated error into (A6.2) gives a value for the apparent crystallite size. Three such values were obtained from the three principal diffraction peaks recorded for each sample and the average, rounded to the nearest power of 5 Angstrom units, taken to give an overall value for crystallite size.

Two examples of the series of calculations undertaken are summarized below:

1. CRYSTALLITE SIZE OF REFERENCE α-FeOOH

θ (Degrees)	B (mm)	b (mm)	$b/_B$	β (mm)	Estimated Crystallite Size ($\mathring{A} = 10^{-10}$m)
10.6	15.5±0.5	2.5	0.16	15.0	131±5
16.6	10.2±0.3	3.2	0.31	9.4	215±6
18.3	11.8±0.3	3.3	0.28	11.1	184±5

$\Rightarrow$ Average crystallite size = 180 ± 20 $\mathring{A}$

= 18 ± 2 nanometres

2. CRYSTALLITE SIZE OF PRECIPITATE FROM RUN 22

($[Fe^{2+}]_I$ = 40 mg/l, See Figure 27C)

θ (Degrees)	B (mm)	b (mm)	b/B	β (mm)	Estimated Crystallite Size ($\mathring{A} = 10^{-10}$m)
7.0	16±1.5	2.5	0.16	15.6	125±11
13.5	18±1.5	2.7	0.15	17.6	114±9
18.1	20±2	3.3	0.17	19.5	105±10

$\Longrightarrow$ Average crystallite size = 115 ± 10 $\mathring{A}$

= 11.5 ± 1 nanometres

6B- TABLES OF ESTIMATED CRYSTALLITE SIZE

N.B. In the following tables the kinetic runs undertaken are characterised by their run number. Relevant details on the nature of each run can be found, if required, in Appendix 7. In the case of Runs 1, 2, 16, 24 and 33 insufficient precipitate was collected to enable the X-ray diffraction pattern to be recorded. Because of the errors involved in estimating the integral breadths of the principal diffraction lines, average crystallite sizes have been rounded off to the nearest power of 5 Angstrom units. Crystallite sizes determined for the reference iron compounds are given in the text and so have not been repeated here.

ARTIFICIAL EFFLUENT RUNS

1. Closed Runs

Run Number	$[Fe^{2+}]_I$ (mg/l)	Estimated Crystallite Size ($\mathring{A} = 10^{-10}m$)	Run Number	$[Fe^{2+}]_I$ (mg/l)	Estimated Crystallite Size ($\mathring{A} = 10^{-10}m$)
3	20	75±10	13	40	130±10
4	30	100±10	14	60	120±10
5	40	110±10	15	60	110±15
6	40	130±10	17	20	55±10
7	20	80±10	18	40	110±10
8	30	105±10	19	40	90±10
9	40	110±10	20	60	125±15
10	50	130±10	27	20	70±10
11	60	140±10	28	20	70±10
12	20	80±10	29	40	105±10

2. Open Runs

Run Number	$[Fe^{2+}]_I$ (mg/l)	Estimated Crystallite Size ($\mathring{A} = 10^{-10}m$)	Run Number	$[Fe^{2+}]_I$ (mg/l)	Estimated Crystallite Size ($\mathring{A} = 10^{-10}m$)
21	20	80±10	25	60	120±15
22	40	115±10	26	75	135±10
23	40	105±10			

TIOXIDE EFFLUENT RUNS

Run Number	Effluent Dilution Ratio	Estimated $[Fe^{2+}]_I$ (mg/l)	Estimated Crystallite Size ($\mathring{A} = 10^{-10}m$)
30	1:1500	18	120±15
31	1:1500	14	110±10
32	1:1500	14	85±15

APPENDIX 7

TABULATED EXPERIMENTAL KINETIC DATA

The following tables give the actual values of dissolved oxygen concentration and pH recorded in the series of kinetic experiments carried out in the present project. Data is also presented for the re-aeration runs discussed in Section 3.3.4. In the case of Runs 10, 12 and 26 it was possible to analyse the precipitate formed, but kinetic data had to be discarded due to erratic behaviour of the oxygen sensor.

A/ CLOSED RUNS AT 25°C

N.B. To reduce the data to manageable proportions values have only been given for each ten minutes of a run. Five-minute values, if required, can be approximated by averaging.

ARTIFICIAL SEA-WATER - ARTIFICIAL EFFLUENT A

TIME (Minutes)	RUN 1 $(Fe^{2+})_I$ = 10 mg/l		RUN 2 $(Fe^{2+})_I$ = 20 mg/l		RUN 3 $(Fe^{2+})_I$ = 20 mg/l	
	O_2 (ppm ± 0.02)	pH (± 0.02)	O_2 (ppm ± 0.02)	pH (± 0.02)	O_2 (ppm ± 0.02)	pH (± 0.02)
0	6.85	8.36	6.80	8.32	7.01	8.34
5	6.11	6.80	6.25	6.65	6.40	6.70
10	5.98	6.78	6.12	6.62	6.28	6.68
20	5.80	6.77	5.83	6.58	6.01	6.60
30	5.69	6.76	5.62	6.55	5.81	6.59
40	5.60	6.77	5.42	6.54	5.62	6.56
50	5.52	6.77	5.28	6.52	5.45	6.55
60	5.49	6.76	5.15	6.50	5.31	6.54
70			5.05	6.48	5.19	6.52
80			4.95	6.47	5.09	6.49
90			4.87	6.46	5.01	6.49
100			4.82	6.45	4.93	6.48
110			4.75	6.44	4.88	6.47
120			4.70	6.43	4.82	6.47

TIME (Minutes)	RUN 4 $(Fe^{2+})_I$ = 30 mg/l		RUN 5 $(Fe^{2+})_I$ = 40 mg/l		RUN 6 $(Fe^{2+})_I$ = 40 mg/l	
	O_2 (ppm $\pm$ 0.02)	pH ($\pm$ 0.02)	O_2 (ppm $\pm$ 0.02)	pH ($\pm$ 0.02)	O_2 (ppm $\pm$ 0.02)	pH ($\pm$ 0.02)
0	6.85	8.36	6.80	8.40	6.90	8.37
5	6.38	6.69	6.31	6.60	6.35	6.58
10	6.12	6.63	6.12	6.55	6.14	6.55
20	5.87	6.52	5.85	6.48	5.90	6.48
30	5.61	6.49	5.60	6.44	5.64	6.44
40	5.44	6.43	5.38	6.41	5.42	6.40
50	5.30	6.40	5.14	6.39	5.20	6.38
60	5.13	6.39	4.94	6.37	4.97	6.34
70	5.00	6.38	4.72	6.34	4.78	6.32
80	4.90	6.35	4.55	6.31	4.61	6.30
90	4.80	6.35	4.38	6.29	4.43	6.27
100	4.71	6.34	4.22	6.28	4.27	6.24
110	4.59	6.33	4.08	6.27	4.13	6.23
120	4.52	6.32	3.95	6.26	4.01	6.23

ARTIFICIAL SEA-WATER - ARTIFICIAL EFFLUENT B

TIME (Minutes)	RUN 7 $(Fe^{2+})_I$ = 20 mg/l		RUN 8 $(Fe^{2+})_I$ = 30 mg/l		RUN 9 $(Fe^{2+})_I$ = 40 mg/l	
	O_2 (ppm $\pm$ 0.02)	pH ($\pm$ 0.02)	O_2 (ppm $\pm$ 0.02)	pH ($\pm$ 0.02)	O_2 (ppm $\pm$ 0.02)	pH ($\pm$ 0.02)
0	6.90	8.32	6.85	8.43	6.98	8.38
5	6.22	6.89	5.96	6.90	6.22	6.68
10	6.16	6.83	5.76	6.82	5.92	6.63
20	5.93	6.74	5.42	6.69	5.58	6.55
30	5.72	6.69	5.12	6.59	5.28	6.48
40	5.54	6.65	4.88	6.52	5.00	6.43
50	5.40	6.60	4.67	6.48	4.78	6.37
60	5.26	6.57	4.49	6.45	4.58	6.33
70	5.16	6.53	4.33	6.42	4.39	6.30
80	5.08	6.51	4.21	6.41	4.20	6.27
90	5.01	6.48	4.10	6.40	4.03	6.24
100	4.91	6.46	4.00	6.39	3.90	6.21
110	4.84	6.44	3.92	6.38	3.80	6.20
120	4.79	6.43	3.86	6.38	3.70	6.17

TIME (Minutes)	RUN 11 $(Fe^{2+})_I$ = 60 mg/l	
	O_2 (ppm ± 0.02)	pH (± 0.02)
0	6.93	8.44
5	5.93	6.80
10	5.58	6.65
20	5.07	6.50
30	4.63	6.40
40	4.23	6.32
50	3.91	6.26
60	3.62	6.20
70	3.39	6.15
80	3.20	6.11
90	3.00	6.09
100	2.85	6.05
110	2.71	6.02
120	2.58	6.00

ARTIFICIAL SEA-WATER - ARTIFICIAL EFFLUENT C

TIME (Minutes)	RUN 13 $(Fe^{2+})_I$ = 40 mg/l		RUN 14 $(Fe^{2+})_I$ = 60 mg/l		RUN 15 $(Fe^{2+})_I$ = 60 mg/l	
	O_2 (ppm ± 0.02)	pH (± 0.02)	O_2 (ppm ± 0.02)	pH (± 0.02)	O_2 (ppm ± 0.02)	pH (± 0.02)
0	6.70	8.42	6.91	8.41	6.92	8.38
5	6.45	6.43	6.78	6.11	6.80	6.07
10	6.34	6.37	6.75	6.08	6.78	6.06
20	6.21	6.35	6.69	6.05	6.65	6.04
30	6.09	6.33	6.61	6.05	6.57	6.03
40	5.95	6.32	6.54	6.04	6.48	6.01
50	5.81	6.29	6.46	6.03	6.40	6.00
60	5.68	6.27	6.36	6.01	6.29	5.99
70	5.52	6.25	6.29	6.00	6.21	5.98
80	5.38	6.24	6.19	5.99	6.12	5.98
90	5.23	6.21	6.09	5.98	6.01	5.97
100	5.12	6.20	5.99	5.97	5.92	5.95
110	5.00	6.19	5.88	5.95	5.83	5.93
120	4.88	6.17	5.79	5.93	5.73	5.91

B/ CLOSED RUNS AT 12°C

N.B. To reduce data to manageable proportions values have only been given for each twenty minutes of a run. Ten-minute values, if required, can be approximated by averaging.

ARTIFICIAL SEA-WATER - ARTIFICIAL EFFLUENT A

TIME (Minutes)	RUN 16 $(Fe^{2+})_I$ = 10 mg/l		RUN 17 $(Fe^{2+})_I$ = 20 mg/l		RUN 18 $(Fe^{2+})_I$ = 40 mg/l	
	O_2 (ppm ± 0.02)	pH (± 0.02)	O_2 (ppm ± 0.02)	pH (± 0.02)	O_2 (ppm ± 0.02)	pH (± 0.02)
0	8.50	8.25	8.46	8.25	8.50	8.37
10	8.07	6.79	8.11	6.62	8.22	6.61
20	7.95	6.78	8.00	6.60	8.11	6.59
40	7.82	6.77	7.82	6.58	7.96	6.55
60	7.74	6.76	7.69	6.56	7.82	6.52
80	7.65	6.75	7.55	6.54	7.70	6.51
100	7.58	6.74	7.42	6.52	7.58	6.49
120	7.49	6.73	7.29	6.50	7.43	6.47
140	7.42	6.73	7.19	6.49	7.30	6.43
160	7.37	6.72	7.08	6.48	7.16	6.41
180	7.32	6.72	6.98	6.46	7.03	6.40
200	7.29	6.71	6.88	6.45	6.93	6.38
220			6.81	6.44	6.82	6.35
240			6.74	6.43	6.74	6.34

TIME (Minutes)	RUN 19 $(Fe^{2+})_I$ = 40 mg/l O_2 (ppm ±0.02)	pH (± 0.02)	RUN 20 $(Fe^{2+})_I$ = 60 mg/l O_2 (ppm ± 0.02)	pH (±0.02)
0	8.60	8.27	8.65	8.28
10	8.36	6.43	8.43	6.31
20	8.28	6.41	8.34	6.30
40	8.13	6.39	8.20	6.29
60	8.00	6.37	8.12	6.28
80	7.89	6.36	8.06	6.27
100	7.78	6.35	7.98	6.26
120	7.64	6.34	7.91	6.25
140	7.54	6.33	7.82	6.23
160	7.43	6.32	7.75	6.22
180	7.32	6.30	7.66	6.21
200	7.23	6.29	7.59	6.19
220	7.13	6.27	7.50	6.18
240	7.05	6.26	7.40	6.18

C/ CLOSED RUNS AT 25°C USING REAL SEA-WATER AND TIOXIDE INDUSTRIAL EFFLUENT

N.B. To reduce data values have only been given for each ten minutes of a run. Five-minute values, if required, can be approximated by averaging.

REAL SEA-WATER - ARTIFICIAL EFFLUENT D

TIME (minutes)	RUN 27 $(Fe^{2+})_I$ = 20 mg/l		RUN 28 $(Fe^{2+})_I$ = 20 mg/l		RUN 29 $(Fe^{2+})_I$ = 40 mg/l	
	O_2 (ppm ± 0.02)	pH (±0.02)	O_2 (ppm ± 0.02)	pH (± 0.02)	O_2 (ppm ± 0.02)	pH (± 0.02)
0	6.81	8.25	6.79	8.25	6.91	8.24
5	5.55	6.65	5.60	6.69	5.97	6.38
10	5.41	6.60	5.42	6.65	5.77	6.33
20	5.19	6.57	5.19	6.60	5.43	6.30
30	5.02	6.56	5.01	6.57	5.16	6.28
40	4.89	6.55	4.89	6.56	4.91	6.26
50	4.79	6.55	4.79	6.55	4.71	6.25
60	4.70	6.54	4.69	6.54	4.51	6.23
70	4.63	6.54	4.62	6.54	4.35	6.22
80	4.59	6.53	4.58	6.53	4.20	6.20
90	4.54	6.53	4.53	6.52	4.07	6.18
100	4.50	6.53	4.50	6.52	3.94	6.17
110	4.48	6.52	4.47	6.52	3.83	6.15
120	4.45	6.52	4.44	6.51	3.75	6.14

RUNS INVOLVING TIOXIDE INDUSTRIAL EFFLUENT

Nature of Runs

Run No.	Tioxide Effluent Sample	Nature of Sea-Water	Estimated $(Fe^{2+})_I$ (mg/l)
30	A	Real	18 ± 0.5
31	B	Real	14 ± 0.4
32	B	Artificial	14 ± 0.4
33	B	Real	7 ± 0.3

Data

N.B. To reduce data values have only been given for each thirty minutes of a run.

TIME (minutes)	RUN 30		RUN 31		RUN 32	
	O_2 (ppm ± 0.02)	pH (± 0.02)	O_2 (ppm ± 0.02)	pH (± 0.02)	O_2 (ppm ± 0.02)	pH (± 0.02)
0	6.75	8.26	6.71	8.26	7.05	8.41
30	6.71	6.37	6.69	6.40	7.02	6.32
60	6.67	6.36	6.67	6.40	6.99	6.31
90	6.64	6.34	6.63	6.39	6.94	6.30
120	6.62	6.33	6.59	6.38	6.88	6.29
150	6.59	6.33	6.53	6.37	6.80	6.28
180	6.55	6.32	6.47	6.36	6.71	6.26
210	6.51	6.32	6.40	6.36	6.60	6.24
240	6.48	6.32	6.34	6.35	6.51	6.23
270	6.45	6.32	6.29	6.34	6.41	6.22
300	6.42	6.31	6.22	6.33	6.32	6.21
330	6.38	6.31	6.17	6.33	6.25	6.21
360	6.35	6.31	6.10	6.32	6.18	6.20
390	6.32	6.31	6.04	6.31	6.10	6.20
420	6.29	6.30	5.99	6.30	6.03	6.19

TIME (Minutes)	RUN 33 O_2 (ppm ± 0.02)	pH (± 0.02)
0	6.89	8.29
30	6.64	6.81
60	6.49	6.78
90	6.33	6.75
120	6.21	6.74
150	6.13	6.72
180	6.07	6.71
210	6.03	6.70
240	5.99	6.69

D. OPEN RUNS AT 25°C

Re-Aeration Runs

Measured rate of increase of dissolved oxygen concentration in stirred solutions of oxygen-depleted artificial sea-water open to the air.

RUN A Stirrer Speed = 2 Soln. Vortex ≈ 5mm O_2 Sat = 7.10 ppm		RUN B Stirrer Speed = 3 Soln. Vortex ≈ 7.5 mm O_2 Sat = 7.08 ppm		RUN C Stirrer Speed = 4 Soln. Vortex ≈ 10 mm O_2 Sat = 7.10 ppm	
TIME (Minutes)	O_2 (ppm ± 0.02)	TIME (Minutes)	O_2 (ppm ± 0.02)	TIME (Minutes)	O_2 (ppm ±0.02)
0	2.52	0	4.43	0	4.42
5	2.61	10	4.68	8	4.59
13	2.73	20	4.90	16	4.75
19	2.81	30	5.10	26	4.98
24	2.90	40	5.30	35	5.18
32	3.04	50	5.48	46	5.42
41	3.18	60	5.62	54	5.61
48	3.30	70	5.77	61	5.78
54	3.42	80	5.89	71	5.96
60	3.50	90	6.00	81	6.12
69	3.60	100	6.11	91	6.23
		110	6.20	101	6.38
		120	6.29	106	6.42
		130	6.36	116	6.54
		140	6.41	128	6.62
		150	6.48	141	6.70
				151	6.75
				161	6.79

Ferrous Oxidation Runs

N.B. To reduce data to manageable proportions values have only been given for each ten minutes of a run. Five-minute values, if required, can be approximated by averaging. As pH values were not utilized in the kinetic analysis they have not been included.

Nature of Runs (N.B. All carried out with artificial sea-water)

Run No.	Artificial Effluent	$(Fe^{2+})_I$ (mg/l)	Stirrer Speed	Estimated Re-Aeration Constant Corresponding to Stirrer Speed (min^{-1})
21	A	20 ± 0.3	3	0.010
22	A	40 ± 0.5	3	0.010
23	A	40 ± 0.5	4	0.014
24	A	50 ± 0.75	4	0.014
25	C	60 ± 1	3	0.010

Data

TIME (Minutes)	RUN 21 O_2 (ppm ± 0.02)	RUN 22 O_2 (ppm ± 0.02)	RUN 23 O_2 (ppm ± 0.02)	RUN 24 O_2 (ppm ± 0.02)	RUN 25 O_2 (ppm ± 0.02)
0	7.15	7.08	7.10	6.90	7.10
5	6.51	6.71	6.70	6.50	6.99
10	6.39	6.59	6.60	6.30	6.92
20	6.20	6.39	6.39	6.00	6.82
30	6.03	6.18	6.19	5.75	6.71
40	5.91	5.99	6.03	5.58	6.60
50	5.82	5.80	5.90	5.44	6.52
60	5.73	5.66	5.79	5.34	6.41
70	5.66	5.54	5.70	5.25	6.30
80	5.60	5.44	5.64	5.18	6.21
90	5.56	5.37	5.60	5.12	6.13
100	5.53	5.30	5.56	5.08	6.05
110	5.51	5.27	5.53	5.05	5.99
120	5.50		5.52	5.03	5.93